

**CONVERSION OF METHANOL TO LIGHT OLEFINS ON SAPO-34
KINETIC MODELING AND REACTOR DESIGN**

A Dissertation

by

SAEED M. AL WAHABI

Submitted to the Office of Graduate Studies of
Texas A&M University
in partial fulfillment of the requirements for the degree of

DOCTOR OF PHILOSOPHY

December 2003

Major Subject: Chemical Engineering

CONVERSION OF METHANOL TO LIGHT OLEFINS ON SAPO-34
KINETIC MODELING AND REACTOR DESIGN

A Dissertation

by

SAEED M. AL WAHABI

Submitted to Texas A&M University
in partial fulfillment of the requirements
for the degree of

DOCTOR OF PHILOSOPHY

Approved as to style and content by:

Gilbert F. Froment
(Co-Chair of Committee)

Rayford G. Anthony
(Co-Chair of Committee)

M. Sam Mannan
(Member)

F. Michael Speed
(Member)

Kenneth R. Hall
(Head of Department)

December 2003

Major Subject: Chemical Engineering

ABSTRACT

Conversion of Methanol to Light Olefins on SAPO-34: Kinetic Modeling and Reactor
Design. (December 2003)

Saeed M. Al Wahabi, B.S., King Saud University;

M.S., King Saud University

Co-Chairs of Advisory Committee: Dr. Gibert F. Froment
Dr. Rayford G. Anthony

In this work, the reaction scheme of the MTO process was written in terms of elementary steps and generated by means of a computer algorithm characterizing the various species by vectors and Boolean relation matrices. The number of rate parameters is very large. To reduce this number the rate parameters related to the steps on the acid sites of the catalyst were modeled in terms of transition state theory and statistical thermodynamics. Use was made of the single event concept to account for the effect of structure of reactant and activated complex on the frequency factor of the rate coefficient of an elementary step. The Evans-Polanyi relation was also utilized to account for the effect of the structure on the change in enthalpy. The structure was determined by means of quantum chemical software.

The number of rate parameters of the complete reaction scheme to be determined from experimental data is thus reduced from 726 to 30. Their values were obtained from the experimental data of Abraha by means of a genetic algorithm involving the Levenberg-Marquardt algorithm and combined with sequential quadratic programming.

The retained model yields an excellent fit of the experimental data. All the parameters satisfy the statistical tests as well as the rules of carbenium ion chemistry. The kinetic model also reproduces the experimental data of Marchi and Froment, also obtained on SAPO-34. Another set of their data was used to introduce the deactivation of the catalyst into the kinetic equations.

This detailed kinetic model was used to investigate the influence of the operating conditions on the product distribution in a multi-bed adiabatic reactor with plug flow. It was further inserted into riser and fluidized bed reactor models to study the conceptual design of an MTO reactor, accounting for the strong exothermicity of the process. Multi-bed adiabatic and fluidized bed technologies show good potential for the industrial process for the conversion of methanol into olefins.

DEDICATION

This dissertation is dedicated with all my heart:

To my late father
for all the trust and encouragement he has given me for which I'm forever indebted

To my mother,
whose sincere prayers, sacrifice, and support made this dissertation possible.

To my parents-in-law,
for their sincere prayers and support in several ways.

To my lovely wife,
whose love, endurance, inspiration and endless support made this dissertation possible.

To my sons (Hamody, and Abody),
for their encouraging smiles every morning

And

To my brothers and sisters,
for their motivation and encouragement throughout my graduate studies.

ACKNOWLEDGMENTS

Praise and gratitude to the almighty, Allah, the creator and governor of the universe and his prophet Mohammed, peace upon him.

I would like to express my sincere appreciation to Dr. Gilbert Froment and Dr. Rayford Anthony, the chairmen of my graduate advisory committee, for their moral and academic support, guidance, encouragement, and help during the course of my Ph.D. study.

I am very thankful to Dr. M. Sam Mannan, and Dr. F. Michael Speed for serving as members of my advisory committee and for their helpful comments and suggestions in shaping this dissertation.

I express my deep appreciation to Dr. Tae-Yun Park for his great assistance in my work. I would like to thank Dr. C.V. Philip for his suggestion and assistance on setting up and operating the gas chromatograph.

I also want to thank Amro Taibah, Salem Al-dini, Adel Malallah, Talal Alkharobi, Mishal Alharbi, Samer Elhaj Mahmood, and all the members of the Saudi Student House Club for their continuous support during my stay here in College Station, Texas.

I would like to express my deep gratitude to SABIC for sponsoring my Ph.D. study. Special thanks go to Mr. Saleh Alfawas at SABIC America for his continuing support and assistance.

I want to thank my friends in the catalysis and chemical engineering kinetics group, Dr. Tarek Moustafa, Xianchun Wu, Ammar Alhawaldeh, Sung Hyun Kim, Won-Jae

Lee, Dr. Bo Wang, Dr. Jagannathan Govindhakannan, Rogelio Sotelo-Boyas, Hemendra Khakhan, Celia Maria Rosas, and Luis Carlos Castareda for making my graduate years enjoyable and memorable.

Last but not least, my deep gratitude and appreciation go to my mother, family, parents-in-law, wife and sons, for their sincere prayers, continuous support and encouragement that made this work a success. May Allah bless them all.

TABLE OF CONTENTS

	Page
ABSTRACT	iii
DEDICATION	v
ACKNOWLEDGMENTS	vi
TABLE OF CONTENTS	viii
LIST OF FIGURES	xi
LIST OF TABLES	xvii
CHAPTER I INTRODUCTION	1
CHAPTER II OLEFINS PRODUCTION	3
II.1 Steam Cracking	4
II.2 Fluid Catalytic Cracking	6
II.3 Paraffins Dehydrogenation	7
II.4 Oxidative Coupling of Methane	8
II.5 The Methanol to Olefins Process	9
CHAPTER III METHANOL-TO-OLEFINS. A LITERATURE REVIEW	15
III.1 Introduction	15
III.2 ZSM-5 and SAPO-34 Zeolites	15
III.2.1 Structure	15
III.2.2 Acidity	17
III.3 Conversion of Methanol into Olefins on ZSM-5 and SAPO-34	18
III.4 Catalyst Deactivation	22
III.5 Reaction Mechanism	22
III.5.1 Formation of Dimethylether	23
III.5.2 Formation of Primary Hydrocarbon Products	25
III.5.3 Formation of Higher Olefins	27
III.6 Kinetic Studies	28

	Page
CHAPTER IV KINETIC MODELING OF MTO ON SAPO-34.....	32
IV.1 Introduction.....	32
IV.2 Olefins Formation in Terms of Elementary Steps.....	32
IV.2.1 Construction of Reaction Network.....	32
IV.2.2 Formulation of the Rate Expressions.....	35
IV.2.3 Modeling of Rate- and Equilibrium-Coefficients.....	39
IV.2.3.1 Single Event Concept.....	39
IV.2.3.2 The Evans-Polanyi Relationship.....	42
IV.2.3.3 Thermodynamic Constraints on the Parameters.....	43
IV.2.3.4 Calculation of the Heat of Formation of Carbenium Ions.....	47
IV.2.4 Model Parameter Estimation.....	47
IV.2.4.1 Experimental Data on SAPO-34.....	47
IV.2.4.2 Reactor Model.....	49
IV.2.4.3 Physiochemical Constraints.....	50
IV.2.4.4 Objective Function and Estimation Procedure.....	50
IV.2.4.5 Parameter Values and Comparison of Experimental and Calculated Yields.....	53
IV.2.4.6 Single Event Rate Coefficients for the Various Elementary Steps.....	59
CHAPTER V CATALYST DEACTIVATION.....	63
V.1 Introduction.....	63
V.2 Modeling of Catalyst Deactivation.....	64
V.3 Results and Discussion.....	69
CHAPTER VI CONCEPTUAL REACTOR DESIGN FOR MTO.....	81
VI.1 Introduction.....	81
VI.2 Isothermal Reactor.....	81
VI.3 Multi-bed Adiabatic Reactor.....	85
VI.3.1 SAPO-34-based Process.....	85
VI.3.2 ZSM-5-based Process.....	98
VI.4 Riser Reactor.....	105

	Page
VI.4.1 Fluidization.....	105
VI.4.2 Mathematical Modeling of MTO in a Riser Reactor	108
VI.4.3 Simulation Results.....	110
VI.5 Fluidized Bed Reactor.....	118
VI.5.1 Mathematical Modeling of MTO in a Fluidized Bed Reactor	118
VI.5.2 Simulation Results.....	125
 CHAPTER VII TECHNOLOGY EVALUATION.....	 130
 CHAPTER VIII CONCLUSION AND RECOMMENDATIONS	 132
 NOMENCLATURE.....	 135
 LITERATURE CITED	 139
 APPENDIX A.....	 145
 VITA	 150

LIST OF FIGURES

	Page
Figure II-1. Forecast of ethylene and propylene global demand.	3
Figure II-2. UOP/Hydro MTO process.	12
Figure III-1. Schematic of pore structure of (a) ZSM-5 (b) SAPO-34.	16
Figure III-2. FTIR spectra of SAPO-34 and ZSM-5 zeolites at 200°C.	17
Figure III-3. Product distribution for various modifications of silicate (ZSM-5) at 400°C, WHSV 4 h ⁻¹ and 2.78 (wt/wt) methanol-to-nitrogen ratio.	20
Figure III-4. Catalyst performance of SAPO-34 and Ni-SAPO-34s in methanol conversion. Reaction conditions: 20% MeOH- 80% N ₂ , GHSV 2000h ⁻¹ , temperature 450°C.	21
Figure III-5. Reaction mechanism for the formation of DME by dehydration of methanol over ZSM-5 catalyst.	24
Figure III-6. Reaction scheme for the MTO process.	26
Figure III-7. Reaction scheme Bos et al.	30
Figure IV-1. Kinetic parameter estimation for the SAPO-34 catalyst by the hybrid Genetic Algorithm.	52
Figure IV-2. Experimental and calculated yields for various MTO products on SAPO-34. T=400-450°C, P=1.04 bar, τ=0.8~3 g-cat hr/mol, feed (MeOH + H ₂ O).	56
Figure IV-3. Calculated yields on SAPO-34 of various MTO products compared with experimental data of Table IV-5 as a function of space time. Lines: simulation and symbols: experimental.	57
Figure IV-4. Model verification by comparison with experimental data of Marchi and Froment obtained under entirely different space time. Lines: model and symbols: experimental.	58
Figure IV-5. Single event rate coefficients for the methylation and oligomerization of linear olefins as a function of the C-number of the product.	61

Figure IV-6.	Single event methylation rate coefficients. Effect of reacting olefin structure. Curve (a): all C7-olefins. Produced R+: 2,3-diMe-2-hexyl; 2,5-diMe-3-hexyl; 2,3,4-triMe-3-pentyl. Curve (b): all C7-Olefins. Produced R+: 2-Me-3-heptyl; 4-Me-3-heptyl; 3,3-diMe-4-hexyl; 2,2,4-triMe-3-pentyl.	61
Figure IV-7.	Single event oligomerization rate coefficients. Carbenium ion: ethyl. Effect of olefin structure. Curve (a): 1, propylene; 2, 1-butene; 3, 2-Me-2-butene; 4, 2-Me-3-pentene. Curve (b): 1, 2-Me-4-pentene; 2, 2-hexene; 3, 2-Me-3-pentene.	62
Figure IV-8.	Single event rate coefficients for elementary cracking steps. Curve (a): 2,2-diMe-4-hexyl R+ into 1-butene and 2-Me-2-propyl R+. Curve (b): 2,2,4-triMe-4-pentyl R+ into isobutylene and 2-Me-2-propyl R+. Curve (c): 3,4-diMe-5-hexyl R+ into 2-butene and 2-butyl R+. Curve (d): Single event rate coefficient for the oligomerization step which is the reverse of the cracking step of curve (b).	62
Figure V-1.	Methanol conversion into hydrocarbons on SAPO-34. T=480°C; feed 30/70 wt% methanol-water. $M = \Sigma F'_{MeOH} / W$	63
Figure V-2.	Schematic representation of the trapping of C ₆₊ components inside the SAPO-34 cavities.	65
Figure V-3.	Extrapolation of heats of protonations of C ₆₊ olefins for SAPO-34 based upon corresponding values for ZSM-5.	67
Figure V-4.	Fitting of the experimental data of Marchi and Froment for isothermal fixed bed reactor at 480°C, 1.04 bar total pressure, 32.0 (W/F ⁰ _{MeOH}) and at two methanol partial pressures. Points: experimental data, and lines: simulated.	71
Figure V-5.	Methanol conversion profiles at different process times for isothermal fixed bed reactor at 480°C, 1.04 bar total pressure and with pure methanol feed.	73
Figure V-6.	Methanol conversion profiles at different process times for isothermal fixed bed reactor at 480°C, 1.04 bar total pressure and 0.5 bar methanol partial pressure.	74

Figure V-7.	Ethylene yield profiles at different process times for isothermal fixed bed reactor at 480°C, 1.04 bar total pressure and with pure methanol feed.	75
Figure V-8.	Ethylene yield profiles at different process times for isothermal fixed bed reactor at 480°C, 1.04 bar total pressure and 0.5 bar methanol partial pressure.	76
Figure V-9.	Propylene yield profiles at different process times for isothermal fixed bed reactor at 480°C, 1.04 bar total pressure and with pure methanol feed.	77
Figure V-10.	Propylene yield profiles at different process times for isothermal fixed bed reactor at 480°C, 1.04 bar total pressure and 0.5 bar methanol partial pressure.	78
Figure V-11.	Concentration profiles of C ₆₊ olefins at different process times for isothermal fixed bed reactor at 480°C, 1.04 bar total pressure and with pure methanol feed.	79
Figure V-12.	Concentration profiles of C ₆₊ olefins at different process times for isothermal fixed bed reactor at 480°C, 1.04 bar total pressure and 0.5 bar methanol partial pressure.	80
Figure VI-1.	Evolution of methanol conversion and wt% yield of different products along the length of an isothermal reactor. Temperature: 440°C. Pressure: 1.04 bar. 100% methanol feed.	83
Figure VI-2.	Rate of reaction profiles on SAPO-34 along the length of an isothermal reactor. Temperature: 440°C. Pressure: 1.04 bar. 100% methanol feed. O _i : Olefin with carbon number <i>i</i>	84
Figure VI-3.	Multi-bed adiabatic reactor for SO ₃ synthesis. From Froment and Bischoff.	86
Figure VI-4.	Temperature and methanol conversion profiles in a four-bed adiabatic reactor. Catalyst: SAPO-34. Process time: 0 min. T _f = 648 K for all beds. P = 1.04 bar and P _{MeOH} =0.5 bar (diluted with steam).	89

Figure VI-5.	Yield profiles in a four-bed adiabatic reactor. Catalyst: SAPO-34. Process time: 0 min. $T_f = 648$ K for all beds. $P = 1.04$ bar and $P_{MeOH} = 0.5$ bar (diluted with steam).....	90
Figure VI-6.	Effect of catalyst deactivation on temperature and methanol conversion profiles in a four-bed adiabatic reactor. Catalyst: SAPO-34. Process time: 20 min. $T_f = 648$ K for all beds. $P = 1.04$ bar and $P_{MeOH} = 0.5$ bar.....	92
Figure VI-7.	Effect of catalyst deactivation on yield profiles in a four-bed adiabatic reactor. Catalyst: SAPO-34. Process time: 20 min. $T_f = 648$ K for all beds. $P = 1.04$ bar and $P_{MeOH} = 0.5$ bar.....	93
Figure VI-8.	Effect of catalyst deactivation on temperature and methanol conversion profiles in a four-bed adiabatic reactor. Catalyst: SAPO-34. Process time: 40 min. $T_f = 673, 653, 643,$ and 633 K for beds 1, 2, 3, and 4 respectively. $P = 1.04$ bar and $P_{MeOH} = 0.5$ bar.....	94
Figure VI-9.	Effect of catalyst deactivation on yield profiles in a four-bed adiabatic reactor. Catalyst: SAPO-34. Process time: 40 min. $T_f = 673, 653, 643,$ and 633 K for beds 1, 2, 3, and 4 respectively. $P = 1.04$ bar and $P_{MeOH} = 0.5$ bar.....	95
Figure VI-10.	Effect of catalyst deactivation on the ethylene and propylene yield profiles in a four-bed adiabatic reactor. Catalyst: SAPO-34. $P = 1.04$ bar and $P_{MeOH} = 0.5$ bar.....	96
Figure VI-11.	Ethylene and propylene yield at different process times in a four-bed adiabatic reactor. Catalyst: SAPO-34. $P = 1.04$ bar and $P_{MeOH} = 0.5$ bar.....	97
Figure VI-12.	Temperature and methanol conversion profiles in a four-bed adiabatic reactor. Catalyst: ZSM-5. $T_f = 673$ K for all beds. $P = 1.04$ bar and $P_{MeOH} = 1.04$ bar.....	100
Figure VI-13.	Yield profiles in a four-bed adiabatic reactor. Catalyst: ZSM-5. $T_f = 673$ K for all beds. $P = 1.04$ bar and $P_{MeOH} = 1.04$ bar.....	101

Figure VI-14.	Temperature and methanol conversion profiles in a four-bed adiabatic reactor. Catalyst: ZSM-5. $T_f = 673$ K for all beds. $P = 1.04$ bar and $P_{MeOH} = 0.5$ bar.	102
Figure VI-15.	Yield profiles in a four-bed adiabatic reactor. Catalyst: ZSM-5. $T_f = 673$ K for all beds. $P = 1.04$ bar and $P_{MeOH} = 0.5$ bar.	103
Figure VI-16.	Comparison between the performance of SAPO-34- and ZSM-5-based MTO process in a four-bed adiabatic reactor. $P = 1.04$ bar and $P_{MeOH} = 0.5$ bar. SAPO-34: $T_f = 648$ K for all beds. ZSM-5: $T_f = 673$ K for all beds.	104
Figure VI-17.	Gas / solid contacting regimes, from low to very high gas velocity.	107
Figure VI-18.	Evolution of temperature and methanol conversion along the height of the riser. Feed temperature: 480°C . Methanol mole fraction in the feed: 1.0. Total pressure: 1.04 bar. Flow rates: solid = 196 T/hr, gas = 28 T/hr.	112
Figure VI-19.	C_{6+} olefins content and void fraction profiles along the height of the riser. Feed temperature: 480°C . Methanol mole fraction in the feed: 1.0. Total pressure: 1.04 bar. Flow rates: solid = 196 T/hr, gas = 28 T/hr.	113
Figure VI-20.	Evolution of temperature and methanol conversion along the height of the riser. Feed temperature: 465°C . Methanol mole fraction in the feed: 1.0. Total pressure: 1.04 bar. Flow rates: solid = 4000 T/hr, gas = 28 T/hr.	114
Figure VI-21.	Evolution of wt% yields of different products along the height of the riser. Feed temperature: 465°C . Methanol mole fraction in the feed: 1.0. Total pressure: 1.04 bar. Flow rates: solid = 4000 T/hr, gas = 28 T/hr.	115
Figure VI-22.	C_{6+} olefins content and void fraction profiles along the height of the riser. Feed temperature: 465°C . Methanol mole fraction in the feed: 1.0. Total pressure: 1.04 bar. Flow rates: solid = 4000 T/hr, gas = 28 T/hr.	116

Figure VI-23.	The effect of recycling the catalyst without regeneration on the light olefins yield and on the C ₆₊ olefins content. Feed temperature: 465°C. Methanol mole fraction in the feed: 1.0. Total pressure: 1.04 bar. Flow rates: solid = 4000 T/hr, gas = 28 T/hr.....	117
Figure VI-24.	Two phase model for fluidized bed reactor.....	119
Figure VI-25.	Evolution of the bubble and emulsion gas velocities and the volume fraction taken by the bubble phase and by the emulsion gas along the height of the fluidized bed reactor. Feed temperature: 430°C. Methanol mole fraction in the feed: 1.0. Total pressure: 1.04 bar.....	128
Figure VI-26.	Evolution of methanol conversion and wt% yields of different products along the height of the fluidized bed reactor. Feed temperature: 430°C. Methanol mole fraction in the feed: 1.0. Total pressure: 1.04 bar.....	129

LIST OF TABLES

		Page
Table II-1.	wt% of Products from Cracking Various Feedstocks.	5
Table II-2.	DCC & FCC Technologies: Yield Comparison.....	7
Table II-3.	MTO Overall Material Balance.....	13
Table III-1.	Types of Elementary Steps for the Formation of Higher Olefins.	27
Table IV-1.	Elementary Steps Describing the Formation of Primary Products of the MTO Process.....	33
Table IV-2.	Number of Elementary Steps and Species Involved in the Reaction Network.....	34
Table IV-3.	Expressions for the Net Rate of Formation of Primary Products and Higher Olefins.	36
Table IV-4.	Definition of the Parameters to Be Estimated.....	46
Table IV-5.	A Set of Experimental Data Used for the Parameter Estimation.	48
Table IV-6.	Kinetic Parameters for SAPO-34 Catalyst.....	54
Table IV-7.	Kinetic Parameters for ZSM-5 Catalyst Estimated by Park.....	55
Table VI-1.	Hydrodynamic and Transport Property Correlations.....	122
Table VI-2.	Data Used in the Fluidized Bed Reactor Simulation.....	126

CHAPTER I

INTRODUCTION

The discovery of huge amounts of natural gas in remote locations has led to the construction, in these locations, of mega methanol plants, using available technologies. Methanol, which is a liquid under normal atmospheric conditions, can be shipped more economically than natural gas to more developed areas and the consumer markets. A promising outlet for methanol in the present economic context is the production of olefins. Sooner or later, depending upon the ratio of oil and natural gas prices, the methanol-to-olefins (MTO) route will enter into competition with the conventional steam cracking route based upon simple hydrocarbon mixtures and petroleum fractions. This dissertation has to be seen in this perspective. It expresses in a fundamental way a number of important technical aspects of the commercialization of MTO.

The objectives can be formulated as follows:

- 1) Develop a kinetic model for the formation of olefins from methanol on SAPO-34.
 - a) Write the model in terms of elementary steps without any lumping neither of components nor of steps.
 - b) Estimate the kinetic parameters using the experimental data of Abraha¹ and verify the model prediction using the experimental data of Marchi and Froment².
- 2) Develop a deactivation model.

This dissertation follows the style and format of *Industrial and Engineering Chemistry Research*.

- a) Relate the rate of coke production to the rate of production of C_{6+} olefins trapped inside the cavity of SAPO-34.
 - b) Estimate the deactivation parameters using the data of Marchi and Froment.
 - c) Use the model to explain the observed catalyst deactivation phenomena.
- 3) Combine the kinetic and the deactivation model and utilize them to:
- a) Investigate the influence of the operating conditions on the product distribution in a multi-bed adiabatic reactor with plug flow.
 - b) Study the conceptual design of riser and fluidized bed reactors for MTO.

CHAPTER II

OLEFINS PRODUCTION

Light olefins such as ethylene, propylene and butylenes are important intermediates for the petrochemical industry. Global consumption of ethylene, mainly for the production of polyethylene, is expected to increase to 114 million metric tons by 2005 from 80.5 million tons in 1998 (Figure II-1).^{3,4} On the other hand demand for propylene has increased from 30 million tons in 1992 to 52.5 million tons in 2000 and expected to reach 70 million tons by 2005.

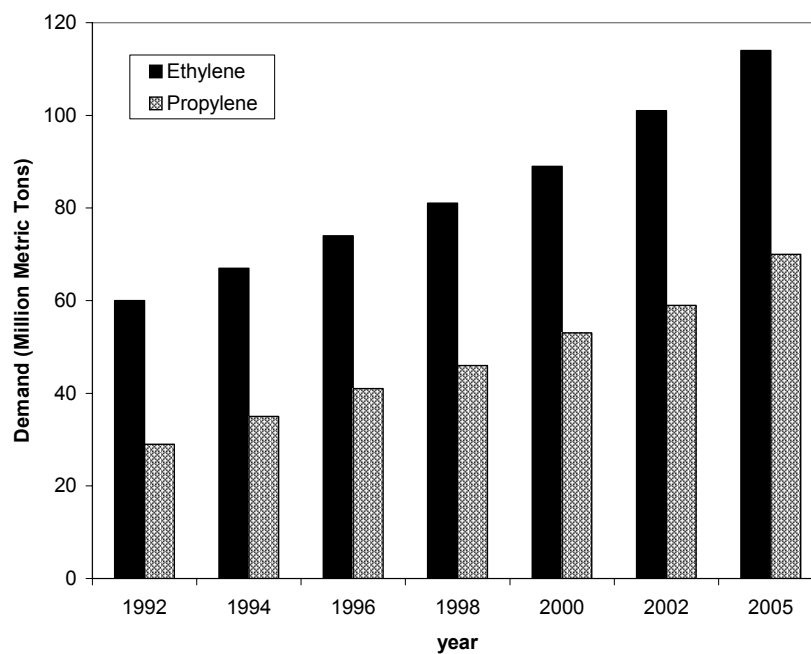


Figure II-1. Forecast of ethylene and propylene global demand.^{3,4}

In 2000, polypropylene accounts for 60% of total propylene demand with an increase of 18% from 1996.

Olefins can be produced using several processes and feedstocks. All processes have in common that they produce a range of products and byproducts. The percentage of the different output products depend on the process and the feedstock used. Currently, there are three main sources of olefins for petrochemicals, Steam Cracking of hydrocarbons (naphtha, ethane, gas oil and LPG), Fluid Catalytic Cracking in oil refineries and Paraffins Dehydrogenation. In addition to these commercial processes, there are some non-commercial technologies under various phases of development such as oxidative coupling of methane, oxidative dehydrogenation of paraffins and Methanol to olefins (MTO) process.

II.1 Steam Cracking

Steam cracking (also known as pyrolysis) of hydrocarbon feedstocks is the main source of olefins production. Virtually all ethylene and around 70% of world propylene are produced by steam cracking.⁴ Hydrocarbon feedstocks most often include ethane, naphtha, and gas oil, although propane and other hydrocarbons may be used. The same process is used regardless of the feedstock employed, although capital and energy requirements will differ depending on both the feedstock and the desired product slate. While there are a number of configurations available to accomplish pyrolysis, essentially all begin with the introduction of hydrocarbon feed and steam into a tubular pyrolysis furnace. In the pyrolysis furnace the feed and steam are heated to a cracking temperature

of about (800-900°C). Temperature requirements for cracking ethane will be higher than for heavier feedstocks.

Table II-1. wt% of Products from Cracking Various Feedstocks.⁵

Product	Ethane	Propane	Naphtha	Gas Oil
Ethylene	76	42	31	23
Propylene	3	16	16	14
C ₄	2	5	9	9
Hydrogen	9	2	2	1
Methane	6	28	17	11

The distribution of the products highly depend on the feed stock used. While lower molecular weight feedstock (e.g., ethane) will give a high percentage of ethylene (see Table II-1); yields of propylene will increase with higher molecular weight feedstock (e.g., naphtha).

Although steam-crackers represent the most important source, propylene supply is very limited due to the low propylene yield. During the last decade, new technologies have been developed for the purpose of enhancing the propylene output of steam crackers. These technologies include Olefins Conversion Technology (OCT) by ABB Lummus⁶, Superflex Technology by Kellogg Brown & Root⁷, and Propylur Technology by Lurgi.⁸ OCT is based on the metathesis reaction which converts one mole of ethylene and one mole of butylenes to form two moles of propylene. When integrated with steam

cracking unit, OCT is claimed to boost the propylene to ethylene ratio from 0.65 (with SC alone) up to 1.0.

On the other hand, Superflex and Propylur technologies can handle wider range of hydrocarbon feeds, generally in the range of C4-C8 and can be designed to produce P/E ratios of about 0.8.

II.2 Fluid Catalytic Cracking

Currently, 31.2 million tons per year or 28% of the world propylene production is being produced in the Fluid Catalytic Cracking (FCC) units.⁴ In FCC, heavy (vacuum) gas oils from refineries are cracked into lighter fractions. The most important product is gasoline with light olefins regarded as byproducts.

Recently, a new catalytic cracking technology was developed, the so-called Deep Catalytic Cracking process (DCC). This process was developed on the basis of a normal riser-cracking process by a Chinese research institute.⁹

DCC produces light olefins from heavy feedstocks with high yields. Two distinct modes of DCC operations are reported, maximum propylene and maximum iso-olefins¹⁰. The key to these processes relies on a highly selective catalysts and appropriate reaction conditions. Table II-2 shows a comparison between the DCC and the conventional FCC units. A substantial increase in the light olefins yields is observed with the new DCC technology.

Table II-2. DCC & FCC Technologies: Yield Comparison.⁹

	DCC (Maximum Propylene)	FCC
Overall Yields, wt%		
C ₂ -	11.9	3.5
C ₃ -C ₄	42.2	17.6
C ₅ + naphtha	26.6	54.8
Light cycle oil	6.6	10.2
Decanted oil	6.1	9.3
Coke	6.0	4.3
Loss	0.6	0.3
Total	100.0	100.0
Olefins Yields, wt%		
Ethylene	6.1	0.8
Propylene	21.0	4.9
Isobutylene	5.1	1.9
Total butylenes	14.3	8.1

II.3 Paraffins Dehydrogenation

Propane dehydrogenation technology has gained importance in recent years due to the increase in consumption of propylene for the production of polypropylene. There are four technologies that can be licensed for propane dehydrogenation. These are CATOFIN from ABB Lummus, Oleflex from UOP, Fluidized Bed Dehydrogenation (FBD) from Snamprogetti, and Steam Active Reforming (STAR) from Phillips Petroleum.

A similar technology can be applied to ethane dehydrogenation, but an economically attractive commercial reactor has not been built.¹¹

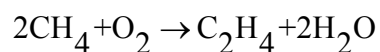
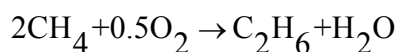
The main drawback of the dehydrogenation technology is that it is equilibrium limited and hence requires high temperatures. The low conversion necessitates a large

separation step to recover products and recycle large volume of unreacted paraffin. To overcome these problems, researchers are focusing in two directions: i) using membrane systems to obtain high conversion at low temperature by separating the hydrogen and shifting the process equilibrium; ii) oxidative dehydrogenation to overcome the equilibrium limitation and to operate at low temperatures.¹²

However, despite some progress made in the membrane area¹³ and in the oxidative dehydrogenation area¹⁴, no commercial plants are believed to be currently operational, although pilot or demonstration plants have been built and operated.

II.4 Oxidative Coupling of Methane

A break-through in the area of methane chemistry occurred in 1982 with the publication of a paper by Keller and Bhasin¹⁵ of Union Carbide (UC), which demonstrated that two molecules of methane could be coupled oxidatively to produce ethane and ethylene:



The initial work showed that the reaction was best carried out in a cyclic mode in which the catalyst was first oxidized and the oxidized material was then exposed to the methane, producing ethane and ethylene. Later, results obtained by Hinsen et al.¹⁶ have shown that a co-feed mode could be used in which both methane and oxygen were fed simultaneously to the catalyst. One year later, Lunsford and co-workers published an

important paper describing the use of Li doped MgO catalysts for the reaction under co-feed conditions, demonstrating that this catalyst has high activity for converting methane to C_{2+} compounds in the presence of O_2 .¹⁷ On the other hand, the introduction of chlorine into the reactants stream has shown to have a very positive effect on the yield of ethylene.¹⁸

During the last decade, a large amount of research in the MOC field has been carried out by the oil and gas companies and other large organizations. Such companies include UC, Arco, BP, Amoco, Mobil, British Gas, Standard Oil Co. and Philips Petroleum.¹⁰ A specific example of catalyst reported by the above include a BP-type catalyst $NaCl/MnO_x/SiO_2$ prepared by the co-gel method¹⁹, which is reported to give a C_{2+} yield of 30% compared to 11.7% for the same catalyst prepared by the traditional route of impregnation.

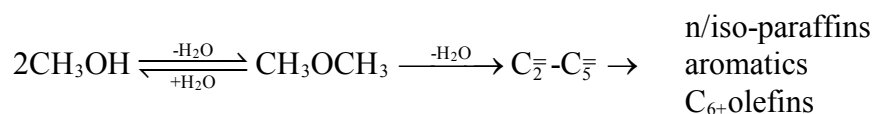
Despite the huge amount of research done on the oxidative coupling of methane, the process still suffers from some drawbacks that need to be solved before it can be commercialized. These drawbacks include limited selectivity to C_2 and high exothermicity of the reaction which requires special reactor design. Additionally, this is complicated by the fact that metals normally used for construction of reactors catalyze the total combustion of methane.²⁰

II.5 The Methanol to Olefins Process

Methanol is a major chemical building block used to manufacture formaldehyde, MTBE, acetic acid and a wide range of other chemical products. The slowdown in MTBE demand, mainly due to the decision taken by California and later by other states

in the US to eliminate its use in the gasoline, is causing some of the producers in the world to explore alternate utilization of their existing methanol plants. One such utilization is the conversion of methanol to olefins (MTO).

The production of light olefins from methanol was first realized around 1977, during the development of Mobil's methanol to gasoline (MTG) process. In the MTG process, where ZSM-5 is used as a catalyst, methanol is first dehydrated to dimethylether (DME). The equilibrium mixture of methanol, DME and water is then converted to light olefins. A final reaction step leads to a mixture of higher olefins, *n/iso*-paraffins, aromatics and naphthenes²¹:



Because they are intermediate in the MTG process, an interruption of the reaction leads to a production of light olefins instead of gasoline. An appropriate process for this purpose was developed later by Mobil.²² Since then several attempts were made to selectively produce light olefins from methanol on zeolite catalysts, not only on medium-pore zeolites but also on small-pore zeolites and to a lesser extent, on large-pore zeolites.

Among all the investigated zeolites, ZSM-5 and SAPO-34 have received a lot of attention due to their excellent catalytic performance for the MTO reaction. Unfortunately the use of ZSM-5 zeolite results in a wide range of products, in particular aromatics and paraffins.²³ In order to improve the selectivity to light alkenes several approaches have been proposed including operating the reactor at high space velocity

and low methanol conversion and introducing some modifications on the catalyst.²⁴ The first solution introduces the need to recycle and results in a rapid catalyst deactivation.²⁵ On the other hand considerable effort has been made to modify the ZSM-5 catalyst for the purpose of increasing its selectivity to light olefins. An extensive review of the literature concerning this has been given by Chang.²⁶ In all cases the production of aromatics could not be avoided at high methanol conversion.

The use of small pore zeolites and in particular SAPO-34 permits the selective formation of light olefins even at 100% methanol conversion.²⁷ This performance has been attributed to the cage structure of SAPO-34, as compared to the channel structure in ZSM-5, and to the intermediate acidity.

Currently, two MTO process technologies are available namely Mobil's MTO process and UOP/Hydro MTO process.

Mobil's MTO process was demonstrated in a 100 BPD fluid bed facility in Germany.²⁸ The process was originally designed for gasoline production and later extended to demonstrate the MTO process. The plant was operated at a pressure between 2.2 and 3.5 bar and a temperature of about 500°C.²² The catalyst used was a modified ZSM-5 zeolite type catalyst. At steady state conditions the olefin yield was more than 60%.

On the other hand, UOP and Norsk Hydro have jointly developed and demonstrated an improved methanol to olefins process which has been ready for license since 1996.²⁹ The process, schematically shown in Figure II-2, offers a high selectivity to light olefins. 80% of the carbon in the methanol feed is converted into ethylene and propylene and

10% to butylenes giving a total light olefins yield of about 90%. By adjusting the operating conditions, ethylene to propylene product weight ratio can be changed from 1.5 to 0.75.³⁰ The catalyst employed is a modified silicoaluminophosphate (SAPO-34) originally discovered by Union Carbide in the 1980s.

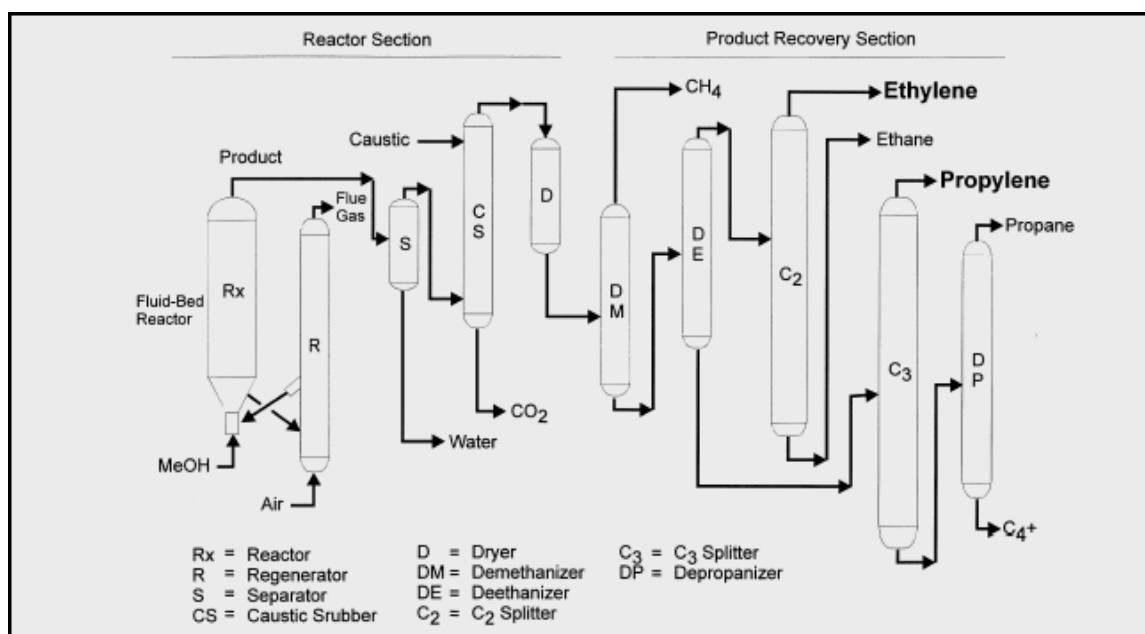


Figure II-2. UOP/Hydro MTO process.²²

Although thermodynamically favored, C₅₊ hydrocarbons are produced at substantially lower level with SAPO-34 than with the ZSM-5 catalyst. This can be

explained by the pore size, which is smaller than the kinetic diameters of these compounds, and by the intermediate acidity of the SAPO-34 catalyst.²

In the overall flow diagram, evaporated methanol is fed directly to the fluidized bed reactor, which is operated to obtain near 100% conversion of methanol. Both neat and crude methanol, which has about 17 wt% of water, can be used as feed stock. The option to use crude methanol opens up for an interesting integration with the methanol unit when located at the same site, thus significant savings can be achieved by not requiring the methanol purification-distillation section. The spent catalyst is circulated to the fluidized bed regenerator, where coke is burned off, and then returned to the reactor to achieve a steady state.

The overall material balance for the production of 500,000 MTA of ethylene is shown in Table II-3. This amount of ethylene production requires 2,330,000 MTA of methanol feed.

Table II-3. MTO Overall Material Balance.²⁹

	Feed, (MTA)	Products (MTA)	Yield on C (%)
Methanol	2,330,000		
Ethylene		500,000	49.0
Propylene		327,000	32.0
Butylenes		100,000	10.0
C ₅₊		22,000	2.0
H ₂ , C ₁₊ paraffins		35,000	3.5
CO _x		5,000	0.5
Coke		31,000	3.0
Water		1,310,000	
Total	2,330,000	2,330,000	100.00

The economics of UOP/Hydro methanol to olefins process were demonstrated by comparing a conventional 500,000 MTA naphtha cracker with a natural gas integrated complex to produce olefins.³¹ For a U.S. gulf coast plant, a return on investment (ROI) of about 30% is achievable for a natural gas based methanol to olefins plant. This compares to about 26% for steam cracker. For a methanol to olefins unit alone, using a methanol cost of \$100/ton, the relevant ROI jumps to more than 36.5%.

CHAPTER III

METHANOL-TO-OLEFINS. A LITERATURE REVIEW

III.1 Introduction

In this chapter a brief review of the ZSM-5 and SAPO-34 zeolites in addition to the reaction mechanism and the kinetic studies reported in the literature concerning the conversion of methanol to light olefins are given. The chapter also summarizes and compares different available technologies for the production of light olefins, mainly ethylene and propylene.

III.2 ZSM-5 and SAPO-34 Zeolites

III.2.1 Structure

The structure of ZSM-5 contains two perpendicularly intersecting channel systems: the sinusoidal channels running parallel to plane [100] are near circular with approximate free dimensions of $5.1 \times 5.5 \text{ \AA}$, while the straight channels of elliptical shape running parallel to [010] have a free cross section of $5.4 \times 5.6 \text{ \AA}$ ³². A simplified picture of the ZSM-5 channel system is shown in Figure III-1 (a).

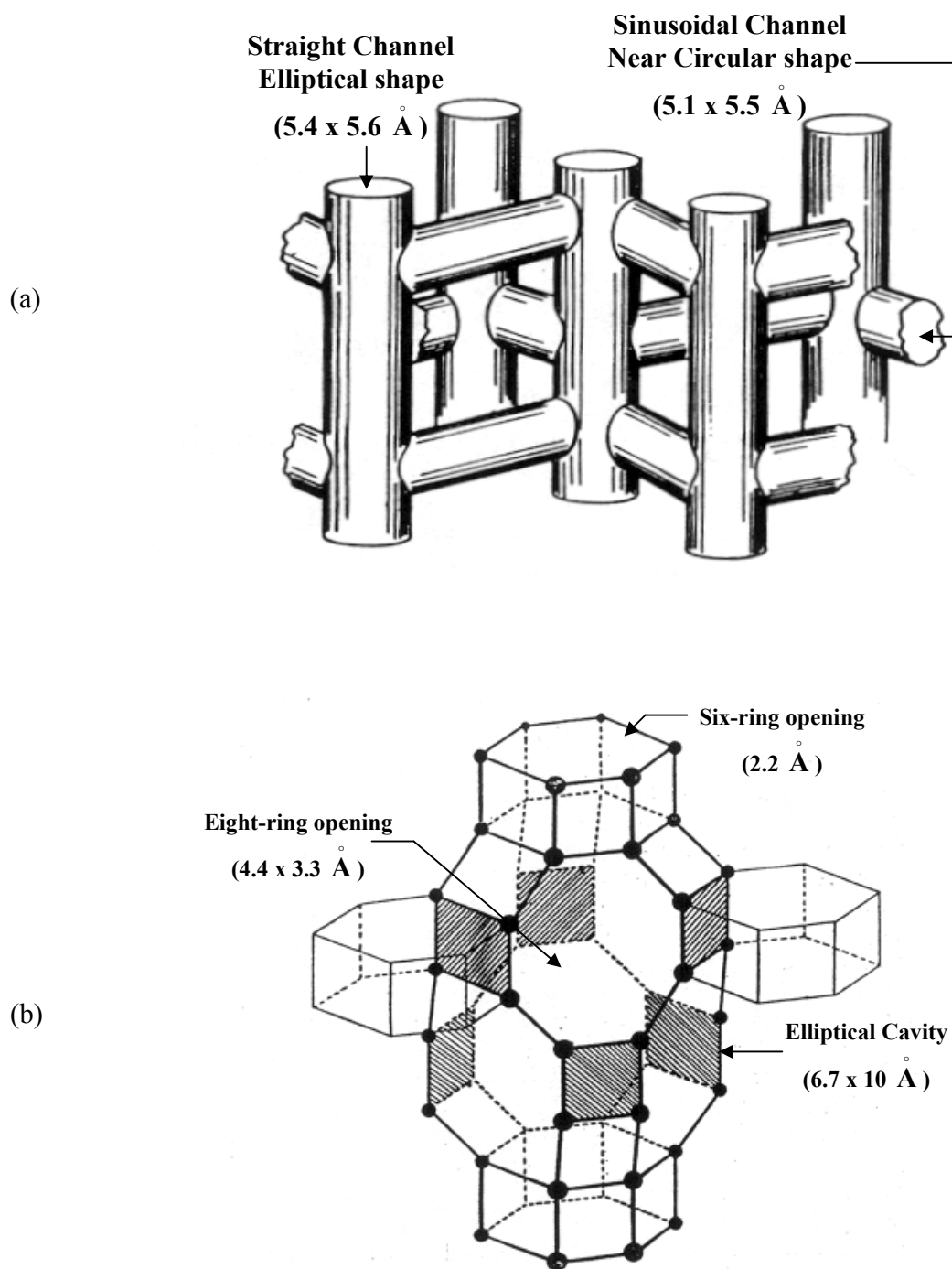


Figure III-1. Schematic of pore structure of (a) ZSM-5³² (b) SAPO-34³³.

On the other hand, SAPO-34 has the chabazite like structure which is shown in Figure III-1 (b). The structure is constructed of doubled six-membered rings forming one cavity per unit cell³³. The dimensions of these roughly elliptical cavities are approximately 6.7 by 10 angstroms. The cavities are interconnected to six others by a 4.4 x 3.1 Å elliptical eight-ring opening.

III.2.2 Acidity

The contribution of the Lewis acidity in the conversion of hydrocarbons is considered to be negligible in comparison to the Bronsted acidity³⁴. Anderson et al.³⁵ showed that the active sites involved in the conversion of methanol on zeolites are not Lewis acids but Bronsted acids.

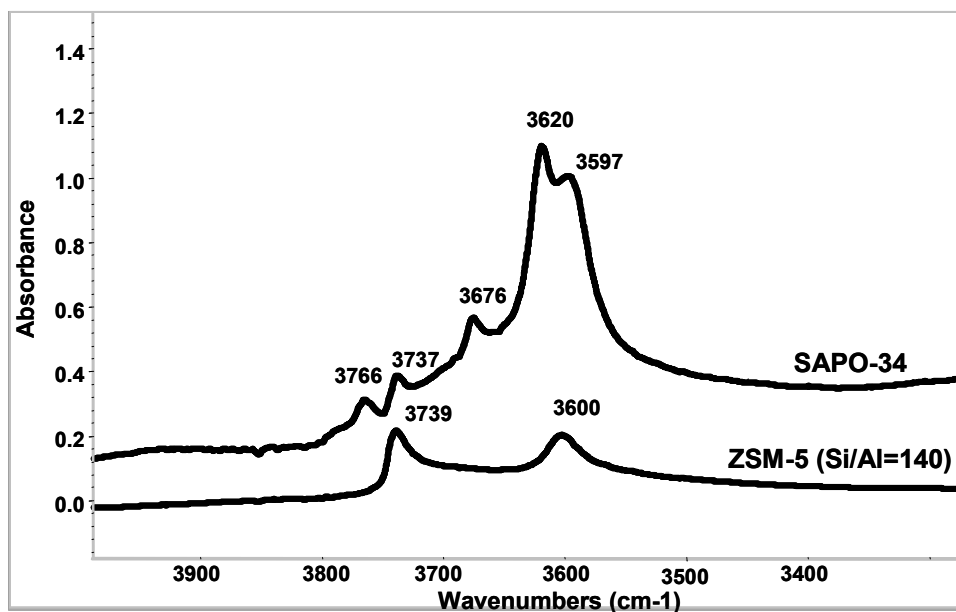


Figure III-2. FTIR spectra of SAPO-34 and ZSM-5 zeolites at 200°C.³⁶

In order to compare the acidity, Wu and Anthony³⁶ tested two samples of HZSM-5 (Si/Al =15) and SAPO-34 (Si/Al = 0.15) using FTIR. The FTIR spectra obtained are shown in Figure III-2. SAPO-34 has more types of –OH groups than ZSM-5. The –OH groups of the SAPO-34 associated with the bands at 3765, 3740, and 3675 cm^{-1} have weak acidity and no activity for acid-catalyzed reactions. The other two kinds of –OH associated with 3620 and 3596 cm^{-1} were believed to have stronger acidity.

The presence of the 3610 cm^{-1} Al-OH groups is believed to be responsible for the high activity of these catalysts for the conversion of methanol into light olefins.²

Whereas the acidity of the ZSM-5 zeolite decreases as the atomic ratio of Si/Al increases, SAPO-34 shows higher concentration of acid sites with increasing Si/Al ratio. This may be explained on the assumption that a SAPO crystal is obtained by silicon substitution into a hypothetical aluminophosphate framework. The predominant mechanism appears to be silicon substitution by phosphorus, which leads to a SAPO crystals having a framework with a net negative charge that are potential Bronsted acid sites.³⁷

III.3 Conversion of Methanol into Olefins on ZSM-5 and SAPO-34

To increase the selectivity toward light olefins, several modifications of the Mobil ZSM-5 catalyst were suggested, especially with respect to ion exchange and impregnation methods. Rodewald³⁸ observed an increase in ethylene selectivity on ZSM-5 catalysts that were exchanged with cations having an ionic radius exceeding 1 angstrom (Cs, Ba). At low conversion, the selectivity toward ethylene on CsZSM-5 was

10% higher than on HZSM-5. At high conversion this difference amount to 40%. This contradict, however, the study done by Dehertog and Froment²³ in which no improvement in the selectivity was observed when using Cs-exchanged ZSM-5 catalyst.

Kaeding and Butter³⁹ modified ZSM-5 with phosphorus compounds. The selectivity toward C₂-C₄ paraffins decreased from 39 to 5 wt%, and toward aromatics from 40 to 20 wt%. The selectivity toward olefins, on the other hand, increased from 1.6 to 39 wt%. the conversion of methanol to hydrocarbons on the P-modified ZSM-5 was only 11.4%, whereas no details on the conversion level of methanol on HZSM-5 were given. For moderate reaction conditions, Dehertog and Froment²³ also reported a significant increase in the maximum yield of light olefins on P-HZSM-5 as compared with HZSM-5. At temperatures above 480°C this effect was no longer observable.

Recently Al-Jarallah et al.⁴⁰ studied the conversion of methanol to light olefins using high silica zeolite of the pentasil type MFI structure (ZSM-5). The reaction was carried out in a fixed bed reaction set-up at 400°C, WHSV = 4 h⁻¹, pressure of 1 bar and a methanol to nitrogen weight ratio of 2.78. The zeolite was modified by impregnation with metal nitrates of Ag, Ca, Cd, Cu, Ga, In, La, and Sr to study their effects on the activity and selectivity of the catalysts. Incorporation of La and Ag led to an improvement in light alkenes selectivity of the silicate by 18% and 14% respectively (see Figure III-3). This was attributed to enhanced shape selectivity of the silicate resulting from reduction in the apparent pore size of the zeolite channels. The activity of the catalyst was slightly decreased due to the formation of higher olefins.

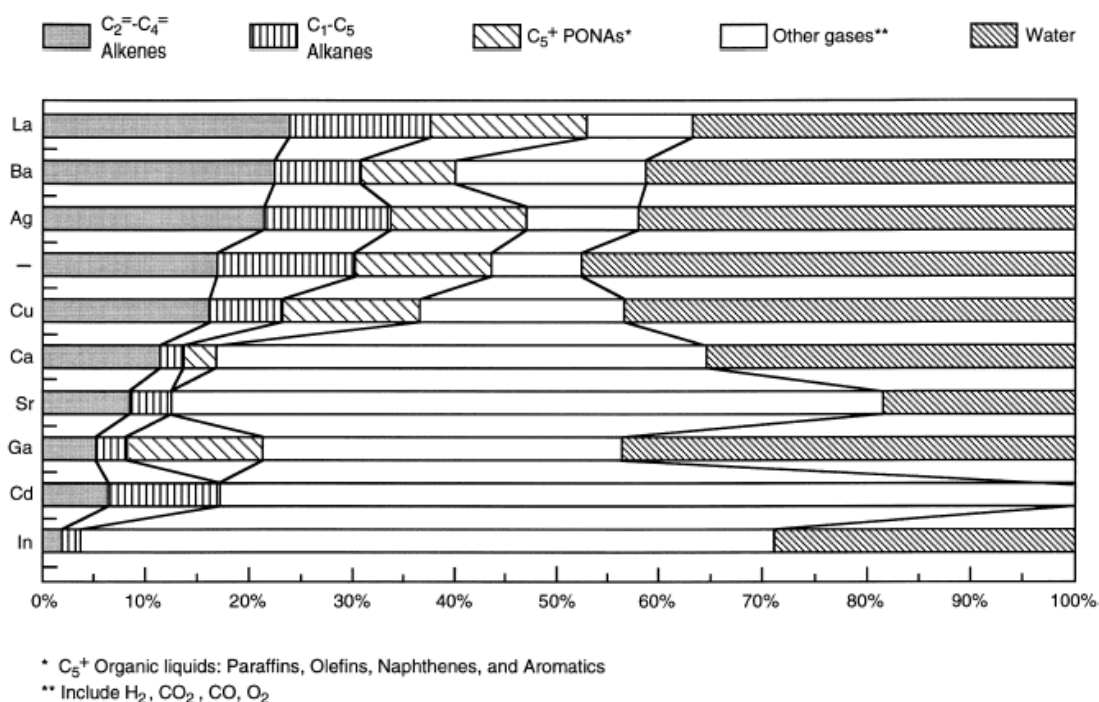


Figure III-3. Product distribution for various modifications of silicate (ZSM-5) at 400°C, WHSV 4 h⁻¹ and 2.78 (wt/wt) methanol-to-nitrogen ratio.⁴⁰

On the other hand, Silicoaluminophosphates (SAPOs), originally developed by UCC early 1980s, and especially SAPO-34 has shown excellent catalytic performance for the selective conversion of methanol to light olefins. At 100% methanol conversion, Kaiser²⁷ reported a combined molar selectivity to light olefins of about 96%. Very low yields of methane and other saturated hydrocarbons were also found. SAPO-34 was also tested by Marchi and Froment². At 480°C and 0.96 h⁻¹ WHSV (MeOH) products yields in (g product/100 g MeOH fed) were as follows: ethylene 18.1 (equivalent to a yield of 41.4 in C-wt %), propylene 16.14 (or 36.9 in C-wt %), butenes 5.5 (or 12.6 in C-wt %),

methane 0.87 and C_{2+} paraffins 2.33. Methanol conversion was approximately 100%. Aromatics or branched isomers were not detected in the effluent. The high selectivity for C_2 - C_4 alkenes and the absence of branched isomers and aromatics were explained by the pore size being smaller than the kinetic diameters of the latter compounds, the intermediate acidity and the low ratio between the concentrations of acid sites on the external surface in relation to that on the internal surface.

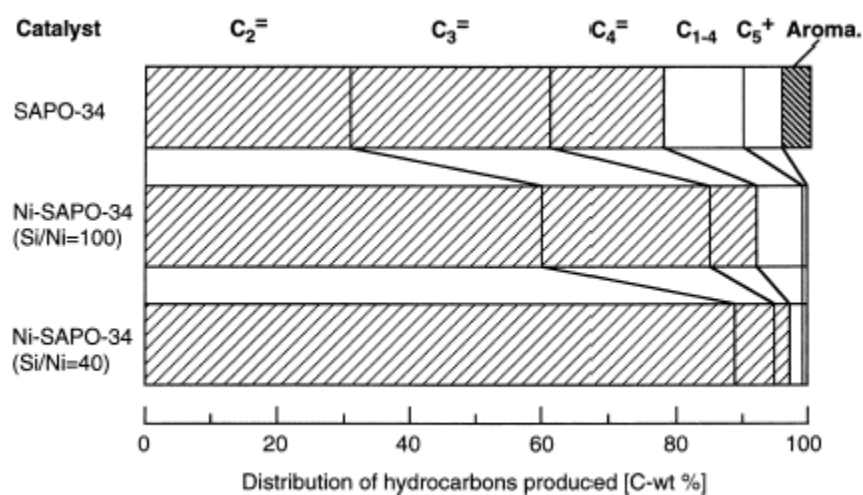


Figure III-4. Catalyst performance of SAPO-34 and Ni-SAPO-34s in methanol conversion. Reaction conditions: 20% MeOH- 80% N_2 , GHSV $2000h^{-1}$, temperature $450^\circ C$.⁴¹

In an attempt to modify SAPO-34 selectivity and life time, Inui et al.⁴¹ reported that nickel-containing SAPO-34 (Ni-SAPO-34) with Si/Ni ratio of 40 prepared by the rapid crystallization method, exhibits a high selectivity to ethylene of 90% at 100% methanol

conversion (see Figure III-4). The catalyst, however, was not easy to reproduce⁴² because the selectivity is very sensitive to those properties which depend on the preparation procedure. Later, Inui and Kang⁴³ reported a reliable procedure for the synthesis of Ni-SAPO-34, and investigated the factors involved in its preparation.

III.4 Catalyst Deactivation

Compared to ZSM-5, SAPO-34 suffers from rapid deactivation during methanol conversion. The big cavities are responsible for this rapid deactivation.²¹ Deactivation starts when aromatics and heavy branched compounds are formed inside the large cages. These molecules cannot diffuse through the porous structure of the SAPO-34 because their kinetic diameter is larger than the pore-opening size. Thus, they remain inside the big cages where they can form carbonaceous deposits blocking the pore openings and preventing the access of molecules to the active sites.

The operating conditions play a very important role in the deactivation rate. Marchi and Froment² have shown that it is possible to suppress the steps that involve coke formation on SAPO-34 by increasing the temperature and the water content in the feed. Water was believed to weaken the strong acid sites responsible for hydrogen transfer reactions. On the other hand the increase of temperature favors the rate of olefins formation with respect to aromatic and oligomer productions.

III.5 Reaction Mechanism

The reaction mechanism of the methanol conversion to hydrocarbons has been discussed in details by Chang²⁴. Three major steps can be distinguished: the formation of

the dimethylether, the initial C-C bond formation, and the subsequent conversion of the primary products to higher hydrocarbons, which proceeds via classical carbenium ion mechanisms, well known from hydrocarbon chemistry in acid media.

III.5.1 Formation of Dimethylether

The reaction pathways for the formation of DME on ZSM-5 are shown in Figure III-5.⁴⁴ It is generally accepted that the formation of DME from methanol precedes the formation of hydrocarbons. Since it is the acidity that enters into the carbenium ion mechanism, it is entirely logical to accept this mechanism for SAPO-34 also. The steps dealt with in Figure III-5 relate to light components which are not subject to the configuration constraints of SAPO-34.

Experiments by Chang²⁴ showed that an essentially identical reaction path is obtained when using DME instead of MeOH. The formation of DME takes place according to the following steps:

1. Reversible adsorption of methanol molecules on the Bronsted acid sites of the SAPO-34.
2. Dehydration of the protonated methanol to form the surface methoxy.
3. Reaction of gas phase methanol with the surface methoxy group to form a surface associated dimethyloxonium ion (DMO^+).
4. Formation of DME by the deprotonation of the DMO^+ .

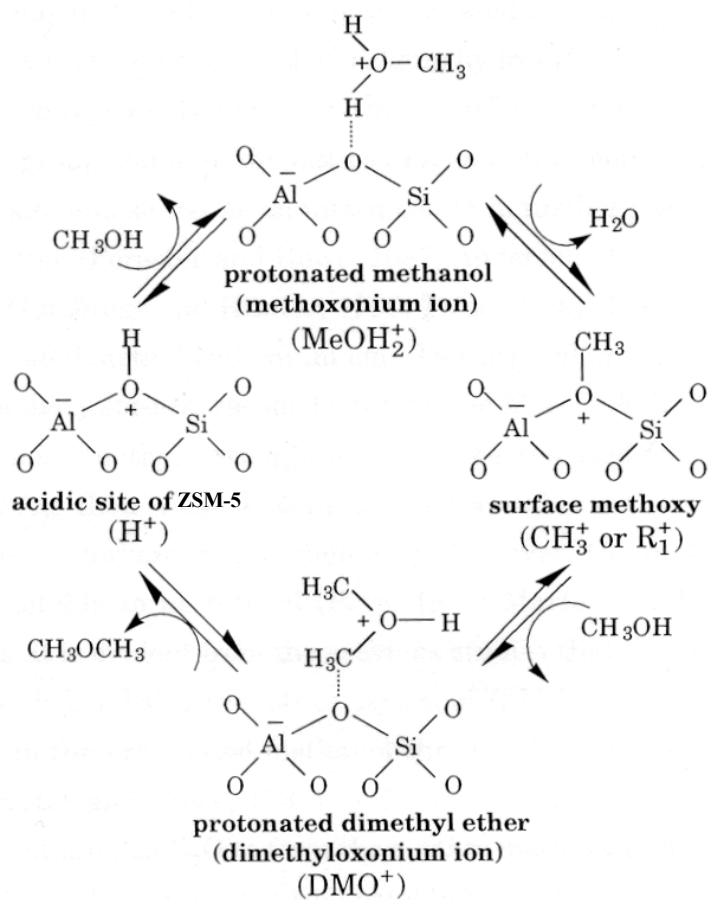


Figure III-5. Reaction mechanism for the formation of DME by dehydration of methanol over ZSM-5 catalyst.⁴⁴

III.5.2 Formation of Primary Hydrocarbon Products

A great deal of attention has been given in the literature to understanding the mechanism for the formation of primary hydrocarbon products. The suggested mechanisms have been extensively reviewed and discussed^{21, 24, 46}.

Recently, Park and Froment^{44, 45} developed a kinetic model for the MTO process on ZSM-5 catalyst. Among all the mechanisms considered, only the surface-bonded oxonium methylene mechanism suggested by Hutchings et al.⁴⁶ was shown to be valid. According to this mechanism, shown schematically in Figure III-6, proton transfer from the surface methoxy to a nearby basic zeolite site (e. g. an adjacent Al-O site) yields a surface-bonded oxonium methylene (CH_2), which reacts with protonated dimethylether (DMO^+) to produce a surface-bonded ethyl and/or propyl carbenium ion (R_2^+, R_3^+). Deprotonation of the R_2^+ and R_3^+ forms gas-phase ethylene and propylene respectively.

At low methanol conversion, methane is also a major primary product. Methane forms by hydride donation from methanol to the surface methoxy.

In this research, the surface-bonded oxonium methylene mechanism will be considered for the kinetic model development.

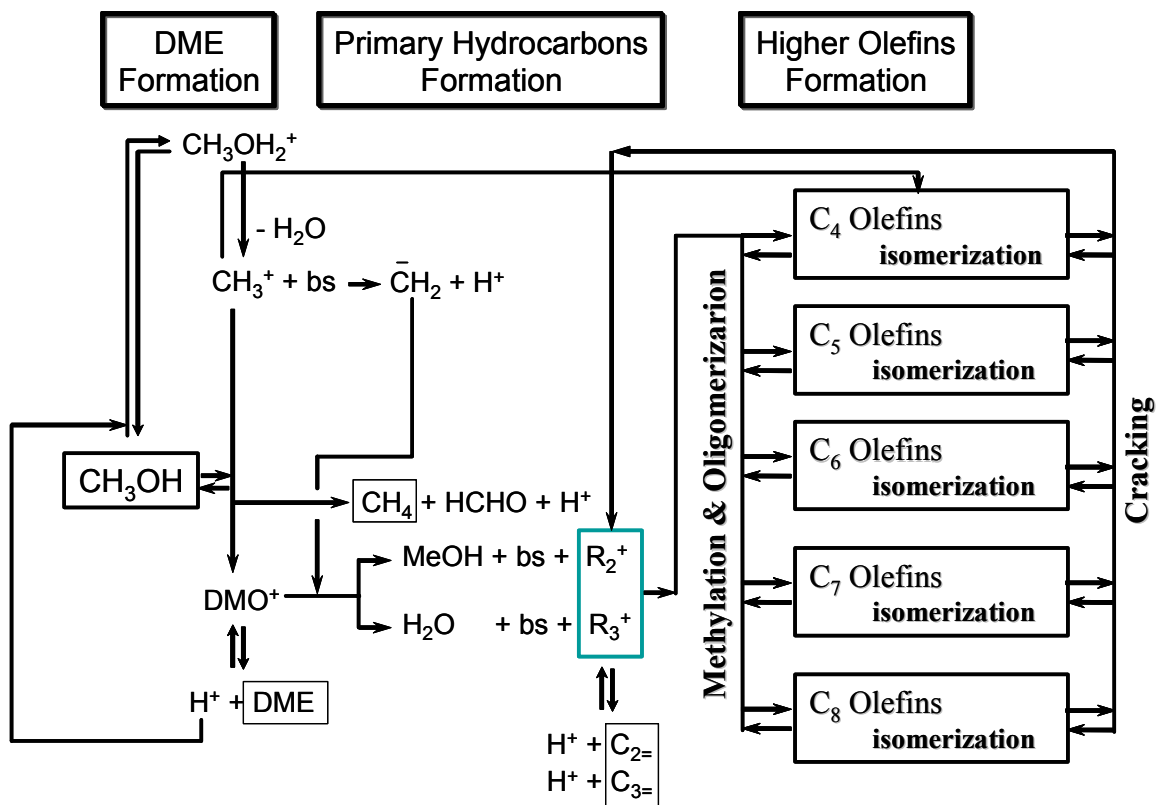


Figure III-6. Reaction scheme for the MTO process.⁴⁴

III.5.3 Formation of Higher Olefins

In MTO, as in any hydrocarbon transformation on heterogeneous acidic catalysts, the conversion of the primary products to higher hydrocarbons proceeds via the carbenium ion mechanisms. Methylation, oligomerization and cracking via β -scission of surface carbenium ions are typical elementary steps for increasing or decreasing the number of carbon atoms in the olefinic products.

Table III-1. Types of Elementary Steps for the Formation of Higher Olefins.

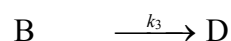
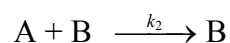
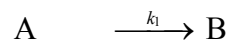
Elementary Step Type	Example			
Rearrangement				
Hydride Shift		\rightleftharpoons		
Methyl Shift		\rightleftharpoons		
PCP Branching		\rightleftharpoons		
β -scission		\rightarrow		+
Deprotonation		\rightleftharpoons		+ H^+
Protonation		+ H^+	\rightleftharpoons	
Methylation		+ R_1^+	\rightarrow	
Oligomerization		+	\rightarrow	

Within the same number of carbon atom, the structure of the carbenium ions is modified by various types of rearrangements, including methyl shift and protonated cyclopropane (PCP) branching. As a result, almost all olefin isomers can be formed by the elimination steps of deprotonation of those carbenium ions. Table III-1 summarizes the elementary steps describing the formation of higher olefins with carbenium ions as intermediates.

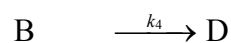
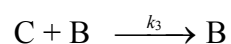
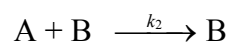
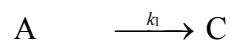
At higher space times based upon methanol (or higher methanol conversion), the olefins are converted into paraffins and aromatics. The formation of these products is generally explained in terms of hydride transfer followed by cyclization of olefinic carbenium ions. The present study focuses on the reaction network corresponding to conditions where the amount of paraffins and aromatics is negligible. This is almost always true for SAPO-34, and true for ZSM-5 at moderate methanol conversion.

III.6 Kinetic Studies

The complexity of the reaction network of the methanol conversion into hydrocarbons, has led many researchers to lump reactants and products into a small number of groups. Based on the autocatalytic nature of the methanol reaction over ZSM-5, Chen and Reagan⁴⁷ used the following simple model:



Where A, B and D represent the oxygenates, the olefins and the aromatics/paraffins, respectively. Chang⁴⁸ modified the scheme of Chen and Reagan by adding a bimolecular step accounting for the carbene insertion into the primary olefins:



Where C represents the carbenes (:CH₂) and A, B, and D are defined as the same as before.

Schoenfelder et al.⁴⁹ developed a lumped-species reaction scheme, involving seven lumps. These lumps are: oxygenates (A), ethene (B), propene (C), butene (D), paraffins (E), methane, carbon monoxide, hydrogen (F), and water (W).

Bos et al.⁵⁰ developed a kinetic model for the MTO process based on SAPO-34. The final reaction scheme, Figure III-7, consisted of 12 reactions involving 6 product lumps plus coke. Reactions 8 and 12 are considered to be second order. All other reactions are of first order. The rate of reactions for different reactions shown in Figure III-7 are as follows:

$$r_i = k_i x_{MeOH} P \quad i = 1, 2, \dots, 7 \quad (\text{III-1})$$

$$r_8 = k_8 x_{C_3} P x_{MeOH} P \quad (\text{III-2})$$

$$r_i = k_i x_{C_3} P \quad i = 9, 10 \text{ and } 11 \quad (\text{III-3})$$

$$r_{12} = k_{12} x_{C_4} P x_{MeOH} P \quad (\text{III-4})$$

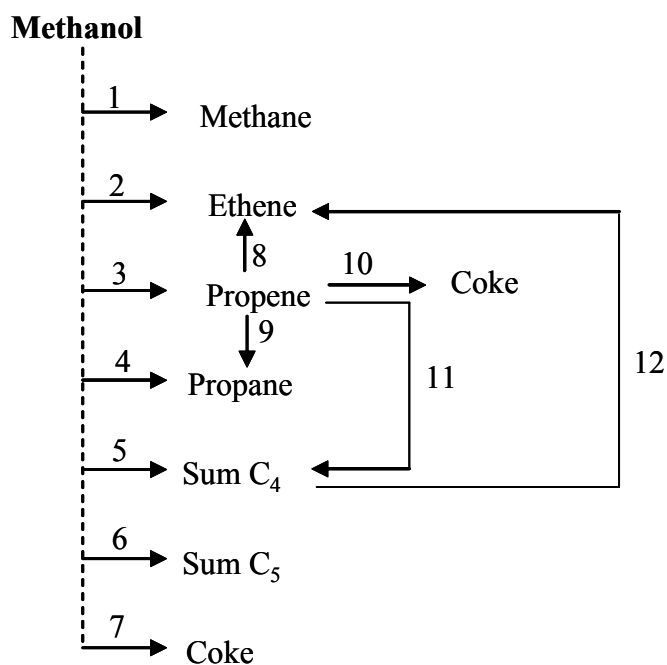


Figure III-7. Reaction scheme Bos et al.⁵⁰

The problem with these lumped models is that they do not reflect the underlying chemistry and the estimated rate and equilibrium coefficient always are dependent on the feed composition and reaction conditions.

Recently Park and Froment^{44,45} modeled the kinetics of the MTO process on a ZSM-5 catalyst on the basis of a detailed mechanistic reaction scheme. A total of eight kinetic

models were tested. The finally retained model corresponds to a mechanism that proceeds over oxonium methylide formed from a methoxy ion interacting with a basic site of the catalyst. The ylide subsequently reacts with dimethyloxonium ions to generate in parallel the primary products ethylene and propylene. Through steps of carbenium ion chemistry, the latter lead to higher olefins and, to a lesser extent, to paraffins and aromatics.

In the present work, it is this detailed reaction mechanism that will be followed in the kinetic modeling of MTO on SAPO-34.

CHAPTER IV

KINETIC MODELING OF MTO ON SAPO-34

IV.1 Introduction

The development of a realistic kinetic model for a process requires detailed information on the mechanism of the reactions. For some processes, however, such as MTO the reaction network consists of hundreds of elementary steps. The complex nature of the MTO reaction network has led many researchers to model the methanol conversion reaction by lumping various products into a few species. Unfortunately, lumped kinetic models can not predict the product composition, and their rate and equilibrium coefficients are dependent on feed composition and reaction conditions.⁴⁴

In this work, the rate coefficients of the elementary steps involved in the MTO network have been modeled by the single event kinetics approach introduced by Froment and co-workers⁵¹ and the Evans-Polanyi relation. This procedure provides a tremendous reduction in the number of parameters to be estimated.

IV.2 Olefins Formation in Terms of Elementary Steps

IV.2.1 Construction of Reaction Network

As discussed in Figure III-6, the MTO process can be divided into three sections; (i) the formation of dimethylether, (ii) the formation of the primary hydrocarbons, and (iii) conversion of the primary products to higher olefins.

Table IV-1 shows the elementary steps describing the formation of the primary products. These steps are constructed based on the mechanism that proceeds via the reaction between surface-bonded oxonium methyl ylides and the protonated DME.

Table IV-1. Elementary Steps Describing the Formation of Primary Products of the MTO Process.

Elementary Steps	Rate or Equilibrium Constants
DME Formation	
$MeOH + H^+ \rightleftharpoons MeOH_2^+$	$K_{Pr}(MeOH)$
$MeOH_2^+ \rightleftharpoons R_1^+ + H_2O$	$k'_F(R_1^+), k'_C(R_1^+)$
$R_1^+ + MeOH \rightleftharpoons DMO^+$	$k'_F(DMO^+), k'_C(DMO^+)$
$DMO^+ \rightleftharpoons DME + H^+$	$K_{Pr}(DME)$
Methane Formation	
$R_1^+ + MeOH \rightarrow CH_4 + HCHO + H^+$	$k'_F(CH_4)$
Primary Olefins Formation	
$R_1^+ + bs \rightleftharpoons OM + H^+$	$k'_{Sr}(R_1^+; bs), k'_{Sr}(OM; H^+)$
$OM + DMO^+ \rightarrow R_2^+ + MeOH + bs$	$k'_{Sr}(OM; DMO^+; R_2^+)$
$R_2^+ \rightleftharpoons O_2 + H^+$	$k'_{De}(R_2^+), k'_{Pr}(O_2)$
$OM + DMO^+ \rightarrow R_3^+ + H_2O + bs$	$k'_{Sr}(OM; DMO^+; R_3^+)$

The reaction network for the formation of higher olefins, however, is much more complicated and contains a large number of elementary steps. To generate the network for such a complex processes, Froment and co-workers⁵¹⁻⁵⁶ developed a computer algorithm in which the various species are characterized by vectors and Boolean relation matrices. Recently Park and Froment^{44,45} utilized this algorithm for the generation of the

MTO reaction Network on ZSM-5. The generated network is adapted for the development of the kinetic model for the MTO reaction on SAPO-34. The olefins and carbenium ions involved in the reaction network are shown in Tables A-1 and A-2, respectively. The number of elementary steps generated by the computer algorithm and species involved in the reaction network are summarized in Table IV-2.

Table IV-2. Number of Elementary Steps and Species Involved in the Reaction Network.

Number of Species	
Olefins	142
Carbenium Ions:	83
Total	225
Number of Elementary Steps	
Protonation:	142
Deprotonation	142
Hydride Shift	88
Methyl Shift	42
PCP Branching	151
Methylation	88
Oligomerization	52
β -scission	21
Total	726

The same number of products and elementary steps are used for SAPO-34 as for ZSM-5. It is true that heavy components that are detected with ZSM-5 do not appear among the products obtained with SAPO-34. Yet, they are actually formed and trapped

inside the SAPO-34 cavities. Further explanation in this regard will be given in CHAPTER VI.

IV.2.2 Formulation of the Rate Expressions

The kinetic expressions for the formation of the primary products and for the higher olefins are formulated based on the reaction mechanism presented in Figure III-6.

In these derivations the following points are considered:

- The olefin isomers were shown to be in equilibrium, so that their partial pressures can be obtained from the composition of the equilibrium mixture.
- The concentration of various adsorbed species can be calculated using the classical Hougen-Watson formalism if an elementary step including the adsorbed species is in pseudo equilibrium in the reaction network. If not the pseudo steady state approximation can be used instead.
- The elementary steps of protonation deprotonation, and the various rearrangements are considered to reach equilibrium, thus their rates are not directly involved in the net rate of production of higher olefins. However, it is important to take them into account because the surface concentration of the carbenium ions involved in the kinetic model is determined by these reactions also.

A summary of the rate expressions for the formation of the primary products and for the higher olefins is presented in Table IV-3.

Table IV-3. Expressions for the Net Rate of Formation of Primary Products and Higher Olefins.⁴⁵

Rate Equations
$\mathfrak{R}_{CH_4} = \mathcal{G}_{R_1^+} \cdot P_{MeOH}$
$\mathfrak{R}_{DME} = k_F(DMO^+) \cdot \mathcal{G}_{R_1^+} \cdot P_{MeOH} - k_C(DMO^+) \cdot \mathcal{G}_{DMO^+}$ $- (k_{sr}(OM; DMO^+ : R_2^+) + k_{sr}(OM; DMO^+ : R_3^+)) \cdot \mathcal{G}_{OM} \cdot \mathcal{G}_{DMO^+}$
$\mathfrak{R}_{O_2} = k_{De}(R_2^+) \cdot \mathcal{G}_{R_2^+} - k_{pr}(O_2) \cdot P_{O_2} \cdot \mathcal{G}_{H^+} - r_{Me}(1,1) - r_{Ol}(1,1)$
$\mathfrak{R}_{O_3} = r_{Me}(1,1) - r_{Me}(2,1) - r_{Ol}(2,1) + k_{sr}(OM; DMO^+ : R_3^+) \cdot \mathcal{G}_{OM} \cdot \mathcal{G}_{DMO^+}$
$\mathfrak{R}_{O_4} = 3r_{Me}(2,1) - r_{Me}(3,1) - r_{Me}(3,2) - r_{Me}(3,3) - r_{Me}(3,4) + 3r_{Ol}(1,1)$
$\mathfrak{R}_{O_5} = 2 \cdot (r_{Me}(3,1) + r_{Me}(3,2) + r_{Me}(3,3) + r_{Me}(3,4)) + 3r_{Ol}(2,1)$
$r_{Me}(i, j) = k_{Me}(i, j) \cdot \mathcal{G}_{R_1^+} \cdot P_{O_{ij}}$
$r_{Ol}(i, j) = k_{Ol}(i, j) \cdot \mathcal{G}_{R_{mn}^+} \cdot P_{O_{ij}}$
Surface Coverages
$N_{R_1^+} = k_F(R_1^+) \cdot K_{Pr}(MeOH) \cdot P_{MeOH} + k_C(DMO^+) \cdot K_{Pr}(DME) \cdot P_{DME}$
$D_{R_1^+} = k_C(R_1^+) \cdot P_{H_2O} + (k_F(DMO^+) + k_F(CH_4)) \cdot P_{MeOH} + k_{Me}(1,1) \cdot P_{O_2} + k_{Me}(2,1) \cdot P_{O_3}$ $+ k_{Me}(3,1) \cdot P_{O_{41}} + k_{Me}(3,2) \cdot P_{O_{42}} + k_{Me}(3,3) \cdot P_{O_{43}} + k_{Me}(3,4) \cdot P_{O_{44}}$
$D_{OM} = k_{sr}(OM; H^+) + (k_{sr}(OM; DMO^+ : R_2^+) + k_{sr}(OM; DMO^+ : R_3^+)) \cdot K_{Pr}(DME) \cdot P_{DME}$
$A_1 = D_{R_1^+} \cdot k_{Sr}(R_1^+; bs)$
$A_2 = D_{R_1^+} \cdot D_{OM} + k_{Sr}(R_1^+; bs) \cdot (D_{OM} - N_{R_1^+} - k_{Sr}(OM; H^+))$
$A_3 = N_{R_1^+} \cdot D_{OM}$
$\eta_{R_1^+} = (2 \cdot A_1)^{-1} \cdot (-A_2 + \sqrt{(A_2)^2 + 4 \cdot A_1 \cdot A_3})$
$\mathcal{G}_{bs} = \frac{D_{OM}}{D_{OM} + k_{Sr}(R_1^+; bs) \cdot \eta_{R_1^+}}$
$\mathcal{G}_{OM} = \frac{k_{Sr}(R_1^+; bs) \cdot \eta_{R_1^+}}{D_{OM} + k_{Sr}(R_1^+; bs) \cdot \eta_{R_1^+}}$

Table IV-3. (Continued).

Surface Coverages
$\eta_{R_2^+} = \frac{k_{sr}(OM; DMO^+ : R_2^+) \cdot K_{Pr}(DME) \cdot P_{DME} \cdot \mathcal{G}_{OM} + k_{Pr}(O_2) \cdot P_{O_2}}{k_{De}(R_2^+) + k_{Ol}(1,1) \cdot P_{O_2} + k_{Ol}(2,1) \cdot P_{O_3}}$
$ads = 1 + K_{Pr}(MeOH) \cdot P_{MeOH} + K_{Pr}(DME) \cdot P_{DME} + \eta_{R_1^+} + \eta_{R_2^+} + K_{Pr}(O_3) \cdot P_{O_3} + K_{Pr}(O_{41})$ $+ K_{Pr}(O_{44}) \cdot P_{O_{44}} + K_{Pr}(O_{51}) \cdot P_{O_{51}} + K_{Pr}(O_{53}) \cdot P_{O_{53}} + K_{Pr}(O_{54}) \cdot P_{O_{54}} + K_{Pr}(O_{56}) \cdot P_{O_{56}}$
$\mathcal{G}_{H^+} = \frac{1}{ads}$
$\mathcal{G}_{MeOH_2^+} = K_{Pr}(MeOH) \cdot P_{MeOH} \cdot \mathcal{G}_{H^+}$
$\mathcal{G}_{DMO^+} = K_{Pr}(DME) \cdot P_{DME} \cdot \mathcal{G}_{H^+}$
$\mathcal{G}_{R_1^+} = \eta_{R_1^+} \cdot \mathcal{G}_{H^+}$
$\mathcal{G}_{R_2^+} = \eta_{R_2^+} \cdot \mathcal{G}_{H^+}$
$\mathcal{G}_{R_{43}^+} = K_{Pr}(O_{41}) \cdot P_{O_{41}} \cdot \mathcal{G}_{H^+}$
$\mathcal{G}_{R_{51}^+} = K_{Pr}(O_{51}) \cdot P_{O_{51}} \cdot \mathcal{G}_{H^+}$
Reaction Rate and Equilibrium Constants
$k_F(DMO^+) = \exp\left[\left(\ln A_F(DME) - \frac{E_F(DME)}{R \cdot T_m}\right) - \frac{E_F(DME)}{R} \cdot \left(\frac{1}{T} - \frac{1}{T_m}\right)\right]$
$k_C(DMO^+) = K_{Pr}(MeOH) \cdot \left(\frac{1}{K_{Hyd}(R_1^+)}\right) \cdot \left(\frac{k_F(DMO^+)}{K(MeOH; DME)}\right) \cdot \left(\frac{1}{K_{Pr}(DME)}\right)$
$K_{Hyd}(R_1^+) = \exp\left[\left(\frac{\Delta S_{Hyd}^\circ(R_1^+)}{R} - \frac{\Delta H_{Hyd}^\circ(R_1^+)}{R \cdot T_m}\right) - \frac{\Delta H_{Hyd}^\circ(R_1^+)}{R} \cdot \left(\frac{1}{T} - \frac{1}{T_m}\right)\right]$
$K(MeOH; DME) = \exp\left(\frac{2441.7}{T} - 1.9686\right)$
$K_{Pr}(DME) = \exp\left[\left(\frac{\Delta S_{Pr}^\circ(DME)}{R} - \frac{\Delta H_{Pr}^\circ(DME)}{R \cdot T_m}\right) - \frac{\Delta H_{Pr}^\circ(DME)}{R} \cdot \left(\frac{1}{T} - \frac{1}{T_m}\right)\right]$

Table IV-3. (Continued).**Reaction Rate- and Equilibrium Constants**

$$k_{sr}(OM; DMO^+ : R_2^+) = \exp \left[\left(\ln A_{sr}(OM; DMO^+ : R_2^+) - \frac{E_{sr}(OM; DMO^+ : R_2^+)}{R \cdot T_m} \right) - \frac{E_{sr}(OM; DMO^+ : R_2^+)}{R} \cdot \left(\frac{1}{T} - \frac{1}{T_m} \right) \right]$$

$$k_{sr}(OM; DMO^+ : R_3^+) = \exp \left[\left(\ln A_{sr}(OM; DMO^+ : R_3^+) - \frac{E_{sr}(OM; DMO^+ : R_3^+)}{R \cdot T_m} \right) - \frac{E_{sr}(OM; DMO^+ : R_3^+)}{R} \cdot \left(\frac{1}{T} - \frac{1}{T_m} \right) \right]$$

$$k_{De}(R_2^+) = \frac{k_{Pr}(O_2)}{K_{Pr}(O_2)}$$

$$k_{Pr}(O_2) = \exp \left[\left(\ln A_{Pr}(O_2) - \frac{E_{Pr}(O_2)}{R \cdot T_m} \right) - \frac{E_{Pr}(O_2)}{R} \cdot \left(\frac{1}{T} - \frac{1}{T_m} \right) \right]$$

$$k_F(R_1^+) = \frac{k_C(R_1^+)}{K_{Hyd}(R_1^+)}$$

$$k_C(R_1^+) = \exp \left[\left(\ln A_C(R_1^+) - \frac{E_C(R_1^+)}{R \cdot T_m} \right) - \frac{E_C(R_1^+)}{R} \cdot \left(\frac{1}{T} - \frac{1}{T_m} \right) \right]$$

$$K_{Pr}(MeOH) = \exp \left[\left(\frac{\Delta S_{Pr}^\circ(MeOH)}{R} - \frac{\Delta H_{Pr}^\circ(MeOH)}{R \cdot T_m} \right) - \frac{\Delta H_{Pr}^\circ(MeOH)}{R} \cdot \left(\frac{1}{T} - \frac{1}{T_m} \right) \right]$$

$$k_F(CH_4) = \exp \left[\left(\ln A_F(CH_4) - \frac{E_F(CH_4)}{R \cdot T_m} \right) - \frac{E_F(CH_4)}{R} \cdot \left(\frac{1}{T} - \frac{1}{T_m} \right) \right]$$

$$k_{sr}(R_1^+; bs) = \exp \left[\left(\ln A_{sr}(R_1^+; bs) - \frac{E_{sr}(R_1^+; bs)}{R \cdot T_m} \right) - \frac{E_{sr}(R_1^+; bs)}{R} \cdot \left(\frac{1}{T} - \frac{1}{T_m} \right) \right]$$

$$k_{sr}(OM; H^+) = \exp \left[\left(\ln A_{sr}(OM; H^+) - \frac{E_{sr}(OM; H^+)}{R \cdot T_m} \right) - \frac{E_{sr}(OM; H^+)}{R} \cdot \left(\frac{1}{T} - \frac{1}{T_m} \right) \right]$$

Table IV-3. (Continued).

Thermodynamic Relations
$\Delta H_{Me}(i, j) = \Delta H_{f,g}(R_{(i+1)k}^+) - \Delta H_{f,g}(R_1^+) - \Delta H_f(O_{ij}) + \Delta q(R_{(i+1)r'}^+) - \Delta q(R_1^+)$
$\Delta H_{Ol}(i, j) = \Delta H_{f,g}(R_{(i+k)m}^+) - \Delta H_{f,g}(R_{ij}^+) - \Delta H_f(O_{kl}) + \Delta q(R_{(i+k)r'}^+) - \Delta q(R_{ij}^+)$
$\Delta q(R_{ir'}^+) = \Delta H_{f,g}(H^+) - \Delta H_{f,g}(R_{ir'}^+) + \Delta H_f(O_3) + \Delta H_{Pr}(O_{ir})$
$\Delta q(R_1^+) = \Delta H_{f,g}(H^+) - \Delta H_{f,g}(R_1^+) + \Delta H_f(MeOH) - \Delta H_f(H_2O) + \Delta H_{Pr}(MeOH) - \Delta H_{Hyd}(R_1^+)$
$\Delta q(R_2^+) = \Delta H_{f,g}(H^+) - \Delta H_{f,g}(R_2^+) + \Delta H_f(O_2) + \Delta H_{Pr}(O_2)$
$\Delta q(R_{54}^+) = \Delta H_{f,g}(H^+) - \Delta H_{f,g}(R_{54}^+) + \Delta H_f(O_{56}) + \Delta H_{Pr}(O_{5r})$

The number of rate and equilibrium coefficients needed for calculating the reaction rate expressions for different products amounts to 253. This means that 504 parameters need to be estimated accounting for the temperature dependency of these rate and equilibrium coefficients. The majority of these parameters come from the detailed reaction network generated by the computer algorithm for the higher olefins production.

IV.2.3 Modeling of Rate- and Equilibrium-Coefficients

IV.2.3.1 Single Event Concept

Because of its large number, estimation of parameters involved in the model is extremely difficult to perform. Therefore, a reduction in the number of parameters is important. For this reason, Froment and co-workers introduced the concept of the “single-event”⁵¹. The concept factors out the structure effect from the change of standard

entropy associated with the transformation of a reactant into a product through an activated complex. From the transition state theory, the rate coefficient can be written as:

$$k' = \frac{k_B \cdot T}{h} \exp\left(\frac{\Delta S^{\ddagger}}{R}\right) \exp\left(-\frac{\Delta H^{\ddagger}}{R \cdot T}\right) \quad (\text{IV-1})$$

According to statistical thermodynamics the standard entropy of a species is determined by several contributions due to the different motions of the species such as translation, vibration, and rotation. The latter is composed of two terms: the intrinsic value, \hat{S}° and a term due to symmetry, σ , which depends on the geometry of the molecule.

$$S_{rot}^\circ = \hat{S}_{rot}^\circ - R \cdot \ln(\sigma) \quad (\text{IV-2})$$

Accounting for the effect of chirality, the rotational contribution S_{rot}° is given by:

$$S_{rot}^\circ = \hat{S}_{rot}^\circ - R \cdot \ln\left(\frac{\sigma}{2^n}\right) \quad (\text{IV-3})$$

where n is the number of chiral centers in a species. The expression in the parenthesis is called a global symmetry number (σ_{gl}). It quantifies all symmetry contributions of a species.

The difference in standard entropy between reactant and activated complex due to symmetry changes is given by:

$$\Delta S_{sym}^{\ddagger} = R \cdot \ln \left(\frac{\sigma_{gl}^r}{\sigma_{gl}^{\ddagger}} \right) \quad (\text{IV-4})$$

This contribution can be substituted for the entropy of activation in (III-1) leading to:

$$k' = \left(\frac{\sigma_{gl}^r}{\sigma_{gl}^{\ddagger}} \right) \frac{k_B \cdot T}{h} \exp \left(\frac{\Delta \hat{S}^{\ddagger}}{R} \right) \exp \left(-\frac{\Delta H^{\ddagger}}{R \cdot T} \right) \quad (\text{IV-5})$$

The rate coefficient of the elementary step, k' , can now be written as a multiple of the single event rate coefficient, \tilde{k} ; where

$$k' = n_e \cdot \tilde{k} \quad (\text{IV-6})$$

The number of single events, n_e , is the ratio of the global symmetry numbers of the reactant and the activated complex.

$$n_e = \frac{\sigma_{gl}^r}{\sigma_{gl}^{\ddagger}} \quad (\text{IV-7})$$

A “single event” frequency factor that does not depend upon the structure of the reactant and activated complex and is unique for a given type of elementary step can be defined as:

$$\tilde{A} = \frac{k_B T}{h} \exp \left(\frac{\Delta S^{\circ}}{R} \right) \quad (\text{IV-8})$$

Because the effect of a difference in structure between the reactant and the activated complex has been factored out by introducing the number of single events, the single event rate coefficient now truly characterizes the reaction itself at the fundamental level. The calculation of the global symmetry numbers of the reacting and produced carbenium ion and of the activated complex requires their configuration. These can be determined by means of quantum chemical packages such as MOPAC, GAMESS and GAUSSIAN.

IV.2.3.2 The Evans-Polanyi Relationship

Whereas the single event concept accounts for the effect of the structure on the frequency factor of an elementary step the relation of Evans and Polanyi⁵⁷ accounts for the effect of structure and chain length upon the enthalpy contribution to the rate coefficient. For elementary steps of a given type (Methylation, Oligomerization, etc.), the activation energy of each elementary step is given by:

$$\begin{aligned}
 E_a(i) &= E_a^\circ - \alpha |\Delta H_r(i)| && \text{(exothermic)} \\
 E_a(i) &= E_a^\circ + (1 - \alpha) |\Delta H_r(i)| && \text{(endothermic)}
 \end{aligned}
 \tag{IV-9}$$

This relation permits the calculation of the activation energy, E_a , for any elementary step or single event pertaining to a certain type, provided the α -coefficient and the E_a° of a reference step of that type are available. Use of modern quantum chemical packages, such as GAUSSIAN, is essential for the calculation of ΔH_r .

The single event rate coefficients for each elementary step can be written based upon the Evans-Polanyi relation as:

$$\tilde{k} = \tilde{A} \cdot \exp\left(\frac{E_a}{R \cdot T}\right) \quad (\text{IV-10})$$

where \tilde{A} is the single event preexponential factor. The intrinsic activation barrier E_a° and the transfer coefficient α take on unique values for a given type of elementary step or single event so that there are only 2 independent rate parameters for this step. The single event concept and the Evans-Polanyi relation drastically reduce the number of rate coefficients.

IV.2.3.3 Thermodynamic Constraints on the Parameters

Despite the remarkable reduction of the number of parameters in the rate expressions due to the introduction of the single event concept and the Evans-Polanyi relation, a large number of equilibrium constants still remain to be estimated. The number of these constants can also be reduced based upon the thermodynamic relationship for the olefin isomerization network.

The equilibrium constant for the isomerization between any two olefins can be expressed as the product of the equilibrium constants for the reactions in their respective isomerization pathways via the common carbenium ions. Using this relation, together with the expression for the rate coefficient based upon the single event and the Evans-Polanyi relation, the protonation equilibrium constant for an olefin can be written as:

$$K_{Pr}(O_{ij}) = K_{Iso}(O_{ij} \rightleftharpoons O_{ir}) \cdot K_{Pr}(O_{ir}) \cdot \left(\frac{\sigma_{gl}^{R_{ij}^+}}{\sigma_{gl}^{R_{ir}^+}} \right) \cdot \exp\left(\frac{\Delta H_{f,g}(R_{ij}^+) - \Delta H_{f,g}(R_{ir}^+)}{R \cdot T} \right) \quad (\text{IV-11})$$

where O_{ir} and R_{ir}^+ represent the olefin and the corresponding carbenium ion in the reference protonation step. Olefins O_{44} and O_{56} are chosen as references for the olefins with carbon numbers 4 and 5 respectively. Similarly, carbenium ions R_{42}^+ and R_{54}^+ are chosen as references for the carbenium ions with carbon numbers 4 and 5 respectively. The subscripts represent the carbon number and the isomer index as shown in Tables A-1 and A-2.

Equation (IV-11) shows that for olefins with the same carbon number, any protonation equilibrium constant can be calculated from the equilibrium constant of a reference protonation and the thermodynamic properties of the gas phase carbenium ions. Thus, there is only a one independent equilibrium constant per carbon number.

The use of the thermodynamic constraints as well as the single event kinetic approach with energy contribution described by the Evans-Polanyi relation reduce the parameters that need to be estimated to 30 parameters. Twenty four of these parameters belong to the formation of the primary olefins, and 8 to the higher olefins formation. The 8 parameters are related to 4 heats of protonations of reference olefins, $\Delta H_{Pr}(O_{ir})$, 1 entropy term in the protonation equilibrium constant, $\Delta \tilde{S}_{Pr}$, the single event frequency factor, \tilde{A} , the intrinsic activation barrier, E_a° , and the transfer coefficient, α . Because of the similarity between methylation and oligomerization, only one single event frequency factor for both types of elementary steps, is considered.

In order to reduce the correlation between preexponential factors and activation energies causing inaccuracies in the estimation, the rate coefficients were parameterized as follows:

Starting from the Arrhenius form of the rate coefficient,

$$k_i = A \cdot \exp\left(-\frac{E_i}{R \cdot T}\right) \quad (\text{IV-12})$$

by introducing the mean temperature, T_m , the rate coefficients can be written as:

$$k_i = \exp\left[\left(\ln A_i - \frac{E_i}{R \cdot T_m}\right) - \frac{E_i}{R} \cdot \left(\frac{1}{T} - \frac{1}{T_m}\right)\right] \quad (\text{IV-13})$$

The definition of the 30 kinetic parameters involved in the model is shown in Table IV-4.

Table IV-4. Definition of the Parameters to Be Estimated.

P#	Definition	P#	Definition
1	$\frac{\Delta S_{Pr}^{\circ}(MeOH)}{R} - \frac{\Delta H_{Pr}^{\circ}(MeOH)}{R \cdot T_m}$	16	$\frac{E_{sr}(OM; H^+)}{R}$
2	$\frac{\Delta H_{Pr}^{\circ}(MeOH)}{R}$	17	$\ln A_{sr}(OM; DMO^+; R_2^+) - \frac{E_{sr}(OM; DMO^+; R_2^+)}{R \cdot T_m}$
3	$\frac{\Delta S_{Hyd}^{\circ}(R_1^+)}{R} - \frac{\Delta H_{Hyd}^{\circ}(R_1^+)}{R \cdot T_m}$	18	$\frac{E_{sr}(OM; DMO^+; R_2^+)}{R}$
4	$\frac{\Delta H_{Hyd}^{\circ}(R_1^+)}{R}$	19	$\ln A_{sr}(OM; DMO^+; R_3^+) - \frac{E_{sr}(OM; DMO^+; R_3^+)}{R \cdot T_m}$
5	$\ln A_c(R_1^+) - \frac{E_c(R_1^+)}{R \cdot T_m}$	20	$\frac{E_{sr}(OM; DMO^+; R_3^+)}{R}$
6	$\frac{E_c(R_1^+)}{R}$	21	$\ln A_{Pr}(O_2) - \frac{E_{Pr}(O_2)}{R \cdot T_m}$
7	$\ln A_F(DME) - \frac{E_F(DME)}{R \cdot T_m}$	22	$\frac{E_{Pr}(O_2)}{R}$
8	$\frac{E_F(DME)}{R}$	23	$\frac{\Delta \tilde{S}_{Pr}}{R}$
9	$\frac{\Delta S_{Pr}^{\circ}(DME)}{R} - \frac{\Delta H_{Pr}^{\circ}(DME)}{R \cdot T_m}$	24	$\frac{\Delta H_{Pr}^{\circ}(O_2)}{R}$
10	$\frac{\Delta H_{Pr}^{\circ}(DME)}{R}$	25	$\frac{\Delta H_{Pr}^{\circ}(O_3)}{R}$
11	$\ln A_F(CH_4) - \frac{E_F(CH_4)}{R \cdot T_m}$	26	$\frac{\Delta H_{Pr}^{\circ}(O_{4r})}{R}$
12	$\frac{E_F(CH_4)}{R}$	27	$\frac{\Delta H_{Pr}^{\circ}(O_{5r})}{R}$
13	$\ln A_{sr}(R_1^+; bs) - \frac{E_{sr}(R_1^+; bs)}{R \cdot T_m}$	28	$\ln(C'_{H^+} \cdot \tilde{A})$
14	$\frac{E_{sr}(R_1^+; bs)}{R}$	29	α
15	$\ln A_{sr}(OM; H^+) - \frac{E_{sr}(OM; H^+)}{R \cdot T_m}$	30	$\frac{E^{\circ}}{R \cdot \alpha}$

IV.2.3.4 Calculation of the Heat of Formation of Carbenium Ions

The heat of reaction of the elementary steps, required for the application of the Evans-Polanyi relation is obtained from the heats of formation of olefins and surface-bonded carbenium ions. The thermodynamic properties of the olefin isomers are calculated using Benson's group contribution method. Those of the surface associated carbenium ions were obtained in two steps. In the first, the properties of free carbenium ions were estimated by means of quantum chemical packages. The second step adds to these values the contributions arising from the link to the protons of the zeolite-surface. The latter leads to a "heat of stabilization" that Park and Froment⁴⁵ found to be a function of the number of C-atoms of the carbenium ions. They related them to their heat of protonation. These are parameters to be determined from the experimental data.

IV.2.4 Model Parameter Estimation

IV.2.4.1 Experimental Data on SAPO-34

Kinetic data used for the parameter estimation were obtained from the experimental data of Abraha¹. The experiments were conducted in a fixed bed reactor at three temperatures: 400°C, 425°C, and 450°C. Experiments at three different space times (g-cat hr/moles methanol fed) were performed. Varying the space time was achieved by changing the feed molar flow rate. The total pressure inside the reactor was 1.04 bar for all the experiments carried out in this study. In order to decrease the deactivation rate of SAPO-34, all the experiments were conducted with 80 mol% water in the feed.

Catalyst powder was pelletized by pressing it into wafers, and then crushing and screening it to 1.1 μm , to avoid internal diffusion resistance. The catalyst bed was diluted 4 times (wt.) with α -alumina in three thin layers.

The data were collected after 15 minutes time on stream and it was assumed that at this time the catalyst did not contain any coke and was not deactivated.

The experimental data used in this work are shown in Table IV-5. Both ethylene and propylene are produced in almost equal quantities, but the temperature affects the ratio to some extent.

Table IV-5. A Set of Experimental Data Used for the Parameter Estimation.¹

T (K)	673.16	673.16	673.16	698.16	698.16	698.16	723.16	723.16	723.16
$P_{\text{MeOH}}^{\text{a}}$ (bar)	0.2	0.2	0.2	0.2	0.2	0.2	0.2	0.2	0.2
W/F^{o} ($\text{gcat} \cdot \text{h/mol MeOH}$)	0.86	1.69	2.98	0.81	1.69	2.99	0.81	1.68	2.97
$X_{\text{MeOH}}^{\text{b}}$	42.8	67.4	76.6	46.5	73.4	81.6	46.9	79.2	87.7
Yield ^c									
CH_4	0.14	0.16	0.32	0.32	0.35	0.42	0.5	0.71	1.57
C_2H_4	5.33	10.78	12.51	6.37	11.46	15.14	7.73	13.56	16.50
C_2H_6	0.04	0.07	0.08	0.05	0.07	0.10	0.05	0.08	0.13
C_3H_6	5.19	11.91	15.22	6.62	12.52	16.73	6.68	11.94	14.21
C_3H_8	0.61	0.00	0.40	0.00	0.03	0.44	0.22	0.72	0.59
C_4H_8	1.92	1.61	4.87	1.60	3.10	4.04	1.41	2.61	2.89
C_4H_{10}	0.37	0.03	0.75	0.34	0.56	0.69	0.28	0.50	0.66
C_5H_{10}	0.0	0.63	0.63	0.05	1.12	0.41	0.00	0.45	0.37
CH_3OCH_3	2.94	0.57	0.74	0.45	0.23	0.86	1.34	0.95	0.811

(a) Feed diluted with water.

(b) Conversion of methanol.

(d) Yield (g produced / 100 g methanol fed).

IV.2.4.2 Reactor Model

The theoretical responses, y_i , are calculated based upon the following continuity equations (an ideal plug flow reactor is assumed):

$$\frac{d\hat{y}_i}{d(W/F_{MeOH}^\circ)} = \frac{100 \cdot M_i}{M_{MeOH}} \cdot \mathfrak{R}_i, \quad i = 1, 2, \dots, m \quad (\text{IV-14})$$

where,

\hat{y}_i = Yield of component i in g-formed per 100 g of methanol fed to the reactor.

F_{MeOH}° = Initial flow rate of methanol at the inlet of the reactor in moles/hr.

W = Amount of catalyst in g.

W/F_{MeOH}° = Space time in g-cat hr/moles of methanol fed.

M_i, M_{MeOH} = Molecular weight of species i and of methanol respectively

This system of coupled differential equations can be solved numerically with the initial condition of zero yield at zero space time. Because of the stiffness of this system, Gear's method was utilized in the integration.

IV.2.4.3 Physiochemical Constraints

the kinetic parameters should satisfy well established physiochemical relations⁵⁸. For the parameters involved in the protonation steps, Boudart's criteria⁵⁹ defines a rigorous set of constraints for the enthalpy, ΔH_{Pr}° , and entropy, ΔS_{Pr}° :

$$\begin{aligned} -\Delta H_{Pr}^{\circ} &> 0 \\ 0 &< -\Delta S_{Pr}^{\circ} < S_g^{\circ} \\ 41.8 &< -\Delta S_{Pr}^{\circ} < 51.04 + 1.4 \times 10^{-3} (-\Delta H_{Pr}^{\circ}) \end{aligned} \quad (IV-15)$$

where S_g° is the standard entropy of the molecule in the gas phase. Other constraints also include, the heat of reactions for each elementary step of methylation and oligomerization, ΔH_{Me} and ΔH_{Ol} , should be negative. Similarly, the activation energies of each elementary step of methylation and oligomerization should be positive.

To ensure that the estimated parameters have meaningful values, the above criteria were inserted as constraints in the optimization routine.

IV.2.4.4 Objective Function and Estimation Procedure

Estimation of the kinetic parameters was performed by minimizing the difference between the experimental and calculated yields of MTO products:

$$S = \sum_{j=1}^m \sum_{l=1}^m w_{jl} \sum_{i=1}^n (y_{ij} - \hat{y}_{ij})(y_{il} - \hat{y}_{il}) \quad (IV-16)$$

where m = number of responses, n = number of experiments, and w_{ji} = elements of the inverse of the covariance matrix of the experimental errors on the responses y .

The kinetic parameters in this work have been estimated by means of the hybrid genetic algorithm developed by Park and Froment.⁶⁰ The Genetic Algorithm (GA) was found to access the global minimum even though the ranges of the parameters are extremely wide and in spite of local minima in the parameter space. More information about the Genetic algorithm can be found in the work of Park and Froment⁴⁵.

In this algorithm, three different routines are linked for the objective of increasing the efficiency and the accuracy of the estimation process. In the beginning, the Genetic algorithm is used to generate the initial guesses for the local optimizer, the Levenberg-Marquardt program. Because the Levenberg-Marquardt algorithm is an unconstrained optimization technique, a constrained optimization technique based upon sequential quadratic programming (SQP), called FFSQP has been used. The function of the latter is to ensure that all the estimated parameters satisfy the constraints discussed before.

Figure IV-1 shows the minimization process performed by the hybrid Genetic Algorithm. The best sets of parameters generated by the GA were used as starting point for the local optimizer. The global minimum was reached after performing 138 iterations in Levenberg-Marquardt and FFSQP starting from the 1179th GA initial guess.

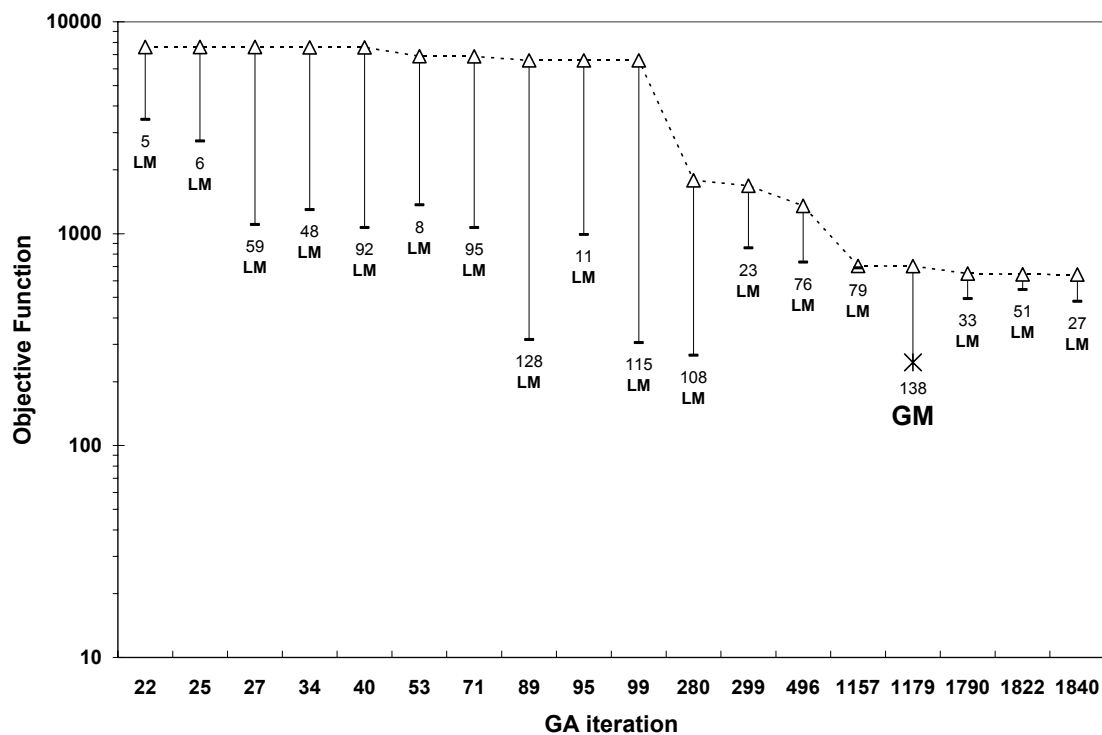


Figure IV-1. Kinetic parameter estimation for the SAPO-34 catalyst by the hybrid Genetic Algorithm.

The best set of parameters at each GA iteration is used as a starting point for the Levenberg-Marquardt optimizer. The numbers at the end of the minimization indicate the number of iterations performed by the Levenberg-Marquardt optimizer.

Legend:
△..... objective function after each GA iteration
 ———— minimization by the Levenberg-Marquardt optimizer
 LM: local minimum GM: global minimum

IV.2.4.5 Parameter Values and Comparison of Experimental and Calculated Yields

Parameters estimated by the hybrid GA are shown in Table IV-6, along with the 95% confidence interval on the parameters. The first column represents the parameters obtained after parameterization of the rate and equilibrium constants as listed in Table IV-4. Kinetic parameters were derived from these parameters using the total concentration of the acidic and basic sites. Because of the similarity between methylation and oligomerization only one single event frequency factor was considered for both types of elementary steps. All the parameters satisfy the statistical tests and the physicochemical constraints discussed earlier. A very small value of the transfer coefficient, α , is obtained. This, according to the Hammond postulate,⁶¹ could be an indication that the transition state lies close to the reactant. A slightly bigger value of α was obtained for ZSM-5 (Si/Al = 200) as shown in Table IV-7⁴⁵. The heats of protonation of the reference olefins flatten out from propylene onwards for SAPO-34. Slight decrease on ΔH_{pr} , however, was observed for ZSM-5. The single event frequency factor of methylation and oligomerization on ZSM-5 is around 25 times bigger than that on SAPO-34.

The kinetic model based on the estimated parameters yields an excellent fit of the experimental data. Parity plots for the yields of different products are shown in Figure IV-2. The fit of experimental yield at 450°C as a function of space time is shown in Figure IV-3. The kinetic model was also able to reproduce the experimental data of Marchi and Froment², also obtained on SAPO-34, as shown in Figure IV-4.

Table IV-6. Kinetic Parameters for SAPO-34 Catalyst.

P #	P-estimate	95% confidence interval		Derived kinetic parameters	values	units
		lower	upper			
1	1.818E-01	1.555E-01	2.081E-01	$\Delta S_{Pr}^o (MeOH)$	-1.22E+02	$J mol^{-1} K^{-1}$
2	-1.055E+04	-1.092E+04	-1.017E+04	$\Delta H_{Pr}^o (MeOH)$	-8.77E+01	$KJ mol^{-1}$
3	-2.726E+00	-3.009E+00	-2.443E+00	$\Delta S_{Hyd}^o (R_1^+)$	-3.32E+01	$J mol^{-1} K^{-1}$
4	-9.009E+02	-9.104E+02	-8.914E+02	$\Delta H_{Hyd}^o (R_1^+)$	-7.49E+00	$KJ mol^{-1}$
5	6.339E+00	5.715E+00	6.963E+00	$A_c (R_1^+)$	1.05E+02	$s^{-1} bar^{-1}$
6	1.224E+02	1.128E+02	1.318E+02	$E_c (R_1^+)$	1.02E+00	$KJ mol^{-1}$
7	5.121E+00	4.850E+00	5.392E+00	$A_f (DME)$	3.09E+01	$s^{-1} bar^{-1}$
8	1.200E+02	1.143E+02	1.257E+02	$E_f (DME)$	9.98E-01	$KJ mol^{-1}$
9	1.155E+01	9.394E+00	1.372E+01	$\Delta S_{Pr}^o (DME)$	-4.18E+01	$J mol^{-1} K^{-1}$
10	-1.183E+04	-1.197E+04	-1.168E+04	$\Delta H_{Pr}^o (DME)$	-9.83E+01	$KJ mol^{-1}$
11	2.016E+00	1.766E+00	2.267E+00	$A_f (CH_4)$	1.00E+13	$s^{-1} bar^{-1}$
12	2.123E+04	2.096E+04	2.150E+04	$E_f (CH_4)$	1.77E+02	$KJ mol^{-1}$
13	5.694E+00	5.521E+00	5.867E+00	$A_{sr} (R_1^+; bs)$	1.67E+16	s^{-1}
14	2.136E+04	2.105E+04	2.167E+04	$E_{sr} (R_1^+; bs)$	1.78E+02	$KJ mol^{-1}$
15	1.374E+01	1.239E+01	1.510E+01	$A_{sr} (OM; H^+)$	1.97E+17	s^{-1}
16	1.738E+04	1.717E+04	1.758E+04	$E_{sr} (OM; H^+)$	1.45E+02	$KJ mol^{-1}$
17	5.192E+00	5.069E+00	5.315E+00	$A_{sr} (OM; DMO^+ : R_2^+)$	2.03E+05	s^{-1}
18	3.798E+03	3.777E+03	3.819E+03	$E_{sr} (OM; DMO^+ : R_2^+)$	3.16E+01	$KJ mol^{-1}$
19	4.613E+00	4.434E+00	4.793E+00	$A_{sr} (OM; DMO^+ : R_3^+)$	2.29E+03	s^{-1}
20	1.013E+03	9.575E+02	1.069E+03	$E_{sr} (OM; DMO^+ : R_3^+)$	8.43E+00	$KJ mol^{-1}$
21	-3.560E+00	-3.759E+00	-3.361E+00	$A_{Pr} (O_2)$	7.64E+03	$s^{-1} bar^{-1}$
22	1.024E+04	1.014E+04	1.033E+04	$E_{Pr} (O_2)$	8.51E+01	$KJ mol^{-1}$
23	-1.292E+01	-1.371E+01	-1.213E+01	$\Delta \tilde{S}_{Pr}$	-1.08E+02	$J mol^{-1} K^{-1}$
24	-6.741E+03	-6.777E+03	-6.705E+03	$\Delta H_{Pr}^o (O_2)$	-5.61E+01	$KJ mol^{-1}$
25	-1.200E+04	-1.205E+04	-1.196E+04	$\Delta H_{Pr}^o (O_3)$	-9.98E+01	$KJ mol^{-1}$
26	-1.200E+04	-1.215E+04	-1.186E+04	$\Delta H_{Pr}^o (O_{4r})$	-9.98E+01	$KJ mol^{-1}$
27	-1.200E+04	-1.205E+04	-1.196E+04	$\Delta H_{Pr}^o (O_{5r})$	-9.98E+01	$KJ mol^{-1}$
28	1.520E+01	1.459E+01	1.581E+01	\tilde{A}	6.27E+05	$s^{-1} bar^{-1}$
29	1.647E-02	1.041E-02	2.254E-02	α	1.65E-02	dimensionless
30	7.067E+05	6.996E+05	7.137E+05	E^o	9.68E+01	$KJ mol^{-1}$

Table IV-7. Kinetic Parameters for ZSM-5 Catalyst Estimated by Park.⁴⁵

\mathcal{P}_i	lower limit ^a	estimate	upper limit ^a	t value	parameter ^b	values	unit
\mathcal{P}_1	-4.6433×10^0	-3.9404×10^0	-3.2374×10^0	11.21	$\Delta S_{Pr}^\circ(\text{MeOH})$	-1.3391×10^2	$\text{J}\cdot\text{mol}^{-1}\cdot\text{K}^{-1}$
\mathcal{P}_2	-8.5333×10^3	-8.3354×10^3	-8.1375×10^3	84.25	$\Delta H_{Pr}^\circ(\text{MeOH})$	-6.9305×10^1	$\text{kJ}\cdot\text{mol}^{-1}$
\mathcal{P}_3	-4.9843×10^0	-4.2179×10^0	-3.4514×10^0	11.01	$\Delta S_{Hyd}^\circ(\text{R}_1^+)$	-8.5028×10^1	$\text{J}\cdot\text{mol}^{-1}\cdot\text{K}^{-1}$
\mathcal{P}_4	-4.1758×10^0	-4.1168×10^3	-4.0578×10^3	139.50	$\Delta H_{Hyd}^\circ(\text{R}_1^+)$	-3.4229×10^1	$\text{kJ}\cdot\text{mol}^{-1}$
\mathcal{P}_5	3.1244×10^0	3.8080×10^0	4.4916×10^0	11.14	$A_C(\text{R}_1^+)$	9.3907×10^5	$\text{s}^{-1}\cdot\text{bar}^{-1}$
\mathcal{P}_6	5.8509×10^3	5.9878×10^3	6.1247×10^3	87.47	$E_C(\text{R}_1^+)$	4.9786×10^1	$\text{kJ}\cdot\text{mol}^{-1}$
\mathcal{P}_7	1.8134×10^1	1.8561×10^1	1.8987×10^1	87.05	$A_F'(\text{DME})$	1.2343×10^9	$\text{s}^{-1}\cdot\text{bar}^{-1}$
\mathcal{P}_8	7.7518×10^0	8.0004×10^2	8.2492×10^2	64.34	$E_F(\text{DME})$	6.6520×10^0	$\text{kJ}\cdot\text{mol}^{-1}$
\mathcal{P}_9	-3.8957×10^0	-3.3374×10^0	-2.7792×10^0	11.96	$\Delta S_{Pr}^\circ(\text{DME})$	-8.6317×10^1	$\text{J}\cdot\text{mol}^{-1}\cdot\text{K}^{-1}$
\mathcal{P}_{10}	-4.9289×10^3	-4.8263×10^3	-4.7237×10^3	94.08	$\Delta H_{Pr}^\circ(\text{DME})$	-4.0128×10^1	$\text{kJ}\cdot\text{mol}^{-1}$
\mathcal{P}_{11}	2.8721×10^{-1}	7.1901×10^{-1}	1.1508×10^0	3.33	$A_F'(\text{CH}_4)$	1.3978×10^{10}	$\text{s}^{-1}\cdot\text{bar}^{-1}$
\mathcal{P}_{12}	1.4284×10^4	1.4687×10^4	1.5090×10^4	72.89	$E_F(\text{CH}_4)$	1.2212×10^2	$\text{kJ}\cdot\text{mol}^{-1}$
\mathcal{P}_{13}	8.3370×10^0	9.0938×10^0	9.8569×10^0	23.83	$A_{sr}'(\text{R}_1^+;\text{bs})$	7.1483×10^{17}	s^{-1}
\mathcal{P}_{14}	1.6298×10^4	1.6574×10^4	1.6850×10^4	120.20	$E_{sr}(\text{R}_1^+;\text{bs})$	1.3781×10^2	$\text{kJ}\cdot\text{mol}^{-1}$
\mathcal{P}_{15}	8.2304×10^0	9.0800×10^0	9.9296×10^0	21.38	$A_{sr}'(\text{OM};\text{H}^+)$	2.3491×10^{14}	s^{-1}
\mathcal{P}_{16}	1.0904×10^4	1.1088×10^4	1.1273×10^4	120.31	$E_{sr}(\text{OM};\text{H}^+)$	9.2193×10^1	$\text{kJ}\cdot\text{mol}^{-1}$
\mathcal{P}_{17}	7.9092×10^0	8.3949×10^0	8.8806×10^0	34.57	$A_{sr}'(\text{OM};\text{DMO}^+;\text{R}_2^+)$	7.7433×10^8	s^{-1}
\mathcal{P}_{18}	2.8230×10^3	2.9090×10^3	2.9950×10^3	67.64	$E_{sr}(\text{OM};\text{DMO}^+;\text{R}_2^+)$	2.4187×10^1	$\text{kJ}\cdot\text{mol}^{-1}$
\mathcal{P}_{19}	7.2316×10^0	7.7135×10^0	8.1955×10^0	32.01	$A_{sr}'(\text{OM};\text{DMO}^+;\text{R}_3^+)$	9.7050×10^{11}	s^{-1}
\mathcal{P}_{20}	8.1202×10^3	8.2635×10^3	8.4068×10^3	115.33	$E_{sr}(\text{OM};\text{DMO}^+;\text{R}_3^+)$	6.8707×10^1	$\text{kJ}\cdot\text{mol}^{-1}$
\mathcal{P}_{21}	-8.7386×10^0	-8.1645×10^0	-7.5950×10^0	28.45	$A_{Pr}'(\text{O}_2)$	8.5785×10^5	$\text{s}^{-1}\cdot\text{bar}^{-1}$
\mathcal{P}_{22}	1.3916×10^4	1.4129×10^4	1.4342×10^4	132.87	$E_{Pr}(\text{O}_2)$	1.1748×10^2	$\text{kJ}\cdot\text{mol}^{-1}$
\mathcal{P}_{23}	-8.9252×10^0	-8.4304×10^0	-7.9357×10^0	34.08	$\Delta \tilde{S}_{Pr}$	-7.0095×10^1	$\text{J}\cdot\text{mol}^{-1}\cdot\text{K}^{-1}$
\mathcal{P}_{24}	-2.3453×10^3	-2.3008×10^3	-2.2563×10^3	103.40	$\Delta H_{Pr}^\circ(\text{O}_2)$	-1.9130×10^1	$\text{kJ}\cdot\text{mol}^{-1}$
\mathcal{P}_{25}	-9.4422×10^3	-9.3039×10^3	-9.1656×10^3	134.55	$\Delta H_{Pr}^\circ(\text{O}_3)$	-7.7358×10^1	$\text{kJ}\cdot\text{mol}^{-1}$
\mathcal{P}_{26}	-9.9335×10^3	-9.9335×10^3	-9.6959×10^3	81.59	$\Delta H_{Pr}^\circ(\text{O}_{4r})$	-8.0616×10^1	$\text{kJ}\cdot\text{mol}^{-1}$
\mathcal{P}_{27}	-1.0488×10^4	-1.0488×10^4	-1.0371×10^4	176.73	$\Delta H_{Pr}^\circ(\text{O}_{5r})$	-8.6230×10^1	$\text{kJ}\cdot\text{mol}^{-1}$
\mathcal{P}_{28}	-1.4485×10^4	-1.4235×10^4	-1.3985×10^4	113.98	$\Delta H_{Pr}^\circ(\text{O}_{6r})$	-1.1836×10^2	$\text{kJ}\cdot\text{mol}^{-1}$
\mathcal{P}_{29}	-1.4767×10^4	-1.4585×10^4	-1.4404×10^4	160.61	$\Delta H_{Pr}^\circ(\text{O}_{7r})$	-1.2127×10^2	$\text{kJ}\cdot\text{mol}^{-1}$
\mathcal{P}_{30}	-1.4962×10^4	-1.4626×10^4	-1.4290×10^4	87.06	$\Delta H_{Pr}^\circ(\text{O}_{8r})$	-1.2161×10^2	$\text{kJ}\cdot\text{mol}^{-1}$
\mathcal{P}_{31}	1.4451×10^1	1.5390×10^1	1.6328×10^1	32.80	\tilde{A}'	1.6111×10^7	$\text{s}^{-1}\cdot\text{bar}^{-1}$
\mathcal{P}_{32}	3.2348×10^{-2}	3.4304×10^{-2}	3.6259×10^{-2}	35.09	α	3.4304×10^{-2}	dimensionless
\mathcal{P}_{33}	3.3719×10^5	3.4183×10^5	3.4647×10^5	147.40	E°	9.7496×10^1	$\text{kJ}\cdot\text{mol}^{-1}$

^a Approximate 95% confidence limit. ^b Original parameters included in the reparametrized form.

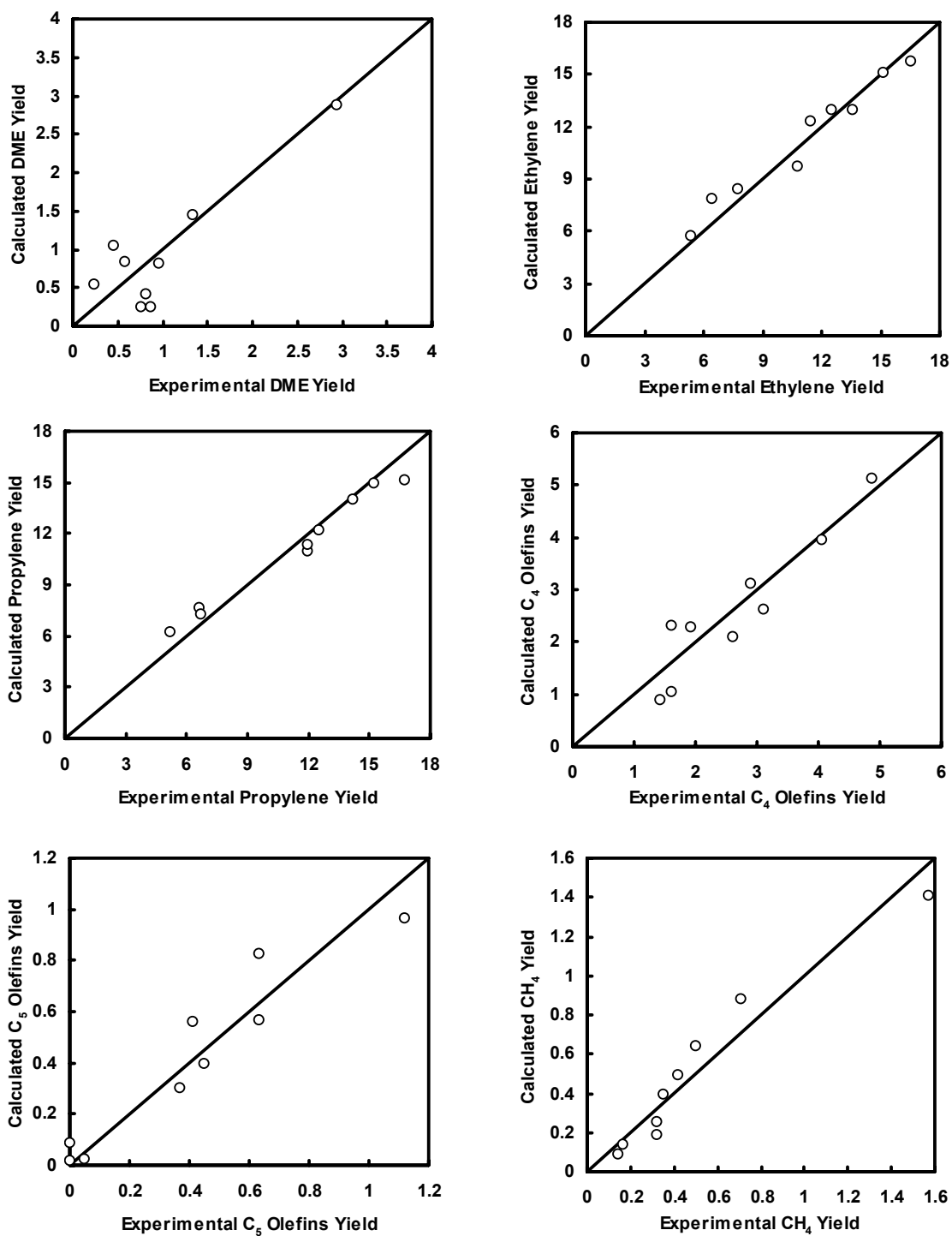


Figure IV-2. Experimental and calculated yields for various MTO products on SAPO-34. T=400-450°C, P=1.04 bar, t=0.8~3 g-cat hr/mol, feed (MeOH + H₂O).

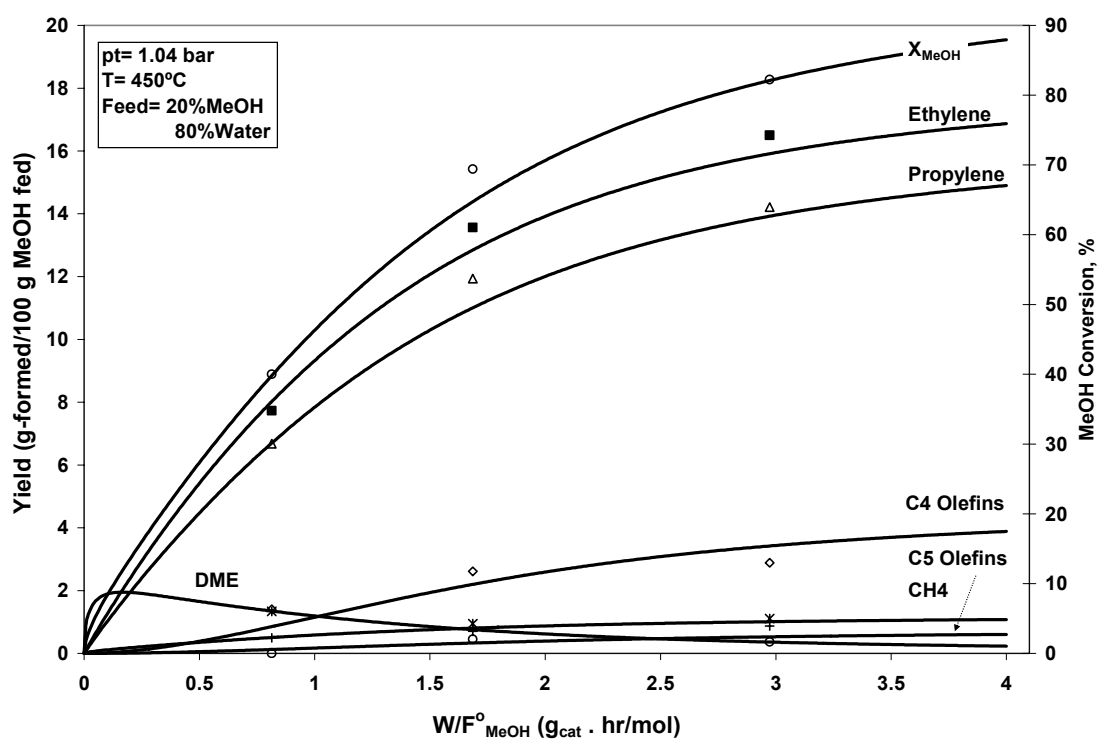


Figure IV-3. Calculated yields on SAPO-34 of various MTO products compared with experimental data of Table IV-5 as a function of space time. Lines: simulation and symbols: experimental.

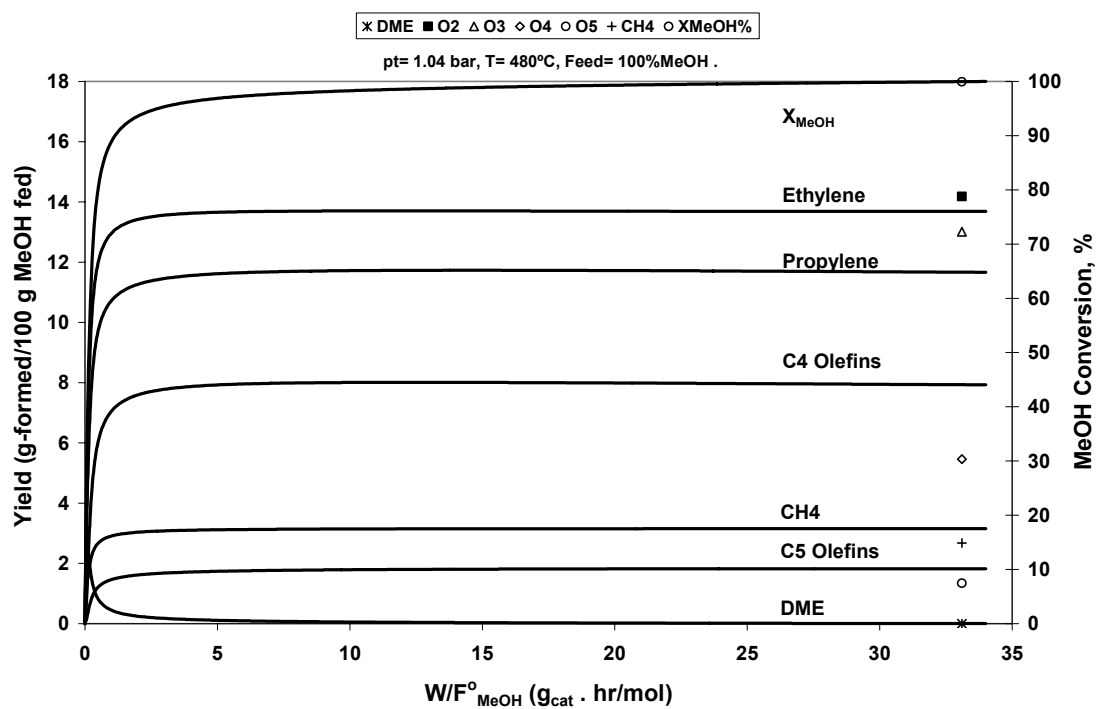


Figure IV-4. Model verification by comparison with experimental data of Marchi and Froment² obtained under entirely different space time. Lines: model and symbols: experimental.

IV.2.4.6 Single Event Rate Coefficients for the Various Elementary Steps

The single event frequency factor for a given type of elementary step is independent of the structure. Because of the energetics, that does not necessarily mean that the single event rate coefficient is independent of the structure too.

Figure IV-5 shows the effect of chain length on the single event rate coefficients (these can be calculated from the parameter values of Table IV-6) for methylation of linear olefins and their oligomerization by means of ethyl- R^+ at 440 °C. The carbenium ions that are produced are all linear and secondary. The single event rate coefficient significantly increases with chain length. Since, by virtue of the single event concept, there is only one frequency factor in this model, this effect solely results from the enthalpy contribution to the single event rate coefficient, \tilde{k} .

Figure IV-6 illustrates the effect of branching, expressed in terms of $n_{C\alpha-C}$ (number of carbon atom in α position with respect to the carbon carrying the positive charge) in the produced R^+ and of the nature of R^+ on the \tilde{k} for methylation. A comparison of curve (a) and curve (b), corresponding to R^+ which are respectively all tertiary and all secondary, reveals that the effect of the nature of R^+ is far more pronounced than that of branching.

Figure IV-7 deals with oligomerization by means of the ethyl carbenium ions. All the produced carbenium ions are secondary. Curve (a) shows how \tilde{k} increases with

chain length and/or $n_{C\alpha-C}$. From curve (b), corresponding to C₆ olefins, branched or straight, it follows that the effect of branching is very weak.

Figure IV-8 shows the evolution of the single event rate coefficient, of the β -scission of various octyl carbenium ions, with temperature. The \tilde{k} values are seen to increase rapidly from 460 °C onwards. A similar behavior is observed for the evolution with temperature of \tilde{k} for an oligomerization, curve (d), which is the reverse of the β -scission in curve (b).

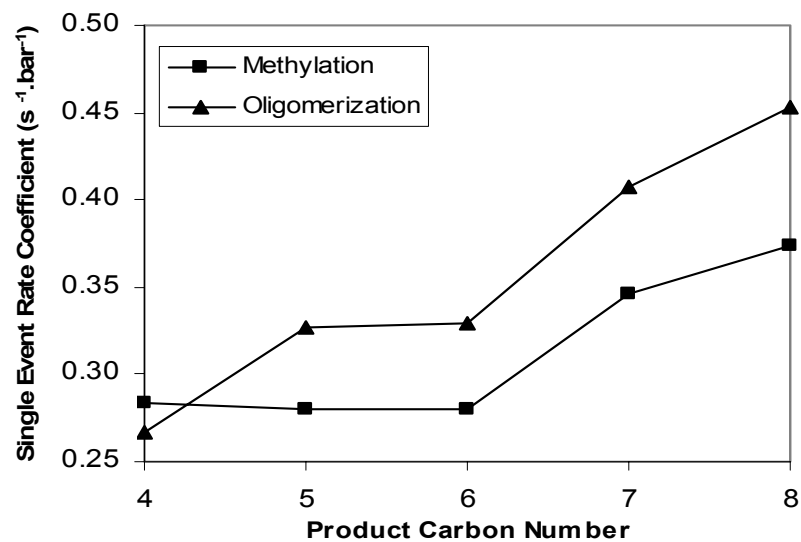


Figure IV-5. Single event rate coefficients for the methylation and oligomerization of linear olefins as a function of the C-number of the product.

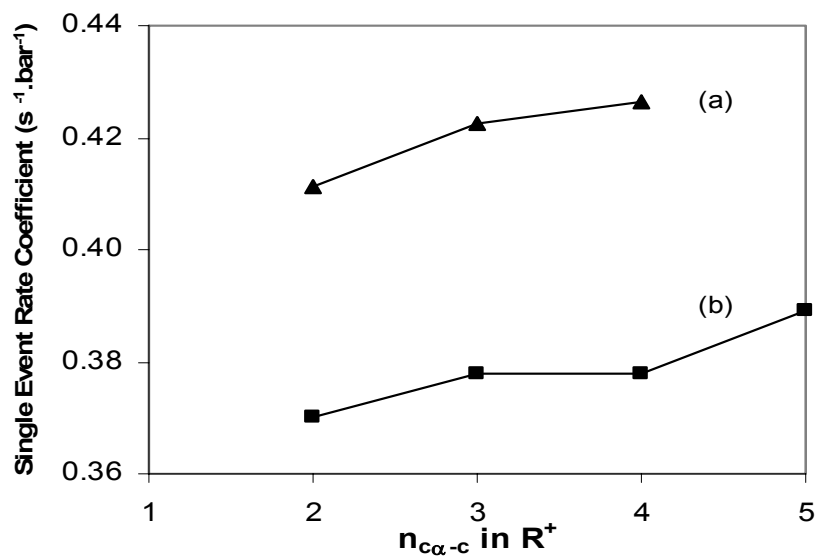


Figure IV-6. Single event methylation rate coefficients. Effect of reacting olefin structure. Curve (a): all C7-olefins. Produced R^+ : 2,3-diMe-2-hexyl; 2,5-diMe-3-hexyl; 2,3,4-triMe-3-pentyl. Curve (b): all C7-Olefins. Produced R^+ : 2-Me-3-heptyl; 4-Me-3-heptyl; 3,3-diMe-4-hexyl; 2,2,4-triMe-3-pentyl.

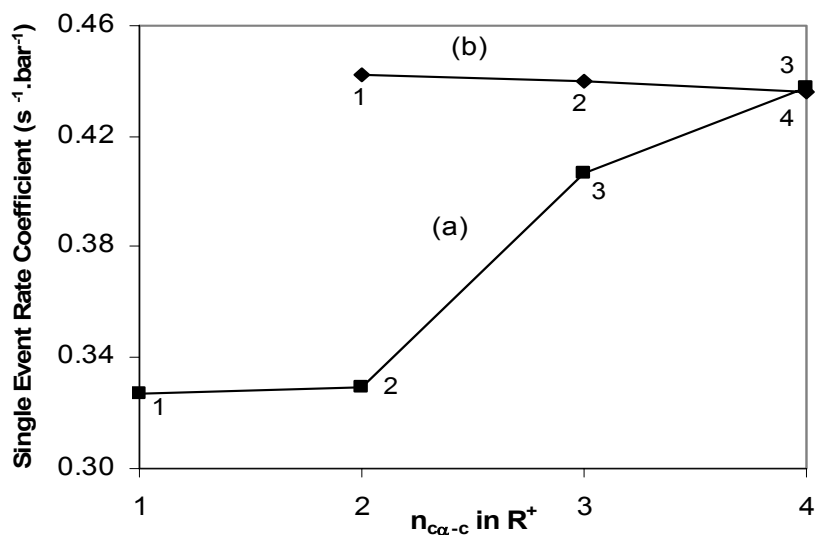


Figure IV-7. Single event oligomerization rate coefficients. Carbenium ion: ethyl. Effect of olefin structure. Curve (a): 1, propylene; 2, 1-butene; 3, 2-Me-2-butene; 4, 2-Me-3-pentene. Curve (b): 1, 2-Me-4-pentene; 2, 2-hexene; 3, 2-Me-3-pentene.

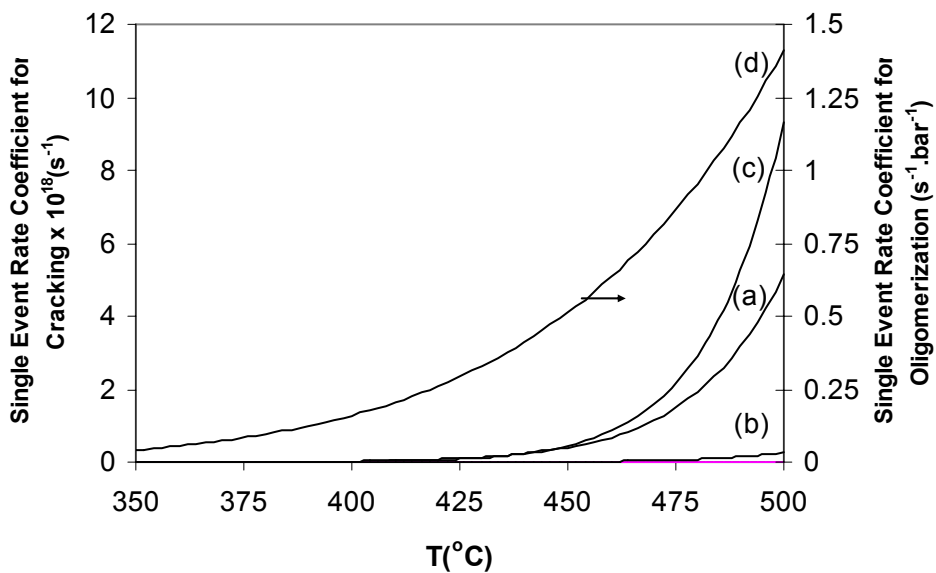


Figure IV-8. Single event rate coefficients for elementary cracking steps. Curve (a): 2,2-diMe-4-hexyl R^+ into 1-butene and 2-Me-2-propyl R^+ . Curve (b): 2,2,4-triMe-4-pentyl R^+ into isobutylene and 2-Me-2-propyl R^+ . Curve (c): 3,4-diMe-5-hexyl R^+ into 2-butene and 2-butyl R^+ . Curve (d): Single event rate coefficient for the oligomerization step which is the reverse of the cracking step of curve (b).

CHAPTER V

CATALYST DEACTIVATION

V.1 Introduction

As discussed in Chapter III, SAPO-34 suffers from relatively rapid deactivation during methanol conversion. The rapid deactivation was attributed to both coverage of the acid sites and blockage of pore structure.²¹ Figure V-1 shows a typical deactivation behavior of a SAPO-34 catalyst, as measured by Marchi and Froment².

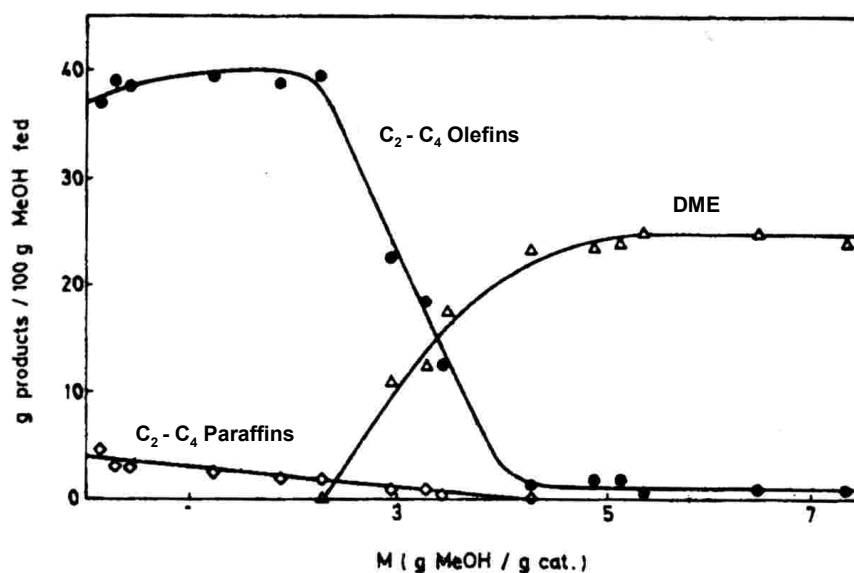


Figure V-1. Methanol conversion into hydrocarbons on SAPO-34.² T=480°C; feed 30/70 wt% methanol-water. $M = \sum F_{\text{MeOH}} / W$.

M is defined as the total weight of methanol fed to the reactor per weight of catalyst. The figure shows that the yield of C₂-C₄ olefins does not decline immediately and DME yield rises only from a certain M-value onwards. This can be explained as follows: because the MTO reactions are very fast, a thin section of the catalyst bed is only utilized. As the catalyst deactivates, the section broadens. Only when it spreads through the entire bed deactivation is observed.

Another important observation about Figure V-1 is that at longer process time, the conversion into olefins drops to zero while the DME yield, after increasing to 30%, becomes constant. That illustrates that the conversion of methanol into DME does not deactivate to the same level as the other reactions. The direct implication of these observations is that a different deactivation functions for the methanol conversion and the yields of olefins has to be defined. That for the olefins is exponential and drops to zero. That for the methanol conversion to DME is a hyperbolic function that does not drop to zero.

In this chapter, the deactivation of SAPO-34 is modeled based upon the elementary steps and the single event concept. The model was then utilized to introduce the deactivation of the catalyst into the kinetic equations for the purpose of simulation of reactor behavior.

V.2 Modeling of Catalyst Deactivation

In the present work the deactivation is ascribed to higher oligomerization products (C₆, C₇, C₈) which because of the cavity structure of SAPO-34, can not leave the catalyst

as shown in Figure V-2. They permanently cover the acid active sites and/or block pores, thus causing deactivation of the catalyst and a decline of the methanol conversion and of the yields of the various products.

The C_{6+} products can not be observed at the exit of the reactor, but their rate of formation and concentration inside the cages can be calculated as follow:

- Because the single event frequency factor for methylation and oligomerization is independent of the structure and the chain length, the frequency factor calculated for the steps involved in the formation of C_4 and C_5 , can be used to calculate the rate of formation of the C_{6+} components.

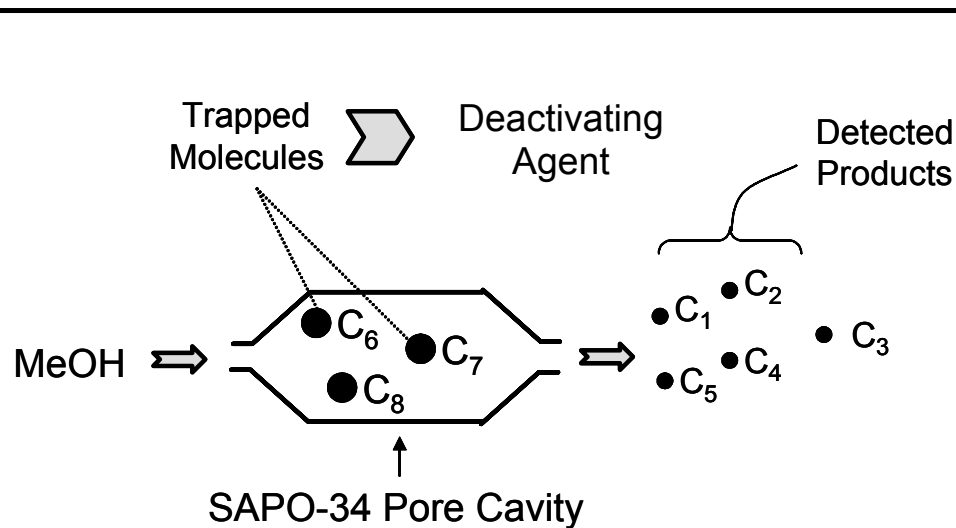


Figure V-2. Schematic representation of the trapping of C_{6+} components inside the SAPO-34 cavities.

- The activation energies of C_{6+} formation and cracking can be calculated from the Evans-Polanyi relationship given the heat of reaction of the elementary step. The latter is obtained from the heats of formation of the reactant and the activated complex and these are calculated by an ab initio quantum chemical approach.
- The heats of protonation of reference olefins, $\Delta H_{pr}(O_{ir})$, for carbon numbers up to C_5 are estimated from experiments, as discussed before. However, heats of protonation for C_{6+} olefins are not known for SAPO-34. To calculate them, it is assumed that the heats of protonation for the reference olefins of different carbon number will have the same trend for SAPO-34 as for ZSM-5. This assumption is verified by comparing the values of $\Delta H_{pr}(O_{ir})$ obtained for SAPO-34 up to C_5 olefins with those of ZSM-5 estimated by Park⁴⁵, as shown in Figure V-3. The heats of protonation of the C_{6+} reference olefins are, then, calculated by extrapolation.

The rate of formation of C_{6+} components can now be formulated at each point along the plug flow reactor. The concentration of the C_{6+} components evolves with time according to:

$$\frac{dC_{C_{6+}}}{dt} = \Phi_c \cdot r_c \quad (\text{V-1})$$

with initial condition,

$$\text{at } t = 0 \quad C_{C_{6+}} = 0 \quad \text{for all } \frac{W}{F_{MeOH}^0}$$

where
$$r_c = \sum_6^8 M_i \mathfrak{R}_i$$

M_i \equiv Molecular weight of component i .

\mathfrak{R}_i \equiv Net rate of formation of component i in (moles/(gcat . hr)).

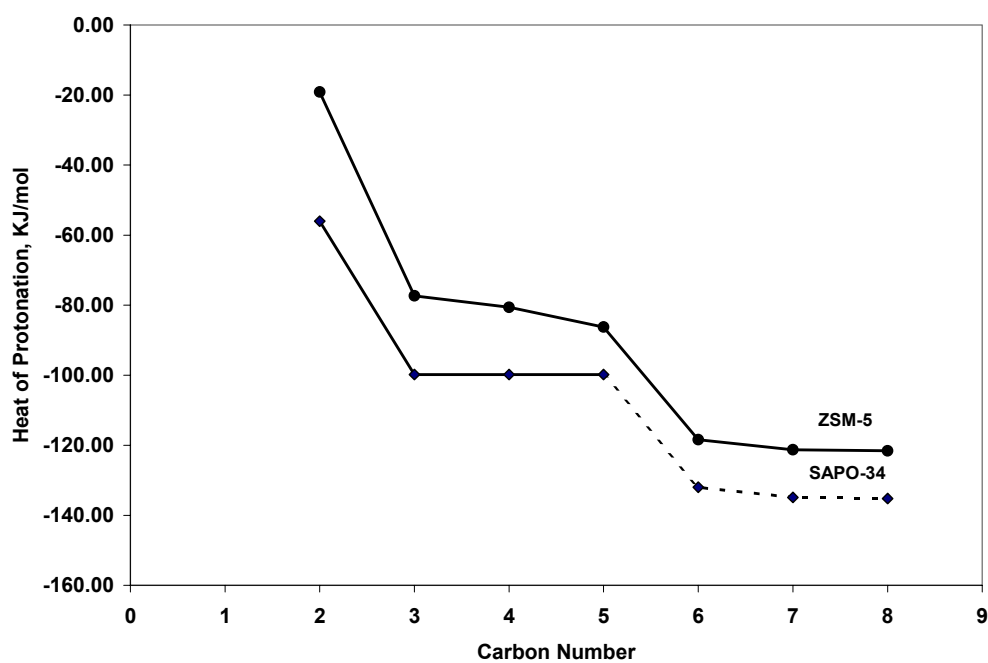


Figure V-3. Extrapolation of heats of protonations of C_{6+} olefins for SAPO-34 based upon corresponding values for ZSM-5. Solid line: estimated from experiments, and broken line: extrapolated.

Φ_c is the deactivation function for C_{6+} olefins formation. It is expressed in terms of the concentration of the C_{6+} olefins using the well proven empirical correlation proposed by Froment and Bischoff⁵⁸ as:

$$\Phi_c = \exp(-\alpha C_{C_{6+}}) \quad (V-2)$$

Equation (V-1) has to be integrated simultaneously with the set of continuity equations describing the behavior of methanol and the various reaction products in the reactor:

$$\frac{d\hat{y}_i}{d(W/F_{MeOH}^o)} = \frac{100 \cdot M_i}{M_{MeOH}} \cdot \Phi_i \cdot \mathfrak{R}_i, \quad i = 1, 2, \dots, m \quad (V-3)$$

where Φ_i are the deactivation functions for the main reactions expressed as follows:

$$\Phi_i = \exp(-\alpha C_{C_{6+}}) \quad \text{for olefins formation} \quad (V-4)$$

$$\Phi_i = \frac{1}{(1 + \beta C_{C_{6+}})} \quad \text{for methanol conversion} \quad (V-5)$$

Equations (V-1) - (V-5) contain two unknown parameters, α and β that need to be estimated. The experimental data of Marchi and Froment² have been utilized for this purpose. The parameters are estimated by minimizing the difference between the

experimental and the calculated methanol conversions and C₂-C₄ yields. Calculated values are obtained by solving the system of partial differential equations above.

Equations (V-3) were integrated along the length of the reactor using Gear's method. Once the yields for the various products are calculated at time=0, equation (V-1) is integrated for a first time interval using the Runge-Kutta method. Because Gear's method uses a variable step size, interpolation between known C₆₊ concentration values are needed to calculate the values at any space time. At this point product yields are calculated based on the new C₆₊ concentration profiles. This mathematical loop is continued until the end of the run.

V.3 Results and Discussion

An accurate fit of the experimental data of Marchi and Froment required deactivation constants to depend upon the partial pressure of methanol in the feed, i.e. on the water dilution. For a methanol partial pressure in the feed of 1,04 bar (no water) α amounted to 60 and β to 7.5. For a methanol partial pressure of 0.5 the corresponding values were 80 and 46, reflecting slower deactivation in the presence of water. The rate coefficients are those calculated from the parameters given in Table IV-6.

Figure V-4 shows the comparison of methanol conversion and C₂-C₄ olefins yield determined by the model with the experimental data of Marchi and Froment performed at 480°C, 1.04 bar total pressure and partial pressures of methanol of 1.04 and 0.5 bar. The data is plotted versus the total amount of methanol fed per g catalyst which is proportional to the run length or process time.

The matching between the model and the experimental data is very good, except for the C₂-C₄ olefins yield for long run lengths in which a slight over-prediction is observed. No experimental data is given for the DME yield.

By studying the Figure, the following observations can be summarized:

- MeOH conversion does not drop instantaneously but instead it remains constant for some time before deactivation breakthrough. This does not mean that the catalyst is not deactivating during that period, however.
- The breakthrough point depends upon the amount of catalyst and the water content of the feed. The larger the water content in the feed, the longer the conversion stays unaffected before deactivation breakthrough.
- The total conversion of methanol drops to 70% for pure methanol feed. That could correspond to equilibrium with DME, which is not reached for short process times because the DME is continuously converted into olefins, without strong effect deactivation yet.

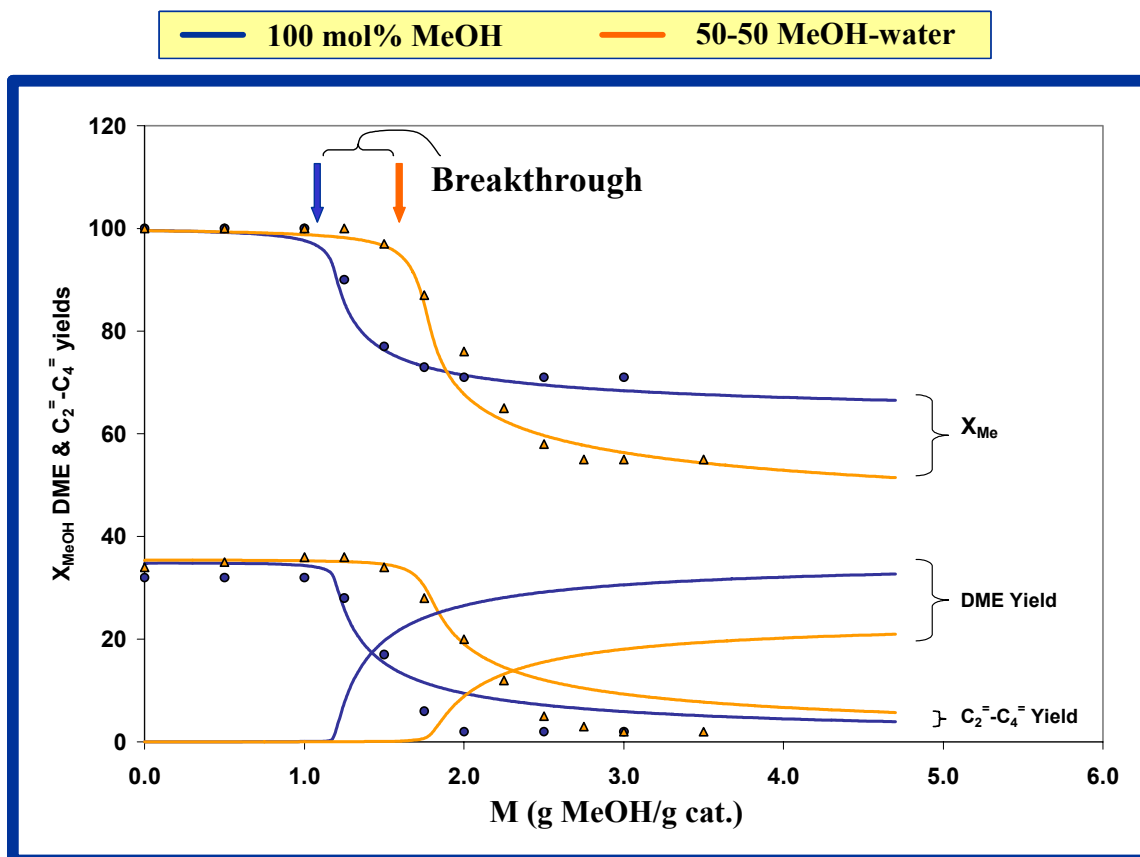


Figure V-4. Fitting of the experimental data of Marchi and Froment for isothermal fixed bed reactor at 480°C, 1.04 bar total pressure, 32.0 (W/F_{MeOH}⁰) and at two methanol partial pressures. Points: experimental data, and lines: simulated.

Figure V-5 and Figure V-6 show the evolution of the methanol conversion in the reactor at different M or process times for 100 and 50 mol% methanol feed compositions respectively. The figures further explain the behavior of the MeOH conversion inside the reactor in the presence of deactivation. The deactivation is not observed at the exit of the reactor until the breakthrough point is reached.

Ethylene and propylene yield profiles are shown in Figure V-7 to Figure V-10. Initial deactivation of the catalyst was seen to increase the formation of ethylene. This has been attributed to the enhancement of the shape-selectivity effects of the catalyst by the deposition of the C_{6+} components in the cavities of the catalyst.⁶²

On the other hand, Figure V-11 and Figure V-12 show that the concentration of the C_{6+} olefins, which are trapped inside the SAPO-34 cavities, reaches a maximum near the inlet of the reactor. This behavior can be explained by rapid production with simultaneous decomposition by beta scission. The cracking of the C_{6+} olefins (into smaller olefins) is fast for small process time, but as time increases the cracking slows down due to deactivation.

The figures also show that it is possible to decrease the formation of C_{6+} component and thus slow down the deactivation of the catalyst by increasing the partial pressure of water in the feed. This effect of water was indeed observed for SAPO-34² and shown to be characteristic of water only. When the partial pressure of methanol in the feed was reduced by using nitrogen instead of water, no reduction of deactivation was observed.

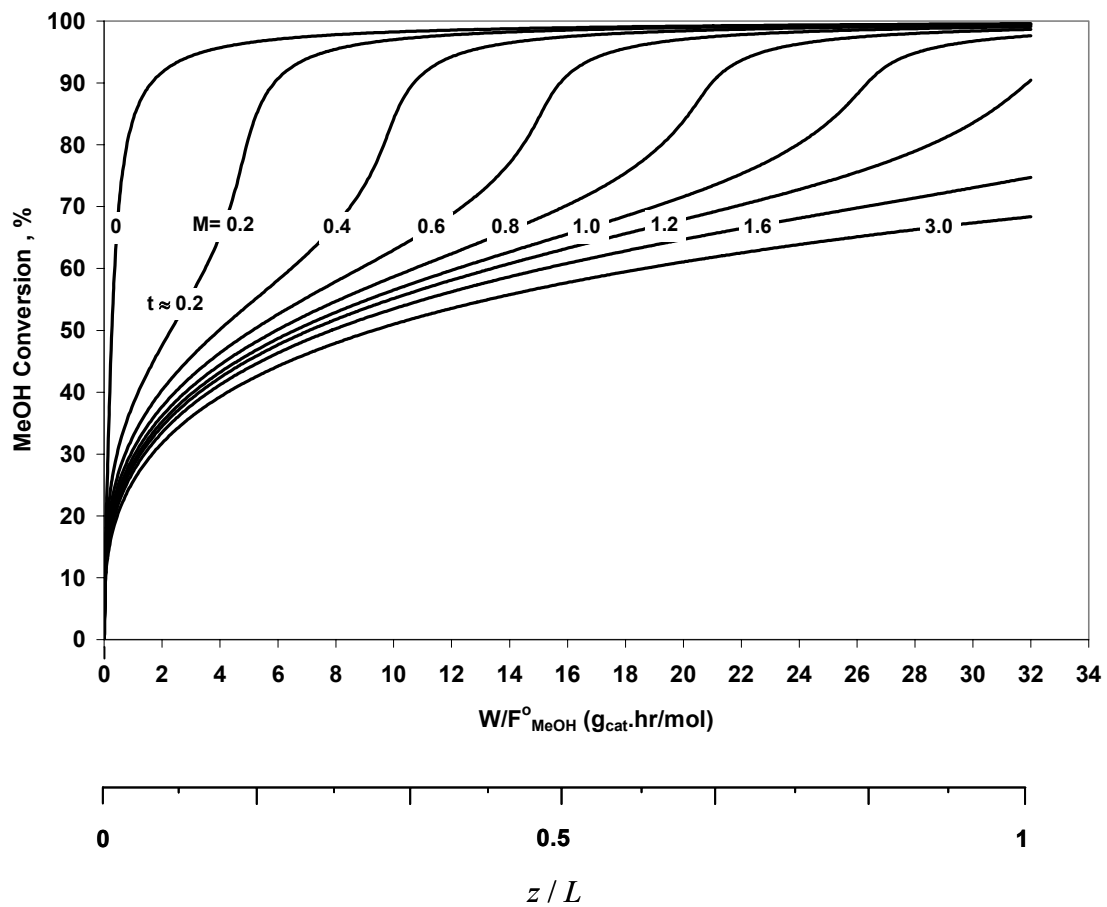


Figure V-5. Methanol conversion profiles at different process times for isothermal fixed bed reactor at 480°C, 1.04 bar total pressure and with pure methanol feed.

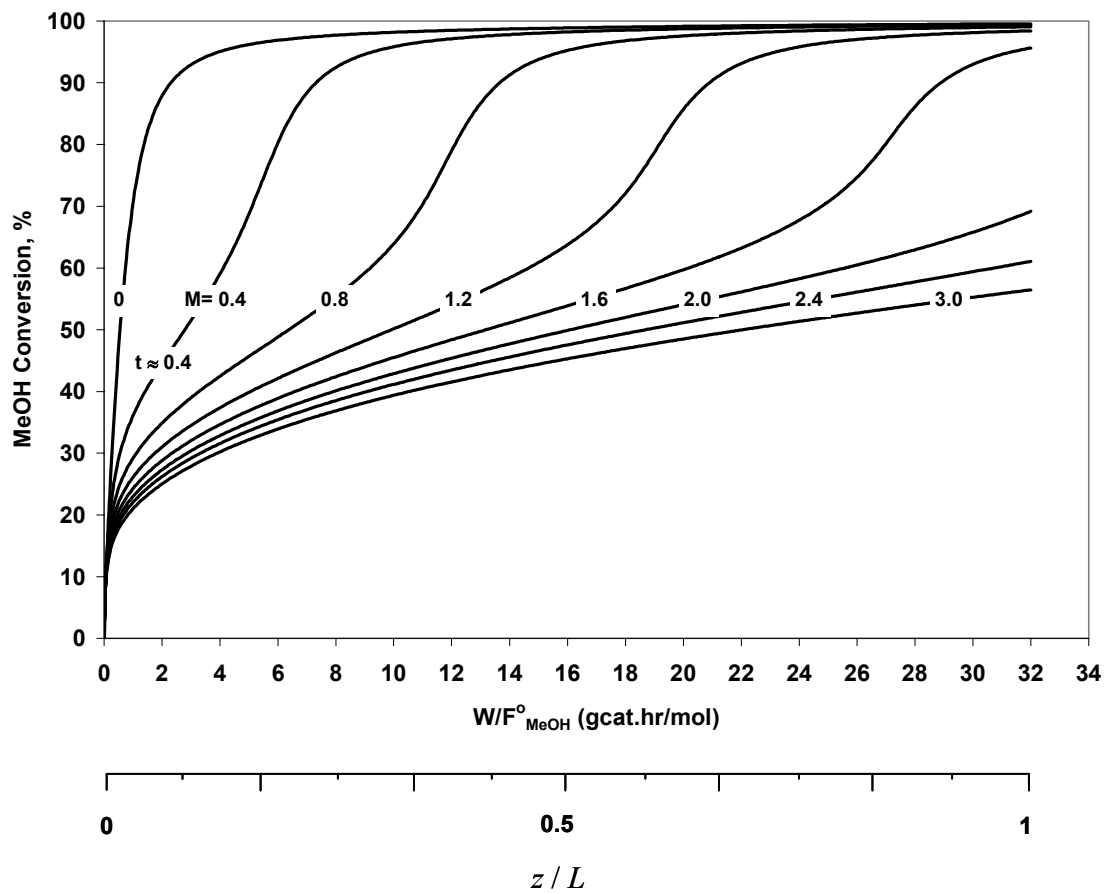


Figure V-6. Methanol conversion profiles at different process times for isothermal fixed bed reactor at 480°C, 1.04 bar total pressure and 0.5 bar methanol partial pressure.

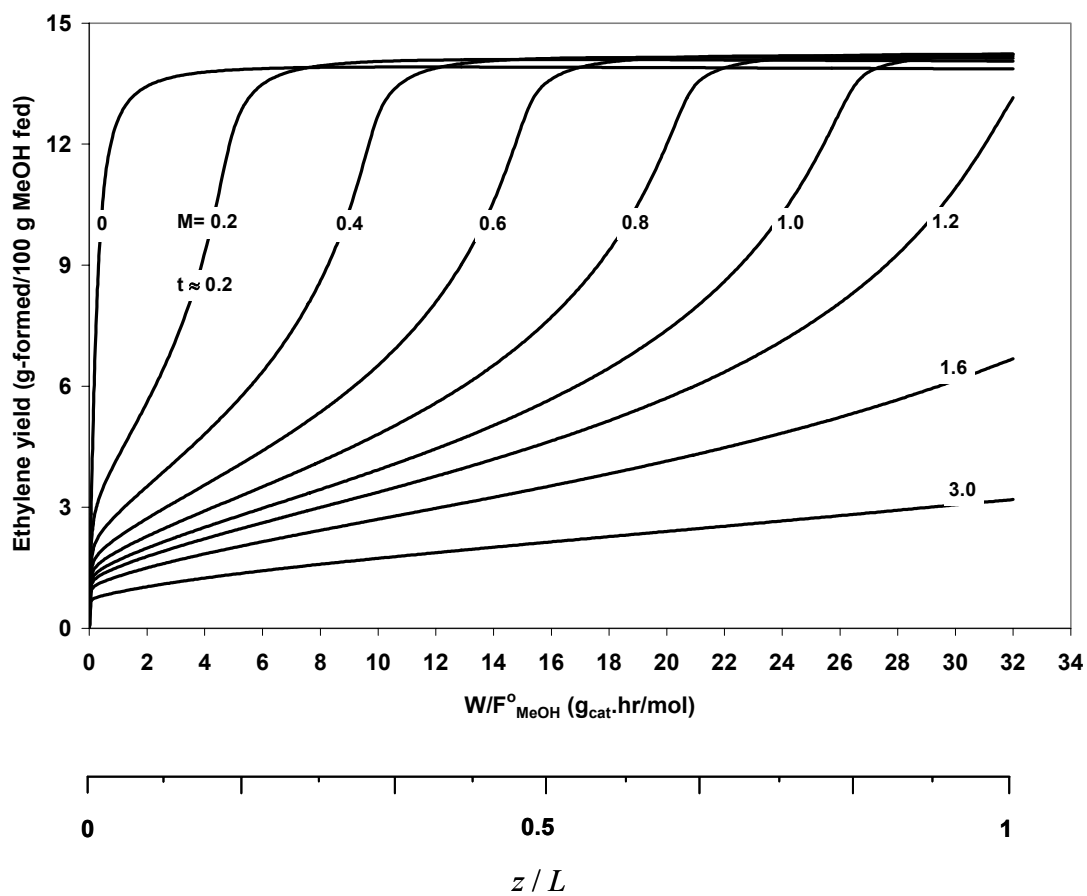


Figure V-7. Ethylene yield profiles at different process times for isothermal fixed bed reactor at 480°C, 1.04 bar total pressure and with pure methanol feed.

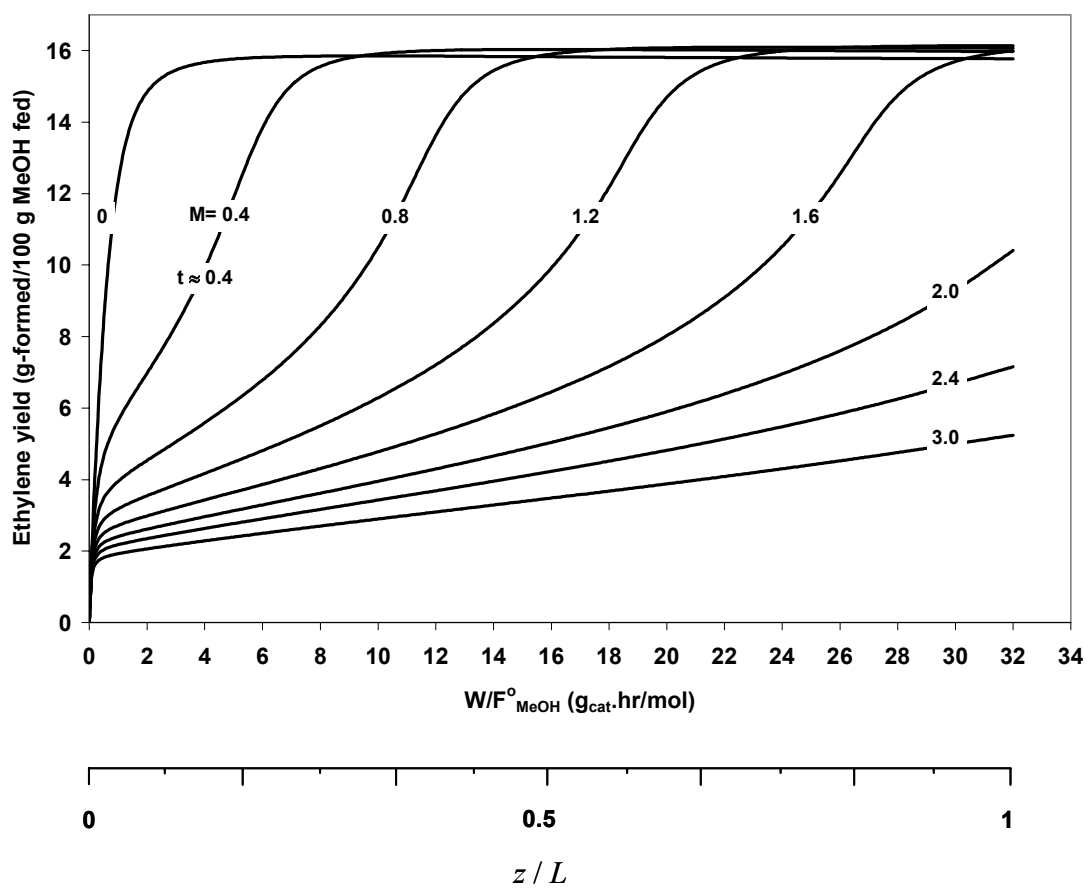


Figure V-8. Ethylene yield profiles at different process times for isothermal fixed bed reactor at 480°C, 1.04 bar total pressure and 0.5 bar methanol partial pressure.

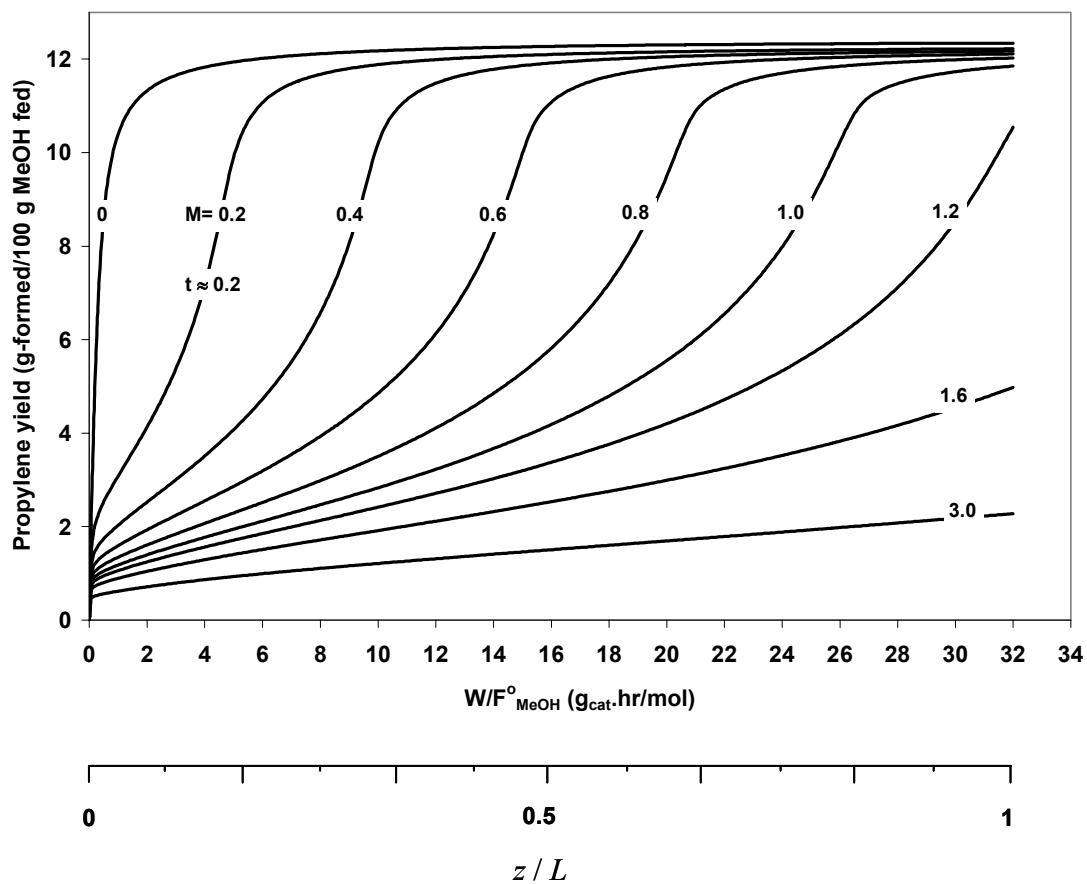


Figure V-9. Propylene yield profiles at different process times for isothermal fixed bed reactor at 480°C, 1.04 bar total pressure and with pure methanol feed.

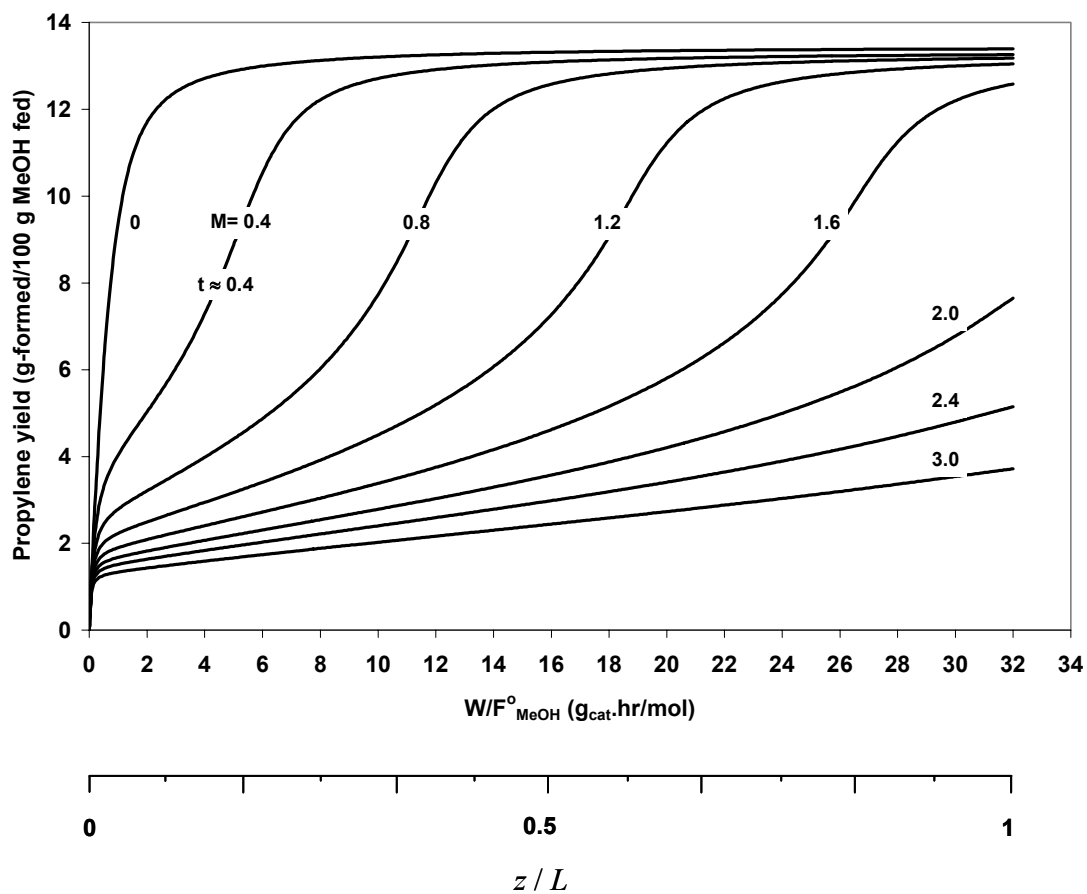


Figure V-10. Propylene yield profiles at different process times for isothermal fixed bed reactor at 480°C, 1.04 bar total pressure and 0.5 bar methanol partial pressure.

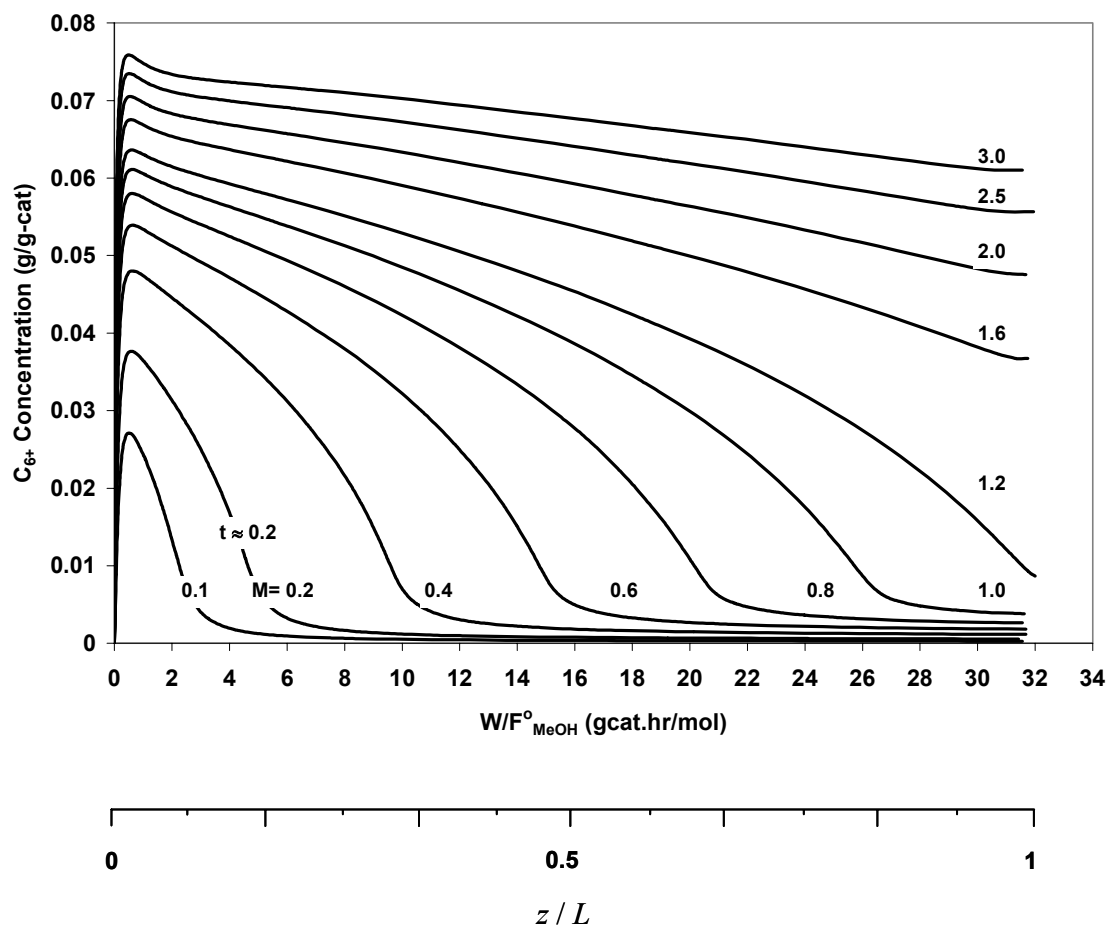


Figure V-11. Concentration profiles of C6+ olefins at different process times for isothermal fixed bed reactor at 480°C, 1.04 bar total pressure and with pure methanol feed.

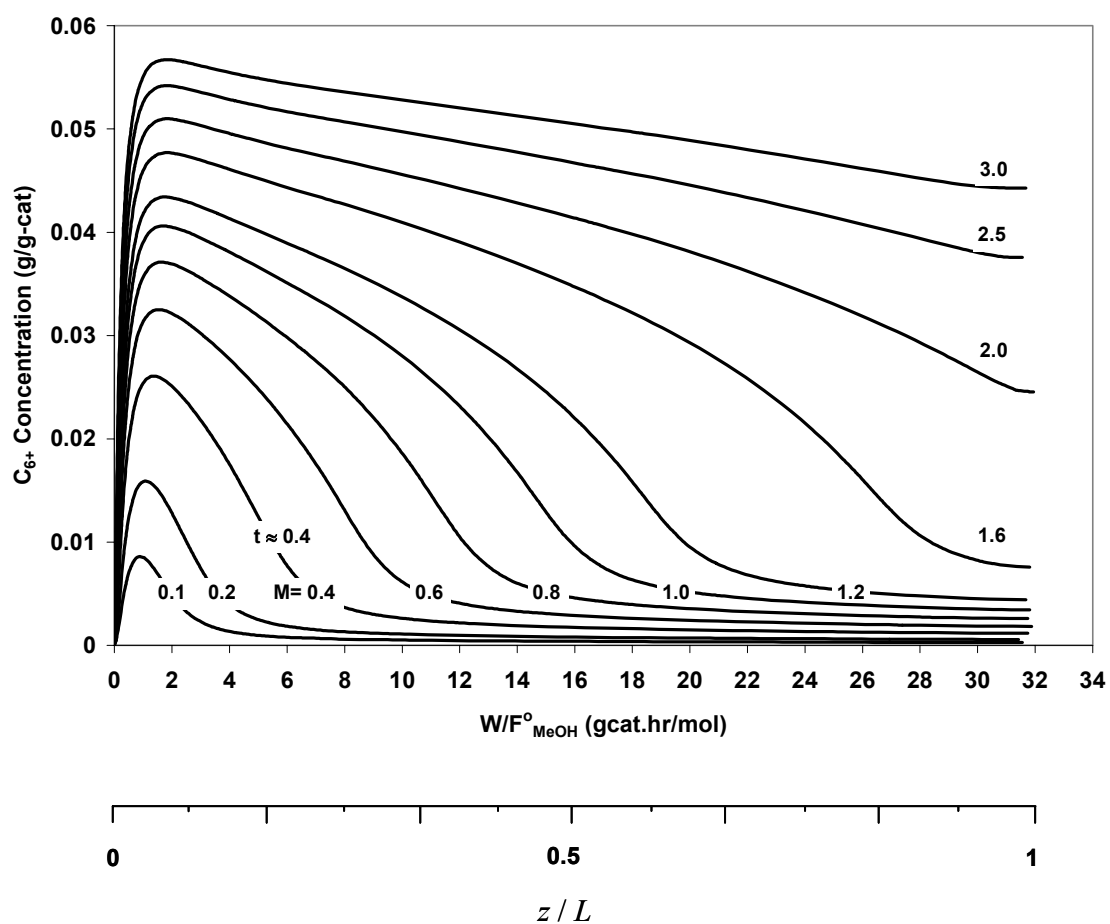


Figure V-12. Concentration profiles of C6+ olefins at different process times for isothermal fixed bed reactor at 480°C, 1.04 bar total pressure and 0.5 bar methanol partial pressure.

CHAPTER VI

CONCEPTUAL REACTOR DESIGN FOR MTO

VI.1 Introduction

On the basis of the kinetic model developed in the previous chapter, several types of reactors have been evaluated for the conversion of methanol to olefins. These range from fixed bed reactors, with isothermal or adiabatic operation, to fluidized bed reactors.

Because of the high exothermicity of the MTO process (the adiabatic temperature rise for a pure methanol feed is of the order of 250°C), temperature limitation represents an important factor governing the selection of the reactor type.

The present chapter discusses the differences in the yields and selectivities to products obtained in various types of reactors. The reactors investigated are: multi-bed adiabatic, riser, and fluidized bed.

VI.2 Isothermal Reactor

The mathematical model for an isothermal reactor has been developed from the basic mass and heat balance equations of the pseudo-homogeneous model. It was checked that there are no gradients inside the catalyst particle and in the film surrounding it. It was also checked that pressure drop inside the reactor is negligible.

The continuity equation can be written,

$$\frac{d\hat{y}_i}{d(W/F_{MeOH}^\circ)} = \frac{100 \cdot M_i}{M_{MeOH}} \cdot \Phi_i \cdot \mathfrak{R}_i, \quad i = 1, 2, \dots, m \quad (\text{VI-1})$$

where Φ_i is the deactivation functions for the main reactions expressed as follows:

$$\Phi_i = \exp(-\alpha C_{C_{6+}}) \quad \text{for olefins formation} \quad (\text{VI-2})$$

$$\Phi_i = \frac{1}{(1 + \beta C_{C_{6+}})} \quad \text{for methanol conversion} \quad (\text{VI-3})$$

The concentration of the C_{6+} components evolves with time according to:

$$\frac{dC_{C_{6+}}}{dt} = \Phi_c \cdot r_c \quad (\text{VI-4})$$

with initial condition,

$$\text{at } t = 0 \quad C_{C_{6+}} = 0 \quad \text{for all } \frac{W}{F_{MeOH}^\circ}$$

$$\text{where} \quad r_c = \sum_6^8 M_i \mathfrak{R}_i$$

Simulation of MTO in an isothermal reactor at 440°C is shown in Figure VI-1. Methanol conversion at the exit of the reactor is around 90%. The ethylene and propylene yields amount to 12 and 13 wt% respectively. The evolution of the rate of disappearance of MeOH and the net rate of production of the products along the reactor is shown in Figure VI-2.

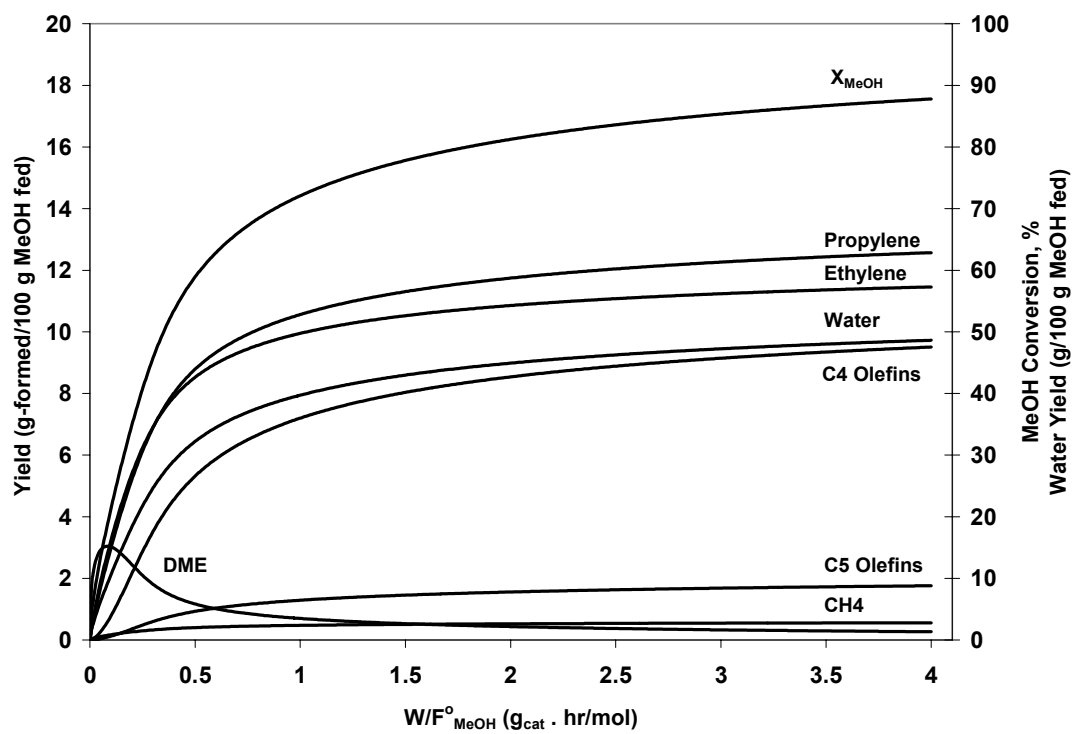


Figure VI-1. Evolution of methanol conversion and wt% yield of different products along the length of an isothermal reactor. Temperature: 440°C. Pressure: 1.04 bar. 100% methanol feed.

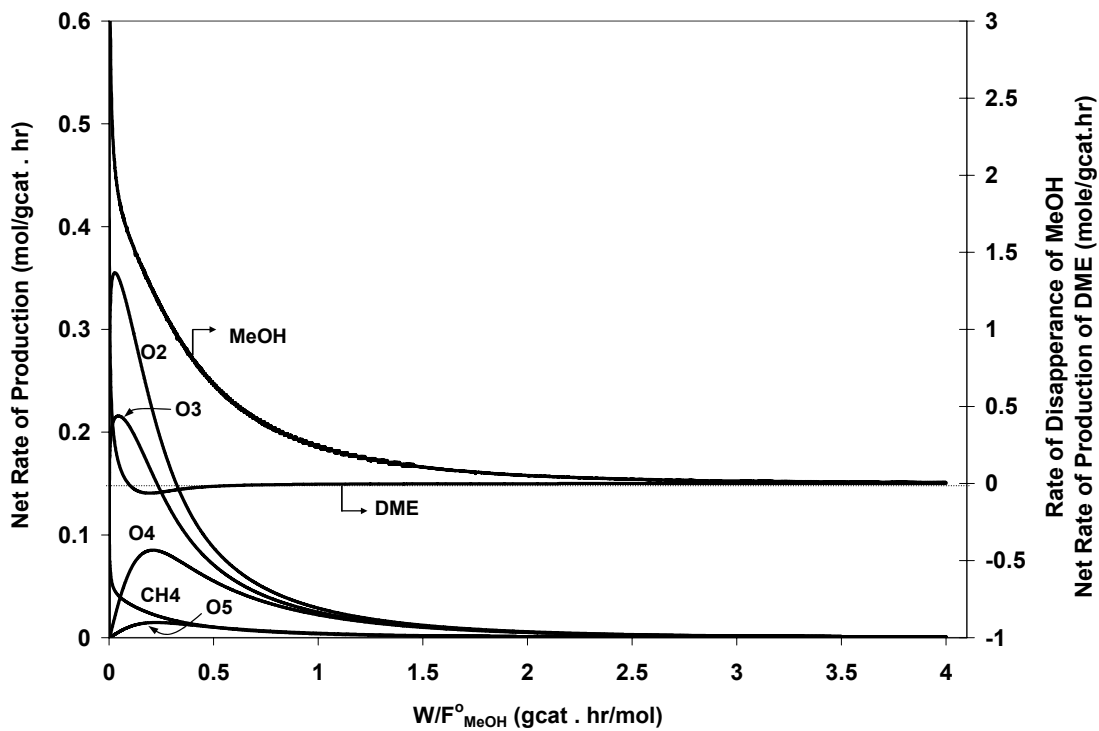


Figure VI-2. Rate of reaction profiles on SAPO-34 along the length of an isothermal reactor. Temperature: 440°C. Pressure: 1.04 bar. 100% methanol feed. O_i : Olefin with carbon number i .

Initially, the production rates increase very rapidly until they reach a maximum near the inlet of the reactor. The position of the maximum varies from one product to another based on the sequence in which they are produced.

The problem with isothermal operations is that it would require a multi-tubular reactor, the cost of which would be prohibitive for the commercialization of this process. Adiabatic operation, then, is required.

VI.3 Multi-bed Adiabatic Reactor

VI.3.1 SAPO-34-based Process

Because of its construction simplicity, an adiabatic reactor is the first and most elementary type of reactor to be considered. In this case the reactor is simply a vessel of relatively large diameter. A single-bed adiabatic reactor, however, is not suitable for highly exothermic process such as MTO. Simulation of such a simple adiabatic reactor leads to a temperature rise of more than 250°C and an unacceptable high methane yield. It would also cause a rapid deactivation of the catalyst by coke formation and even its deterioration. For this reason, a multi-bed adiabatic reactor with intermediate heat exchangers was chosen for this study.

Figure VI-3 shows a schematic diagram of a multi-bed adiabatic reactor used for the process of SO₃ synthesis. A similar design could be used for the MTO process.

The material balance is the same as in the isothermal reactor design.

For an adiabatic reactor, the heat generated by the conversion of methanol is utilized in raising the temperature of the reaction mixture.

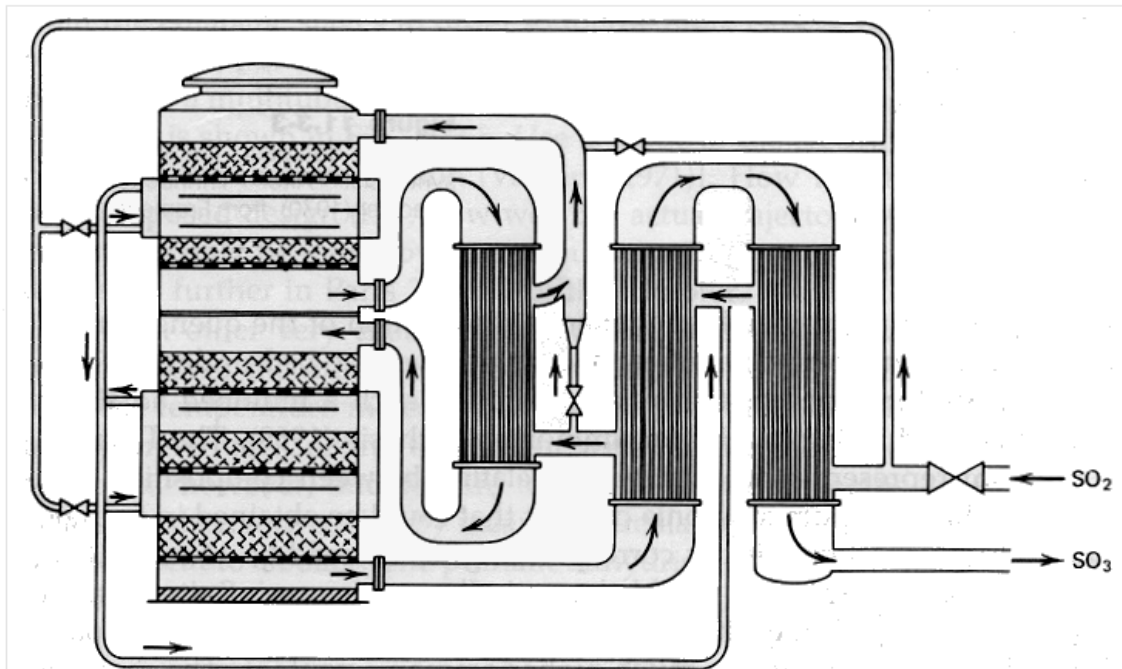


Figure VI-3. Multi-bed adiabatic reactor for SO₃ synthesis. From Froment and Bischoff⁵⁸.

The energy equation can be written as:

$$\frac{\sum_1^{\#comp} F_i C_{pi}}{\Omega} \frac{dT}{dz} = \left[\sum_1^{\#reacts.} r_j (-\Delta H_j) \Phi_j \right] \rho_B \quad (\text{VI-5})$$

But, $W = \Omega \rho_B z$ where Ω is the cross sectional area of the reactor, so that the energy equation becomes:

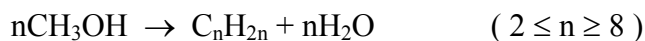
$$\frac{dT}{d(W/F_{MeOH}^\circ)} = \frac{\left[\sum_1^{\#reacts.} r_j (-\Delta H_j) \Phi_j \right]}{\left[\sum_1^{\#comp} F_i C_{pi} \right]} F_M^\circ \quad (\text{VI-6})$$

The heats of reaction appearing in the energy equation are calculated based on the following overall reactions:

- DME (dimethylether):



- Olefins:



The model equations were solved using Gear's routine with variable step size for accuracy adjustment.

Generally, the design of a multi-bed adiabatic reactor represents an optimization problem. The objective of the optimization, in the case of MTO, is to maximize the ethylene and/or propylene yield. The decision variables are the number of beds, the size of each bed and the feed temperature to each bed. Moreover, because of catalyst deactivation, process time is also a decision variable.

In this work, several arrangements of beds and intermediate-coolers, in which the total number of beds was less than five, have been tried. Figure VI-4 and Figure VI-5 show the simulation results, at zero process time obtained with the optimum configuration for maximum ethylene and propylene yield, of the MTO process in a four-bed adiabatic reactor with intermediate cooling. The feed temperature to each bed is 648 K. Temperature rise per bed decreases in the order, $\Delta T_1 > \Delta T_2 > \Delta T_3 > \Delta T_4$. This is because of very rapid methanol conversion into DME in the first two beds and also because the amount of MeOH is gradually converted. As a consequence the rates of methylation and oligomerization decrease and also the associated heat production.

The overall methanol conversion is 93%. The conversion is limited to avoid production of higher olefins and too rapid deactivation, in addition to limiting paraffins and aromatics formation. The yields of propylene, ethylene, and C₄ olefins, at the exit of the reactor, amount to 15, 13, and 8 (kg/100 kg MeOH fed) respectively. More than 50 wt% of the methanol fed to the reactor is converted into water. This is the negative aspect of the MTO process.

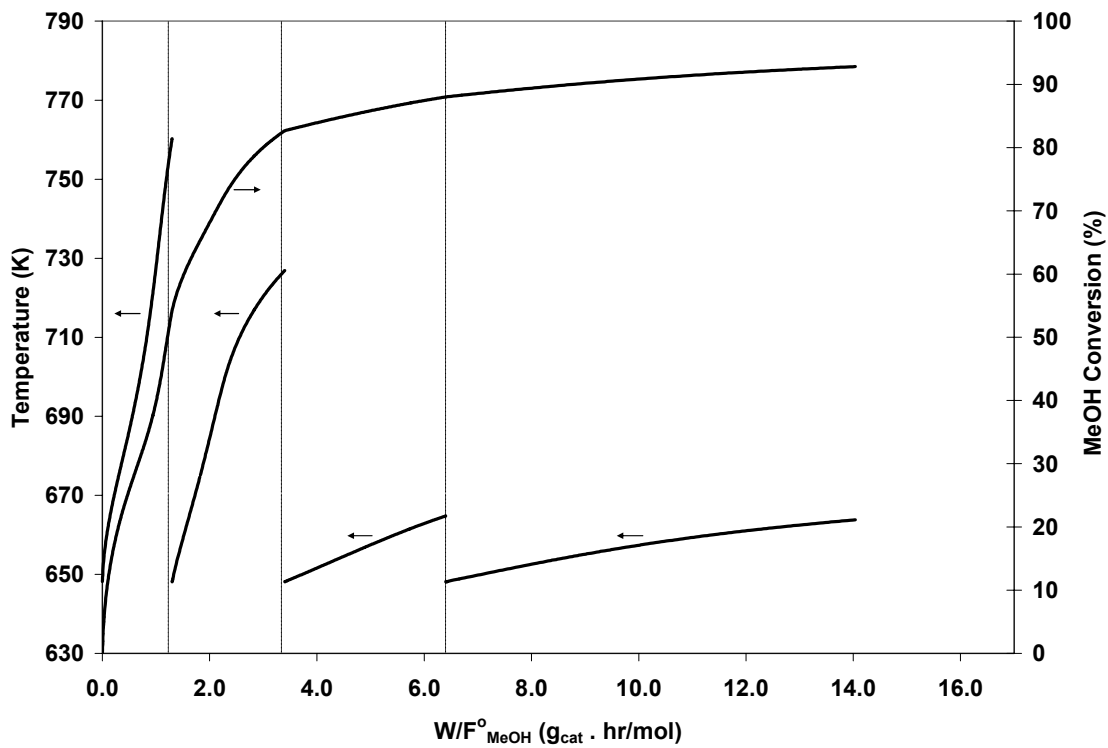


Figure VI-4. Temperature and methanol conversion profiles in a four-bed adiabatic reactor. Catalyst: SAPO-34. Process time: 0 min. $T_f = 648$ K for all beds. $P = 1.04$ bar and $P_{\text{MeOH}} = 0.5$ bar (diluted with steam).

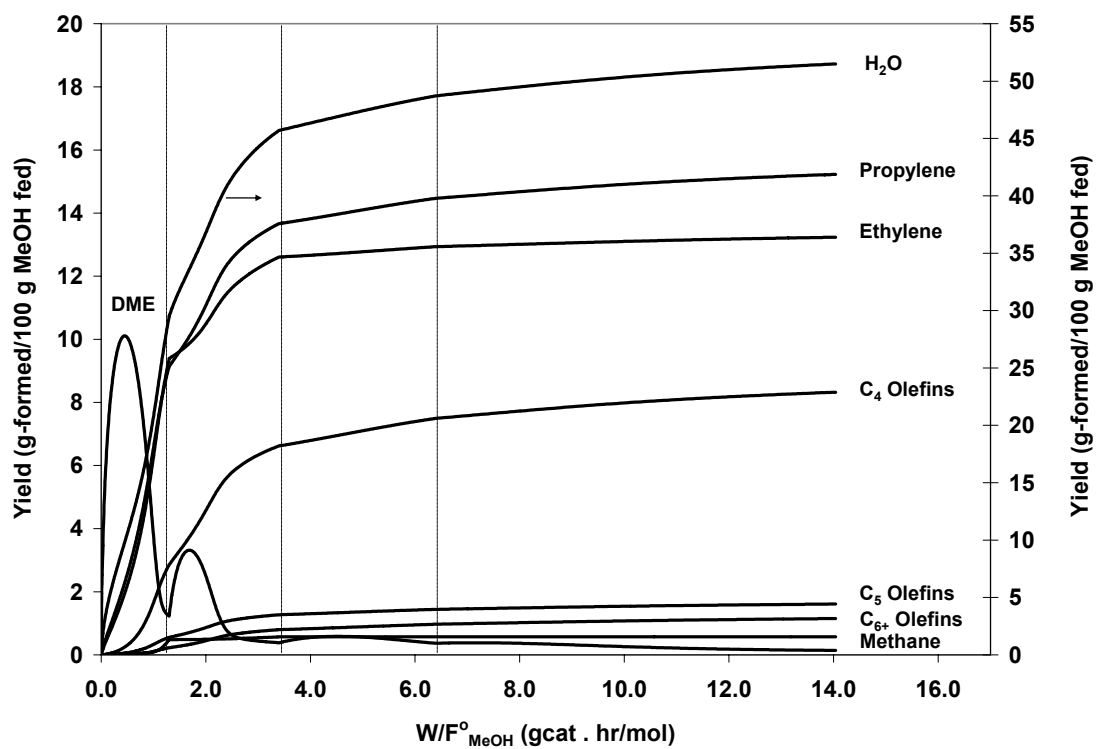


Figure VI-5. Yield profiles in a four-bed adiabatic reactor. Catalyst: SAPO-34. Process time: 0 min. $T_f = 648$ K for all beds. $P = 1.04$ bar and $P_{MeOH} = 0.5$ bar (diluted with steam).

DME formation is very rapid. It reaches a maximum in the first two beds because it is converted into ethylene and propylene, but also methane. Methane is a pure loss and the conditions have to be chosen to keep its yield low. A maximum in the ethylene and propylene has to be avoided by limiting W/F_{MeOH}° and ΔT per bed.

Clearly, initially, most of the reaction takes place in the first two beds. As M increases, the catalyst deactivates and as a result the reaction spreads more evenly over the 4 beds as shown in Figure VI-6 and Figure VI-7.

At higher M , to maintain a relatively high conversion and therefore high ethylene and propylene yield, the inlet temperatures to the beds were raised to compensate for the loss in activity of the catalyst as shown in Figure VI-8 and Figure VI-9.

Figure VI-10 shows the evolution of the ethylene and propylene yield inside the reactor at different process times. Initially, the ethylene and propylene are produced with a weight ratio of ≈ 1.2 (P/E). After 20 minutes, the propylene yield has not changed while the ethylene yield has increased by 8% relative to the yield at zero process time (see Figure VI-11). Until this point no change in feed temperature is made. At 40 minutes process time, changes in the feed temperatures were applied to compensate for the loss of catalyst activity. The ethylene yield has not changed while the propylene yield dropped 30% relative to the value after 20 minutes.

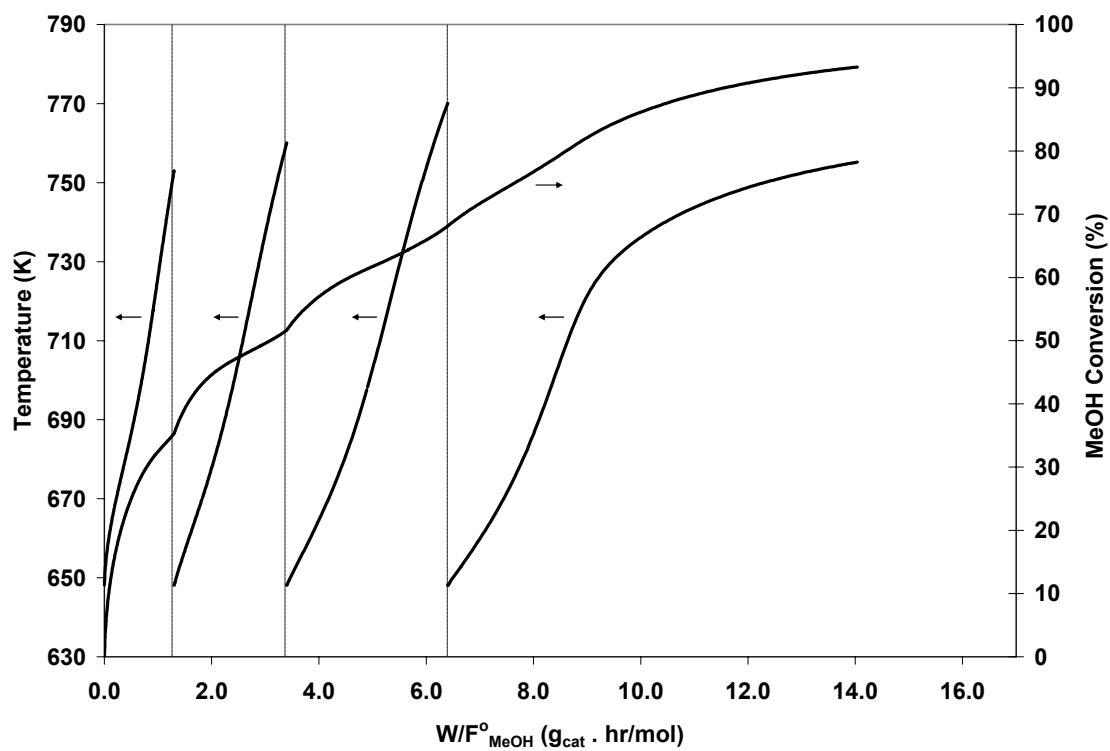


Figure VI-6. Effect of catalyst deactivation on temperature and methanol conversion profiles in a four-bed adiabatic reactor. Catalyst: SAPO-34. Process time: 20 min. $T_f = 648$ K for all beds. $P = 1.04$ bar and $P_{MeOH} = 0.5$ bar.

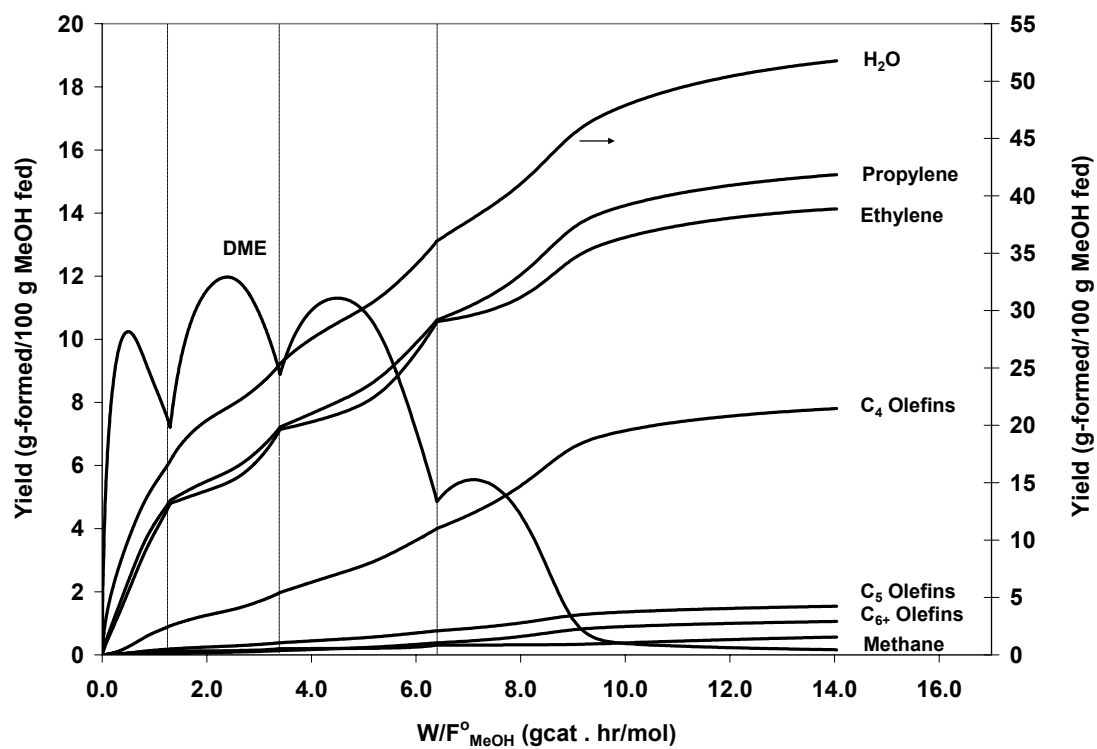


Figure VI-7. Effect of catalyst deactivation on yield profiles in a four-bed adiabatic reactor. Catalyst: SAPO-34. Process time: 20 min. $T_f = 648$ K for all beds. $P = 1.04$ bar and $P_{MeOH} = 0.5$ bar.

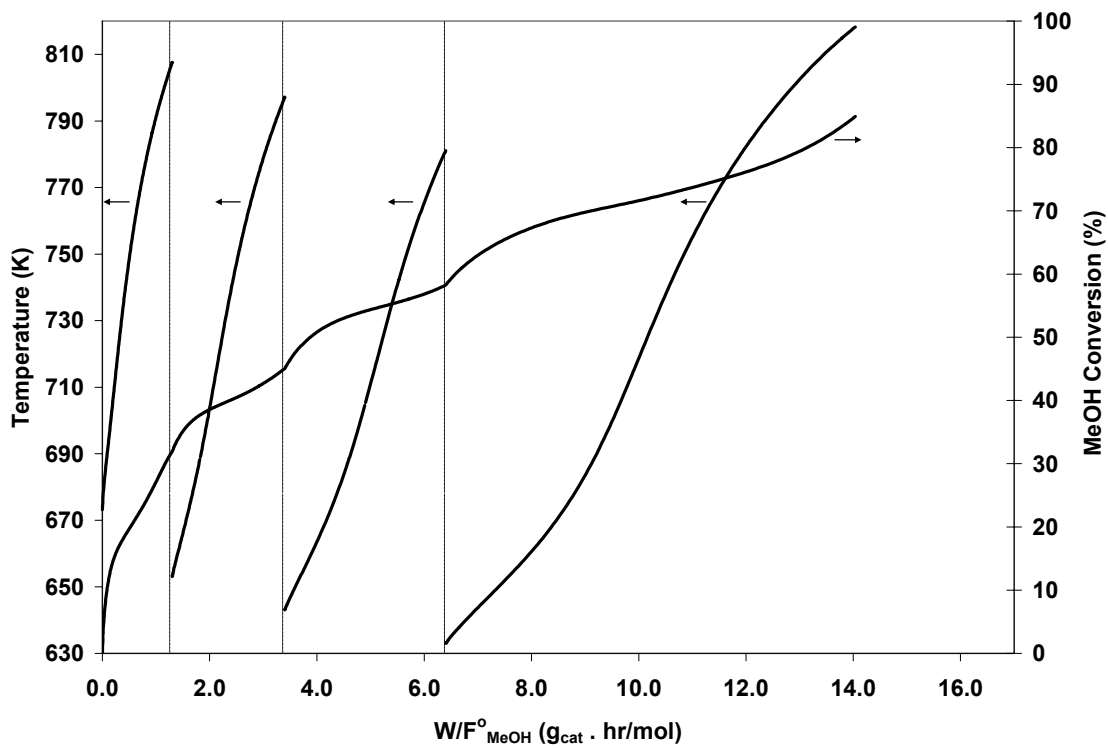


Figure VI-8. Effect of catalyst deactivation on temperature and methanol conversion profiles in a four-bed adiabatic reactor. Catalyst: SAPO-34. Process time: 40 min. $T_f = 673, 653, 643,$ and 633 K for beds 1, 2, 3, and 4 respectively. $P = 1.04$ bar and $P_{MeOH} = 0.5$ bar.

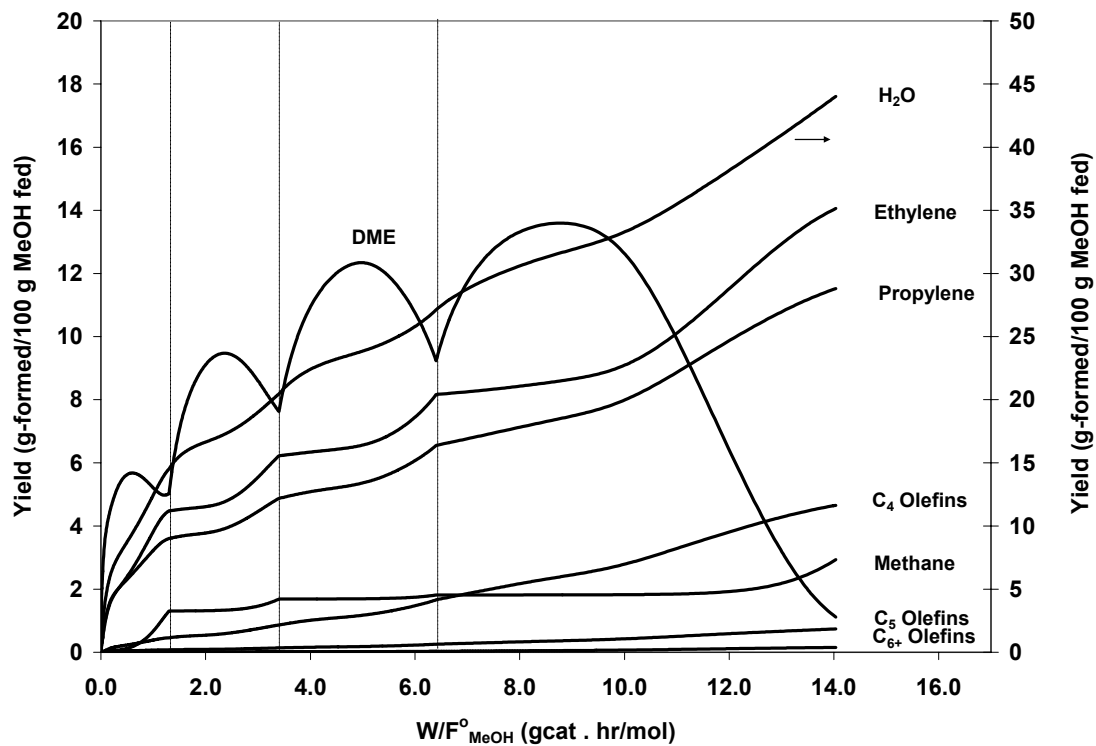


Figure VI-9. Effect of catalyst deactivation on yield profiles in a four-bed adiabatic reactor. Catalyst: SAPO-34. Process time: 40 min. $T_f = 673, 653, 643,$ and 633 K for beds 1, 2, 3, and 4 respectively. $P = 1.04$ bar and $P_{MeOH} = 0.5$ bar.

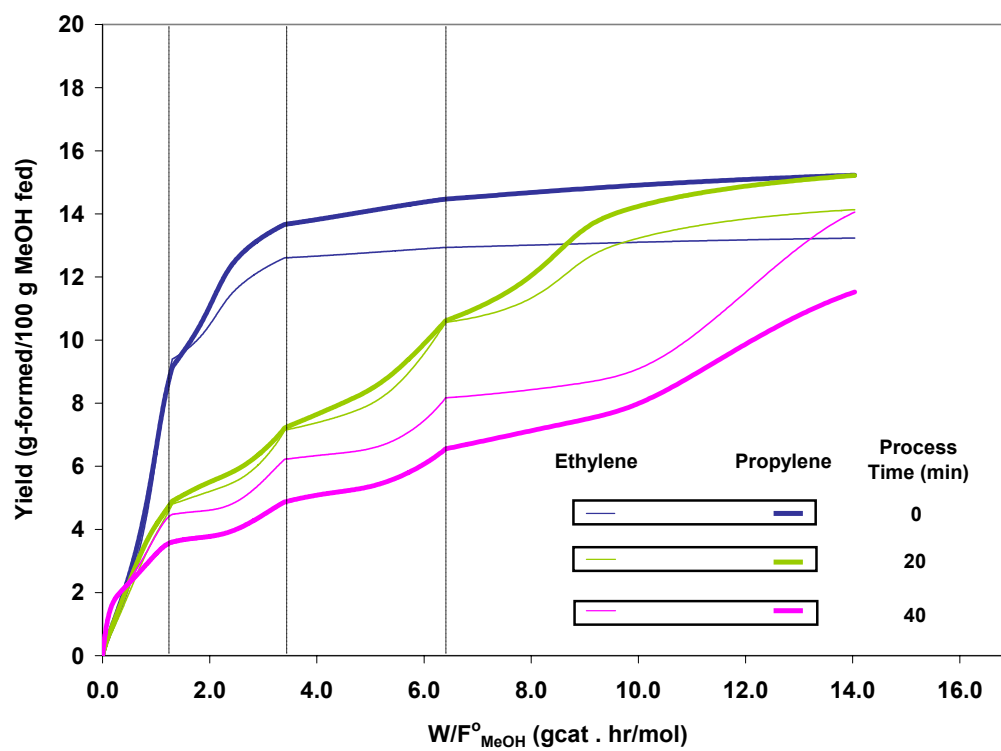


Figure VI-10. Effect of catalyst deactivation on the ethylene and propylene yield profiles in a four-bed adiabatic reactor. Catalyst: SAPO-34. $P = 1.04$ bar and $P_{MeOH} = 0.5$ bar.

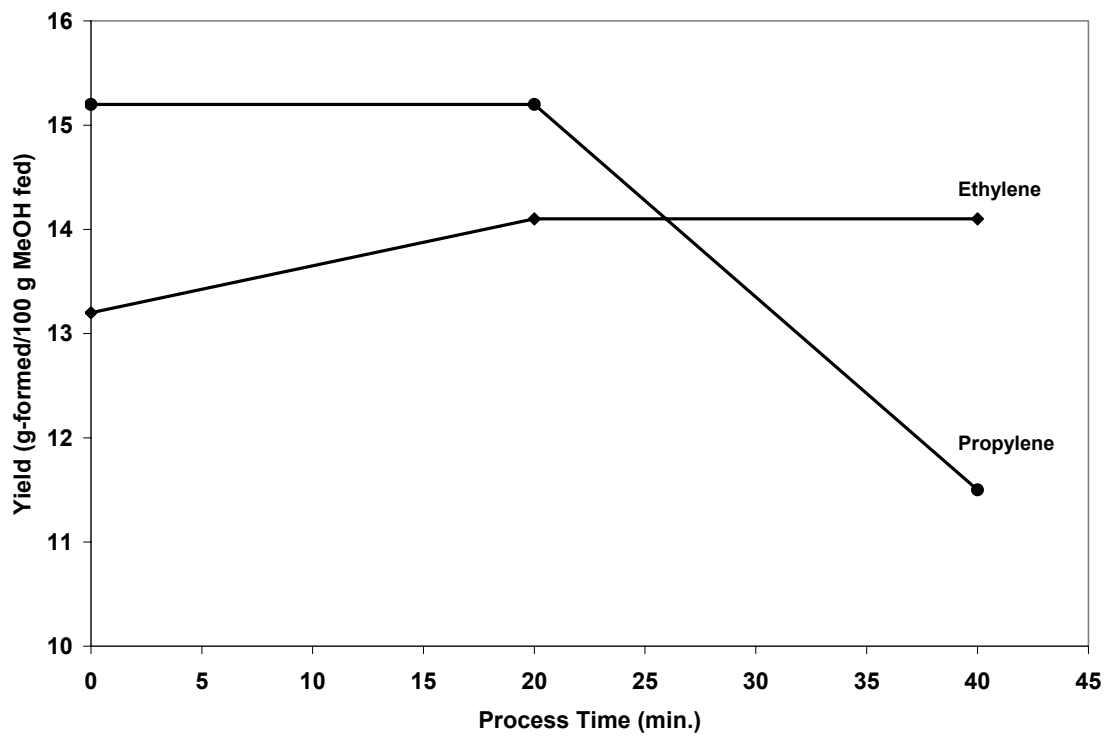


Figure VI-11. Ethylene and propylene yield at different process times in a four-bed adiabatic reactor. Catalyst: SAPO-34. $P = 1.04$ bar and $P_{\text{MeOH}} = 0.5$ bar.

The question now is what is the best time to switch between reaction mode and regeneration mode? Clearly, that again requires optimization. For some time the drop in the activity of the catalyst can be compensated by optimizing the feed temperatures to each bed. However, as the catalyst deactivates beyond an acceptable value and increases in feed temperatures can not compensate for the loss of activity, a decision has to be made to regenerate the catalyst. This periodic operation is a drawback. To maintain the production a second reactor has to be used in parallel, which means increased investment. Operation whereby the regeneration is continuous is an interested alternative. Operating the reactor with a fluidized bed offers this possibility.

VI.3.2 ZSM-5-based Process

For the purpose of comparison with SAPO-34, the simulation of the MTO process on a multi-fixed bed adiabatic reactor with ZSM-5 (Si/Al = 200), was performed. The simulation was based on the model developed by Park and Froment.^{44,45}

The objective was to optimize the yield of propylene under given boundary conditions. The temperature increase per bed was limited to 100 K in order to prevent a high yield of methane. Methane yield was kept below 1 wt% as its production is a pure waste.

The total conversion of methanol is limited to 90% to avoid the production of paraffins and aromatics. Also the temperature is not supposed to exceed 500°C, as higher temperatures would destroy the catalyst.

Because ZSM-5 deactivates much slower than SAPO-34, all the ZSM-5 based reactor simulations presented below do not consider any catalyst deactivation.

Figure VI-12 and Figure VI-13 show the simulation results for a four-bed adiabatic reactor with a pure methanol feed. The feed temperature is 673 K for all beds. The temperature rise per bed was almost constant at 100 K. The amount of catalyst per bed is increasing in the following order: $W_1 < W_2 < W_3 < W_4$. The reason for this is to compensate for the decrease of conversion as the methanol partial pressure decreases. The propylene yield amounts to 7.7%, the ethylene yield to 3%, while the methane-yield is only 0.3%. The DME-yield at the exit is about 10%.

Figure VI-14 and Figure VI-15, on the other hand, show the simulation of a four-bed adiabatic reactor with a 50-50 mol% methanol-water feed. More than two times the amount of catalyst used for the pure methanol case is required to maintain the same conversion, which of course means more investment. However, the ethylene and propylene yields are increased by 26% and 9% respectively. This advantage in addition to decreasing the rate of catalyst deactivation should be weighed against the drawback of the additional investment.

The comparison of the performance of SAPO-34 and ZSM-5 in a four-bed adiabatic reactor with a 50-50 mol% methanol-water feed is shown in Figure VI-16. The exit methanol conversion is the same, $\approx 88\%$, for both cases. Slightly higher W/F_{MeOH}° is needed for ZSM-5 to achieve the same conversion as of SAPO-34. The ethylene, propylene, and C_4 olefins yields for SAPO-34 are 3.4, 1.7, and 1.3 times the corresponding yields for ZSM-5. On the other hand, the C_{5+} yield for ZSM-5 is 6 times that for SAPO-34. Both catalysts give almost the same yield of methane. The low yield of C_{5+} in SAPO-34 is attributed to its small pore size.

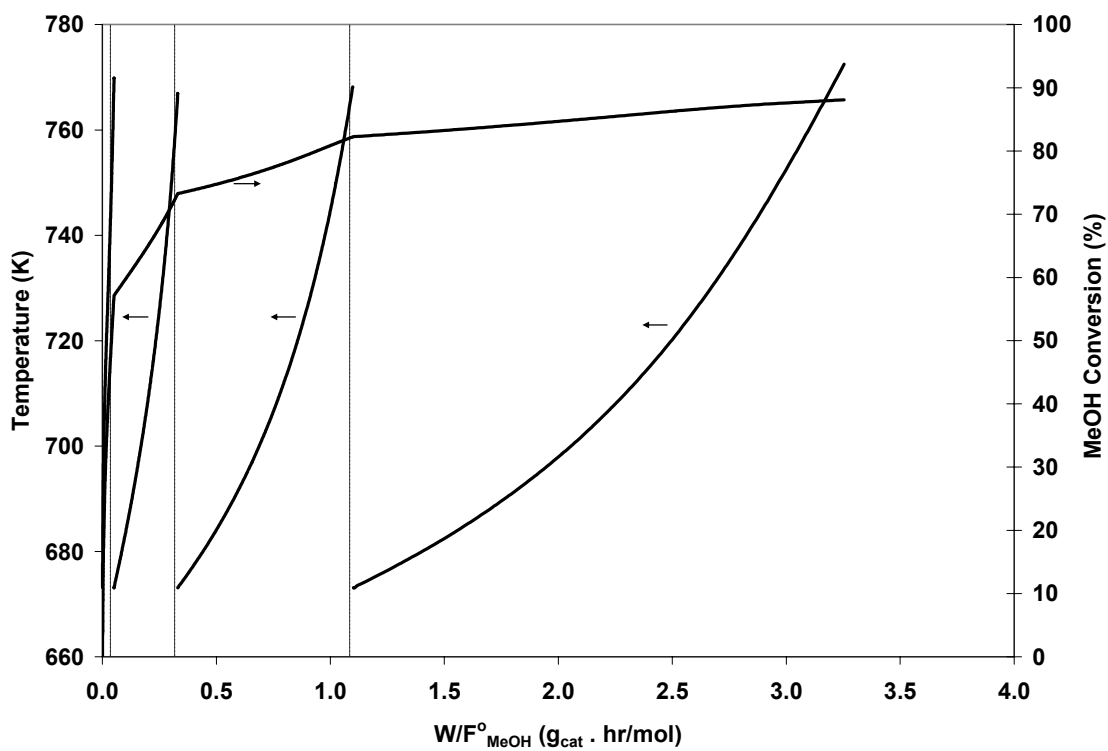


Figure VI-12. Temperature and methanol conversion profiles in a four-bed adiabatic reactor. Catalyst: ZSM-5. $T_f = 673$ K for all beds. $P = 1.04$ bar and $P_{MeOH} = 1.04$ bar.

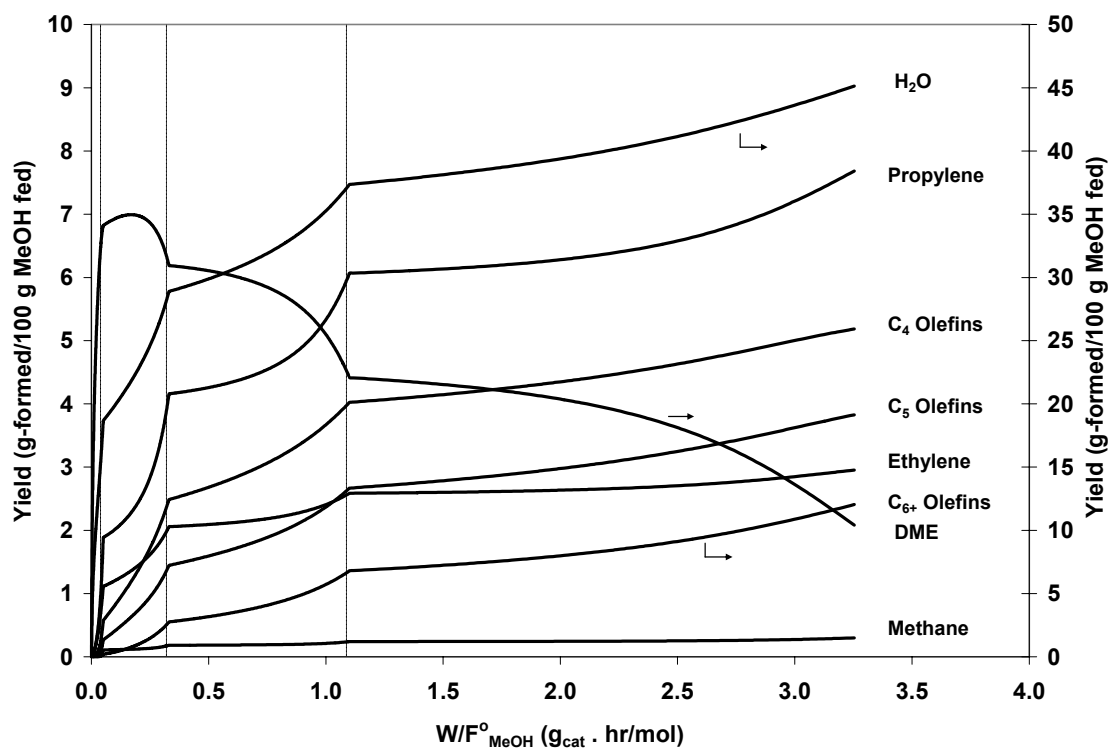


Figure VI-13. Yield profiles in a four-bed adiabatic reactor. Catalyst: ZSM-5. $T_f = 673$ K for all beds. $P = 1.04$ bar and $P_{MeOH} = 1.04$ bar.

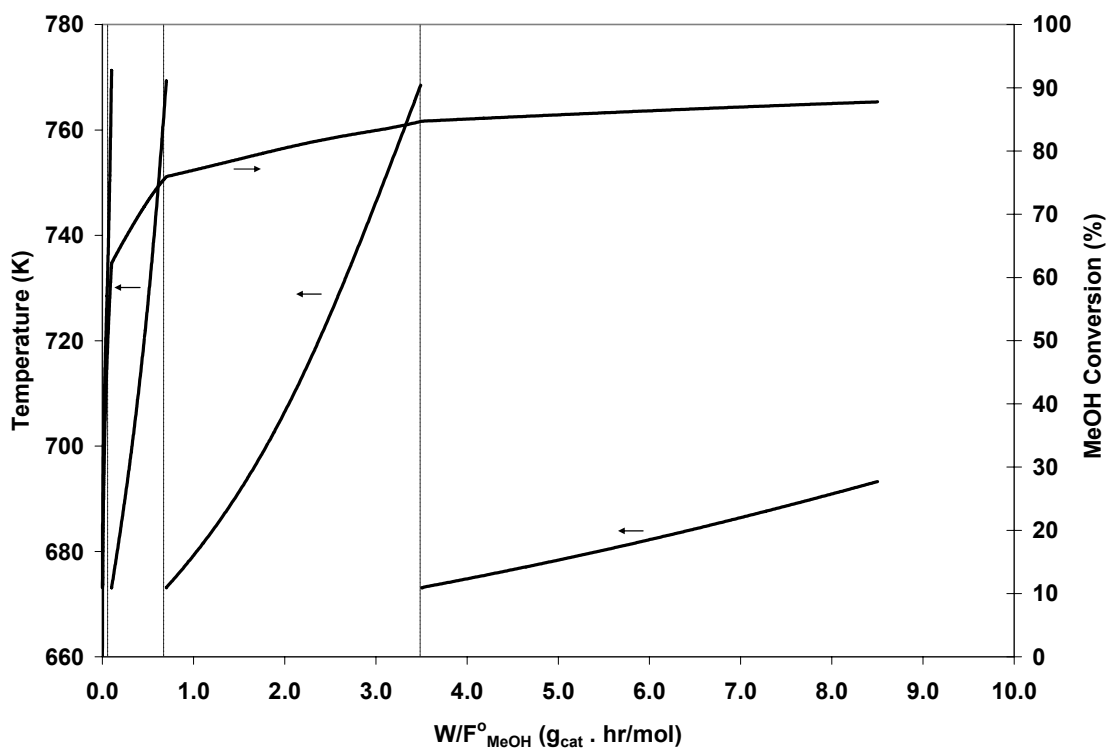


Figure VI-14. Temperature and methanol conversion profiles in a four-bed adiabatic reactor. Catalyst: ZSM-5. $T_f = 673$ K for all beds. $P = 1.04$ bar and $P_{MeOH} = 0.5$ bar.

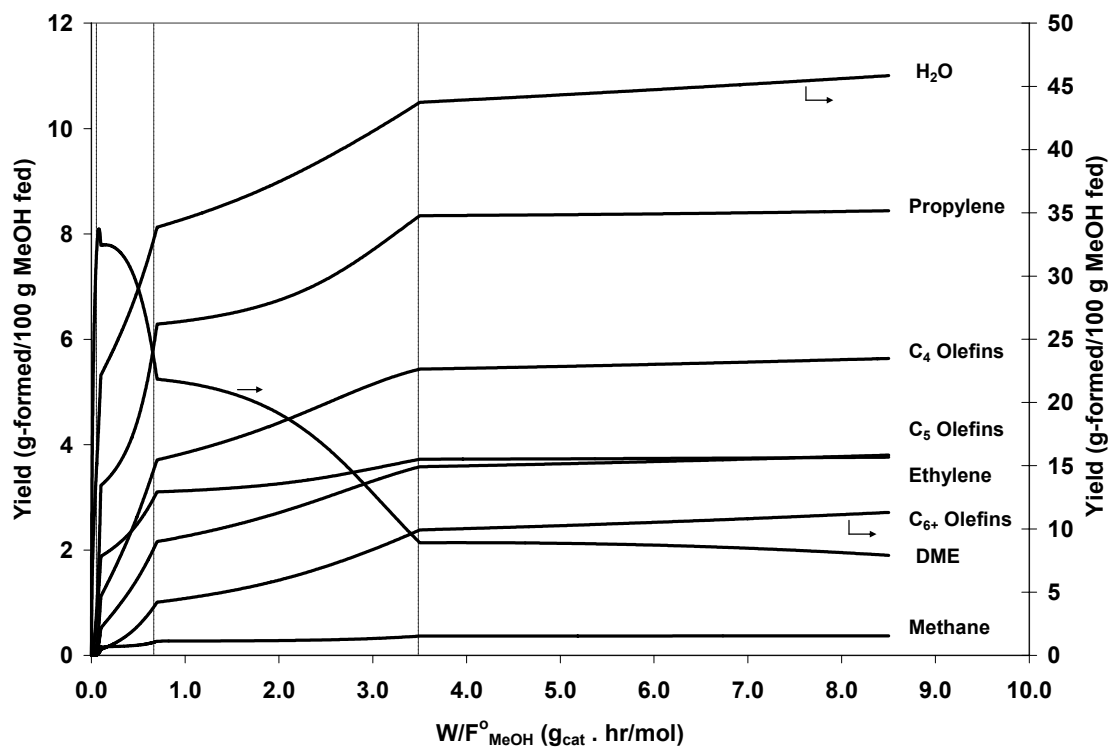


Figure VI-15. Yield profiles in a four-bed adiabatic reactor. Catalyst: ZSM-5. $T_f = 673$ K for all beds. $P = 1.04$ bar and $P_{MeOH} = 0.5$ bar.

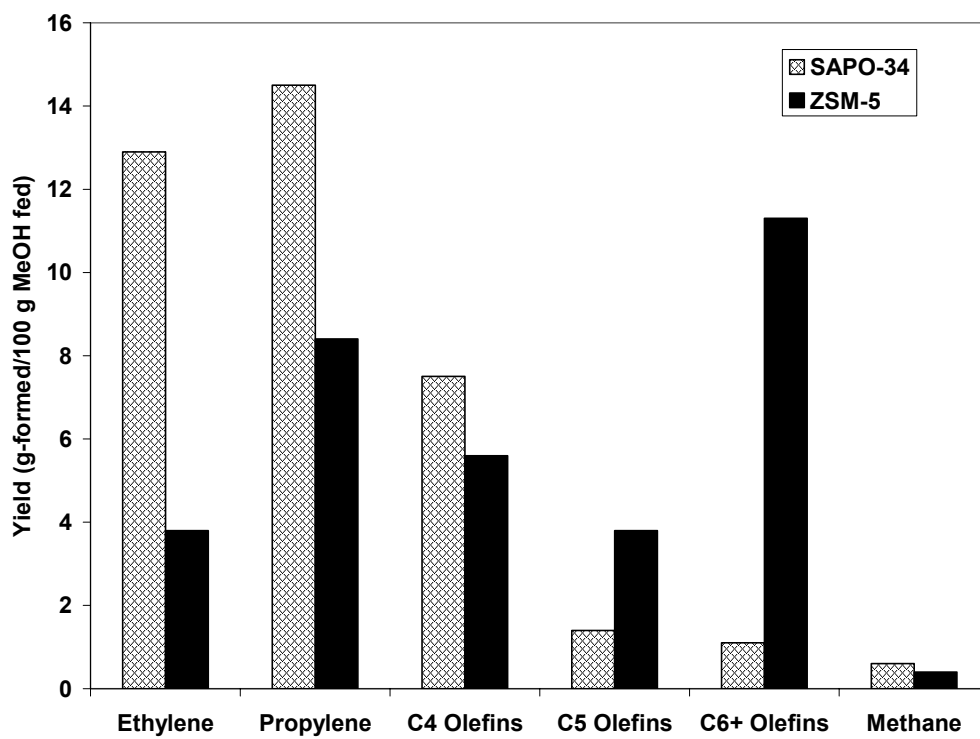


Figure VI-16. Comparison between the performance of SAPO-34- and ZSM-5-based MTO process in a four-bed adiabatic reactor. . $P = 1.04$ bar and $P_{\text{MeOH}} = 0.5$ bar. SAPO-34: $T_f = 648$ K for all beds. ZSM-5: $T_f = 673$ K for all beds.

VI.4 Riser Reactor

VI.4.1 Fluidization

Fluidization is the operation by which an ensemble of solid particles and a fluid is behaving like a fluid. The real breakthrough of fluidized bed technology was associated with the catalytic cracking of gasoil into gasoline, first practiced in 1942 by Exxon. Since then, fluidized bed reactors have found use in many processes such as the oxidation of naphthalene into phthalic anhydride, the ammoxidation of propylene into acrylonitrile, the oxychlorination of ethylene into ethylene dichloride (the first step of vinyl chloride manufacture), and the Union Carbide process for polymerization of ethylene.

Fluidized bed reactors have many advantages over the fixed bed reactors. The most important are as follows:

- Ensembles of fluidized solids behave like liquids, thus can be easily transported from one vessel to another.
- The high turbulence created in the fluid-solid mixture leads to much higher heat transfer coefficients than those which can be obtained in fixed beds. Therefore, a fluidized bed reactor is much more suitable for exothermic processes requiring close temperature control.
- The circulation of solids between two fluidized beds makes it possible to remove or add huge quantities of heat produced or needed in large reactors.

- Fluidized bed operation requires particle sizes which are much smaller than in fixed beds. This reduces the resistance to diffusion through the particles.
- The pressure drop in a fluidized bed is much smaller than in a fixed bed.

On the other hand, fluidized bed technology has a number of disadvantages: mainly axial mixing of the gas, which is detrimental to conversion, nonuniform residence times of solids in the reactor, high attrition rate of catalyst, erosion of pipes and vessels because of abrasion by particles, and complexity of operation.

In fluidization, there are a number of regimes where the fluid bed behaves differently as velocity, gas properties and solid properties are varied. Consider a gas passing upward through a packed bed of fine particles resting on top of a distributor, Figure VI-17. At very low gas flow rates, the gas simply moves through the void spaces between stationary particles without changing the structure of the bed. This represents a fixed or packed bed reactor. As the superficial gas velocity (u_0) increases further, the pressure loss will increase slowly and eventually a point will be reached where the upward drag exerted on the particles by the fluid just equals the weight of the particles.⁶⁵ This point is known as the minimum fluidization and the corresponding gas velocity is the minimum fluidization velocity (u_{mf}).

The magnitude of the minimum fluidization velocity depends on the solid particle properties, such as density and size distribution, as well as the gas properties, particularly the density and viscosity.

A further increase in u_0 will result in bubble formation. For fine particles, such as those used in the FCC process, bubbles do not appear as soon as minimum fluidization is

reached. There is a range of velocities in which uniform expansion is observed with no observed bubbling. However, at a gas velocity of about $3u_{mf}$, bubbles begin to form and bed height begins to increase. This is known as the minimum bubbling point and the corresponding gas velocity as the minimum bubbling velocity u_{mb} . At higher flow rates, agitation becomes more violent and the movement of solids becomes more vigorous. In addition, the bed does not expand much beyond its volume at minimum fluidization. Such a bed was called by Kunii and Levenspiel *bubbling fluidized bed*.⁶³

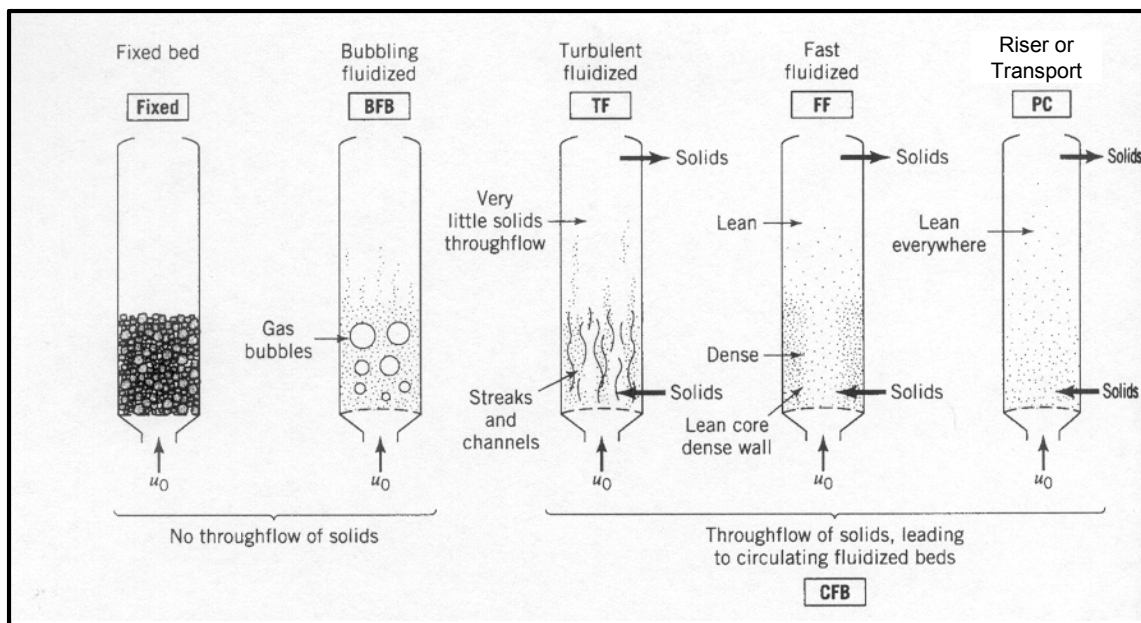


Figure VI-17. Gas / solid contacting regimes, from low to very high gas velocity.⁶⁴

Under certain circumstances, the increase in bubble size as the gas velocity is increased can lead to slug flow. This type of flow is characterized by adjacent bubbles from the gas distributor coalescing to form larger bubbles or slugs that grow to the same order as the vessel diameter, resulting in poor contacting of the gas and solids. In general, slugging can be avoided by reducing the height to diameter ratio.⁵⁸

As the gas velocity is increased beyond the terminal or free-fall velocity, the *turbulent regime* is encountered. This is an interesting regime because the effect of the bubble short-circuiting is much less pronounced than in the bubbling regime, so that high conversion can be more readily obtained. It is encountered in acrylonitrile synthesis reactors, operating at a superficial gas velocity of 0.5 m/s, and in phthalic anhydride synthesis reactors at 0.3 to 0.6 m/s.⁵⁸

With further increase in gas velocity, i.e. in the fast fluidization and dilute phase transport or riser regimes, solids are carried out of the bed with the gas as shown in Figure VI-17. In the riser regime there is no wall or down flow of the particles and the solid volume fraction is very small. The Kellogg-Fischer-Tropsch reactors at Sasol operate in the fast regime and modern catalytic cracking units in the riser flow regime.

VI.4.2 Mathematical Modeling of MTO in a Riser Reactor

In a riser reactor, due to the high gas flow rates all solids are entrained out of the bed and must be continuously replaced. Unlike the bubbling fluidized bed, particles in the riser reactor are equally distributed, with no wall or down flow zone. Therefore, both gas and solid can be assumed to move in plug flow.⁶³

In this work, the riser reactor was modeled using a one-dimensional pseudohomogeneous model with plug flow and slip between the gas and solid phases.⁵⁸

The continuity equations for the gas phase components are,

$$\frac{dy_i}{dz} = 100 \left(\frac{w_i}{w_M F_M^\circ} \right) \rho_s (1 - \varepsilon) \Phi_i \mathfrak{R}_i \quad (\text{VI-7})$$

The void fraction, ε , is given by,

$$\varepsilon = \frac{(u_t + u_{s,g} + u_{s,p}) - \sqrt{(u_t + u_{s,g} + u_{s,p})^2 - 4u_{s,g}u_t}}{2u_t} \quad (\text{VI-8})$$

The terminal or free velocity is calculated from,

$$u_t = \sqrt{\frac{4gd_p(\rho_s - \rho_g)}{3\rho_g C_D}} \quad (\text{VI-9})$$

where C_D is the drag coefficient, a friction factor for flow around a submerged object. The drag coefficient depends upon the Reynolds number as follows:

$$C_D = \frac{24}{\text{Re}} \quad \text{Re} < 0.4$$

$$C_D = \exp\left(-5150 + \frac{69.43}{\ln \text{Re} + 7.99}\right) \quad 1 < \text{Re} < 10^3$$

$$C_D = 0.43 \quad \text{Re} > 10^3$$

The continuity equation for the C_{6+} olefins contained inside the catalyst is,

$$\frac{\dot{m}_s}{\Omega} \frac{dC_{C_{6+}}}{dz} = r_c \rho_s (1 - \varepsilon) \Phi_c \quad (\text{VI-10})$$

The energy equation for an adiabatic riser is written,

$$\frac{dT}{dz} = \frac{\sum r_i (-\Delta H_i) \Phi_i}{\sum F_i C_{p_i} + \dot{m}_s C_{p_s}} \Omega \rho_s (1 - \varepsilon) \quad (\text{VI-11})$$

VI.4.3 Simulation Results

Reactor geometry and catalyst properties data, required for the simulation, were taken to be similar to that employed in the catalytic cracking of gasoil. Simulation data are as follow:

Reactor geometry: $d_t = 0.85$ m; $Z = 40$ m

Catalyst: $\bar{d}_p = 8 \times 10^{-5}$ m; $\rho_s = 1500$ kg cat/m³ cat; $C_{p_s} = 1.003$ kJ/kg K

C_{6+} content of catalyst entering the riser: 0 (g/g cat)

Flow rates: $\dot{m}_s = 196$ T/hr; $\dot{m}_g = 28$ T/hr

Reactor inlet temperature: 480°C.

The results of the simulation are shown in Figure VI-18 and Figure VI-19. Methanol conversion at the exit of the riser was very low (less than 25%) despite the use of a very high riser and high temperature of the feed. The reason behind that is the low volume fraction of catalyst in the reactor. This volume fraction of solid was found to be (Figure VI-19) on the order of 0.2% of the total volume of the riser. This is a very low value in comparison to that usually encountered in the industrial riser reactor (1-8%).⁵⁸

Increasing the feed temperature could increase the conversion, but the value chosen is already close to the limit.

In another simulation, the solid volume fraction was increased by increasing the solid flow rate in the riser. The operating data are the same as in the previous simulation, except that the solid flow rate was increased to 4000 T/hr and the feed temperature was set at 465°C.

Simulation results are shown in Figure VI-20 - Figure VI-22. The methanol conversion at the exit of the riser was 85%. Ethylene and propylene yields were 12.5 and 11.5 wt% respectively. The high temperature chosen for the feed is responsible for the high ethylene yield with respect to that of propylene. The adiabatic temperature rise was less than 6°. This is primarily due to the high flow rate of solid which consumes most of the generated heat. The solid void fraction was on the order of 4%.

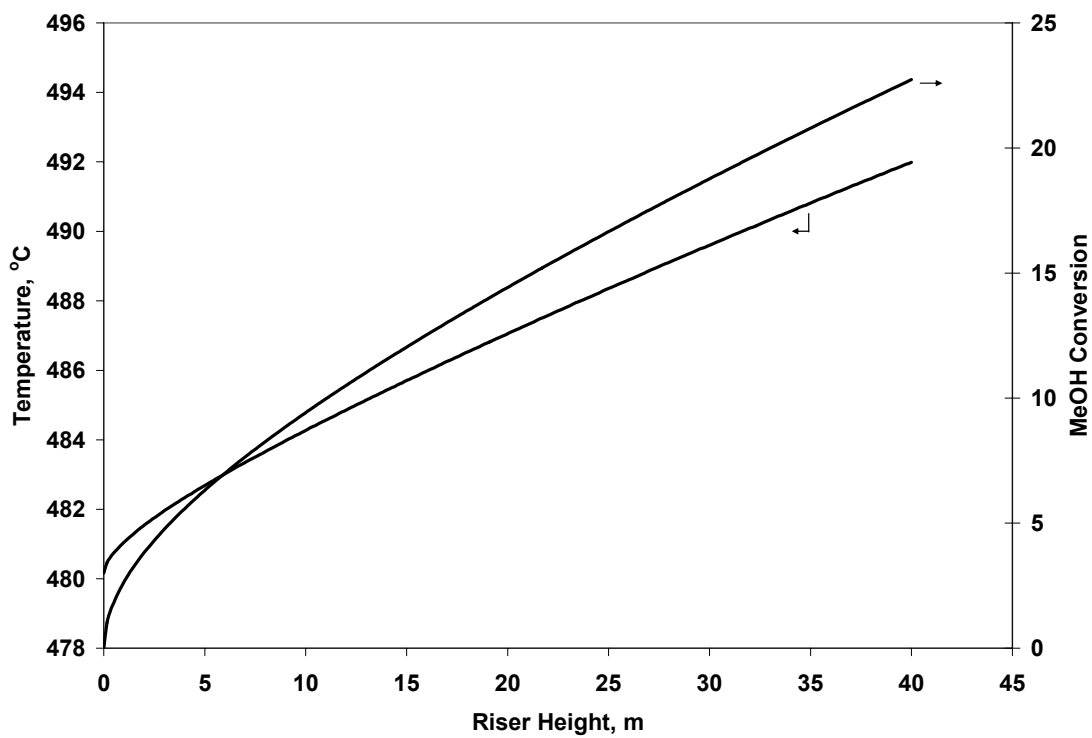


Figure VI-18. Evolution of temperature and methanol conversion along the height of the riser. Feed temperature: 480°C. Methanol mole fraction in the feed: 1.0. Total pressure: 1.04 bar. Flow rates: solid = 196 T/hr, gas = 28 T/hr.

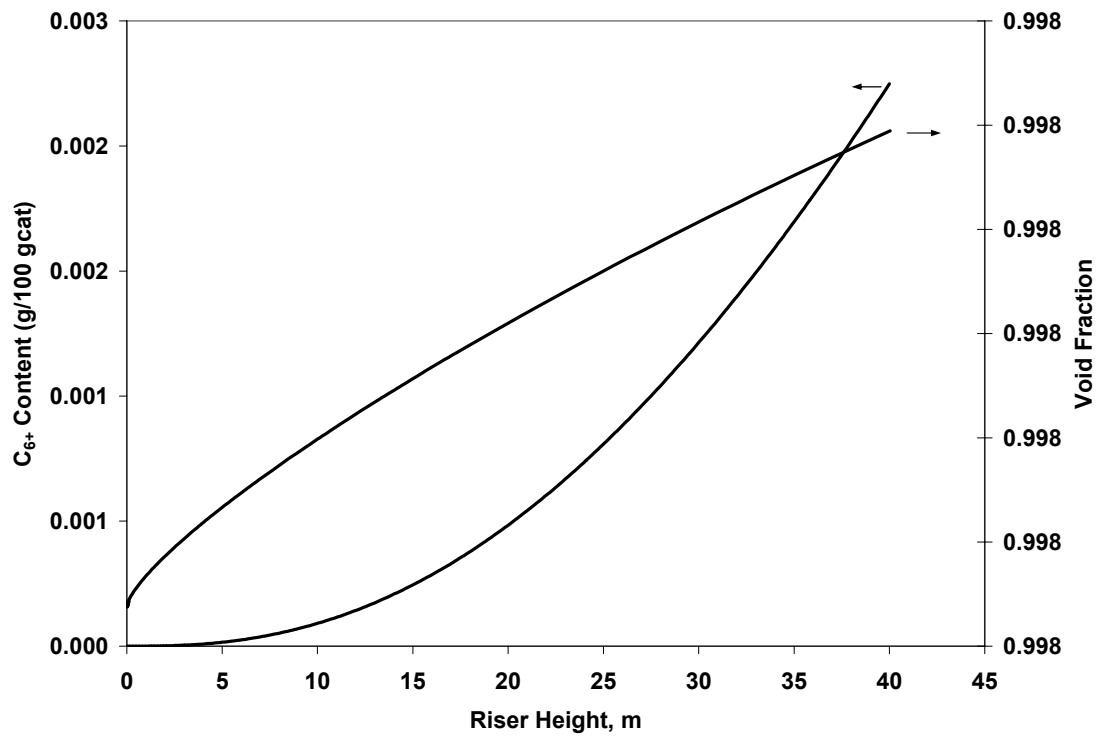


Figure VI-19. C₆₊ olefins content and void fraction profiles along the height of the riser. Feed temperature: 480°C. Methanol mole fraction in the feed: 1.0. Total pressure: 1.04 bar. Flow rates: solid = 196 T/hr, gas = 28 T/hr.

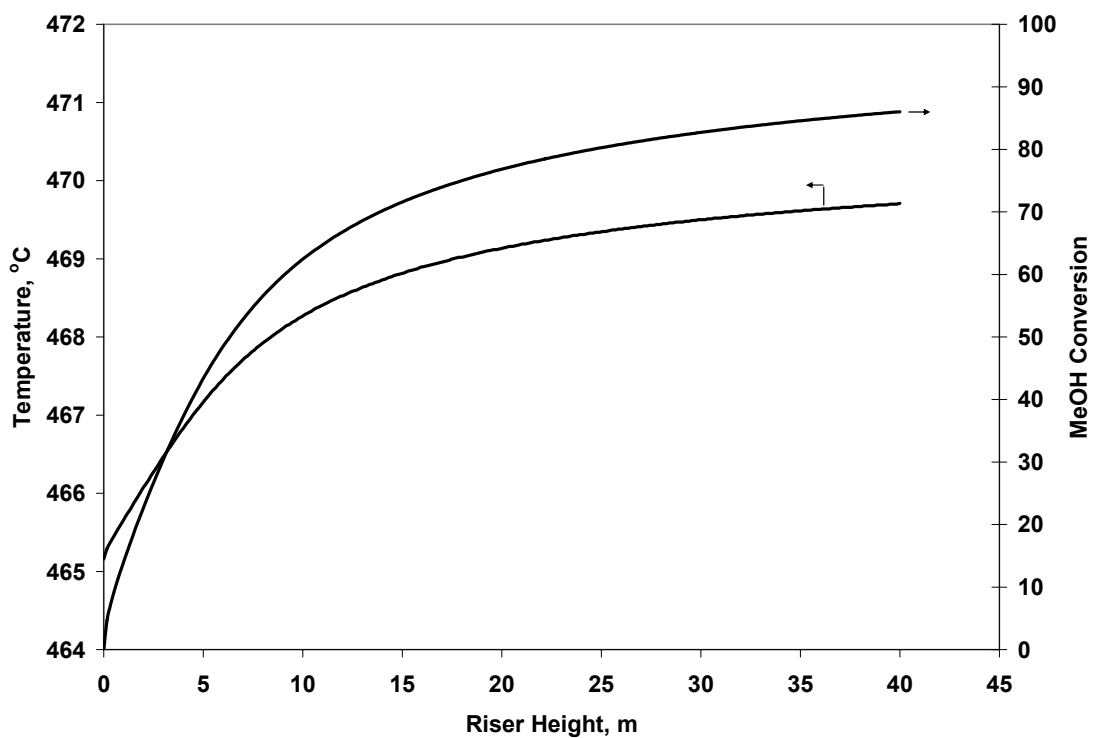


Figure VI-20. Evolution of temperature and methanol conversion along the height of the riser. Feed temperature: 465°C. Methanol mole fraction in the feed: 1.0. Total pressure: 1.04 bar. Flow rates: solid = 4000 T/hr, gas = 28 T/hr.

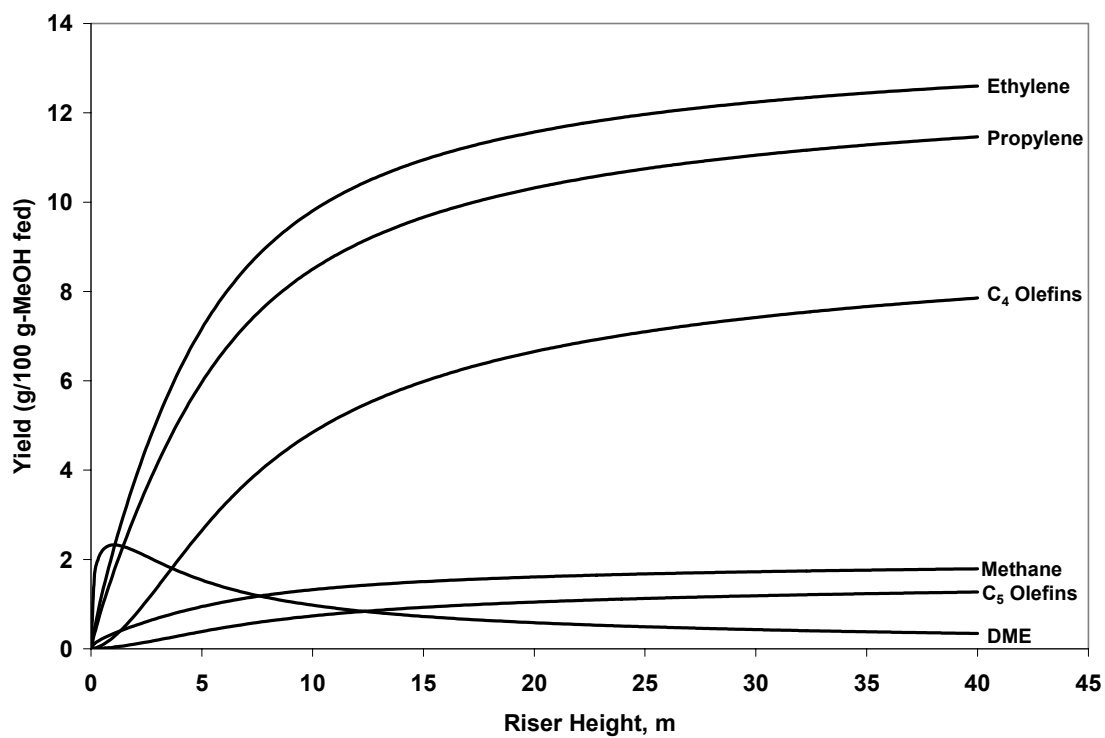


Figure VI-21. Evolution of wt% yields of different products along the height of the riser. Feed temperature: 465°C. Methanol mole fraction in the feed: 1.0. Total pressure: 1.04 bar. Flow rates: solid = 4000 T/hr, gas = 28 T/hr.

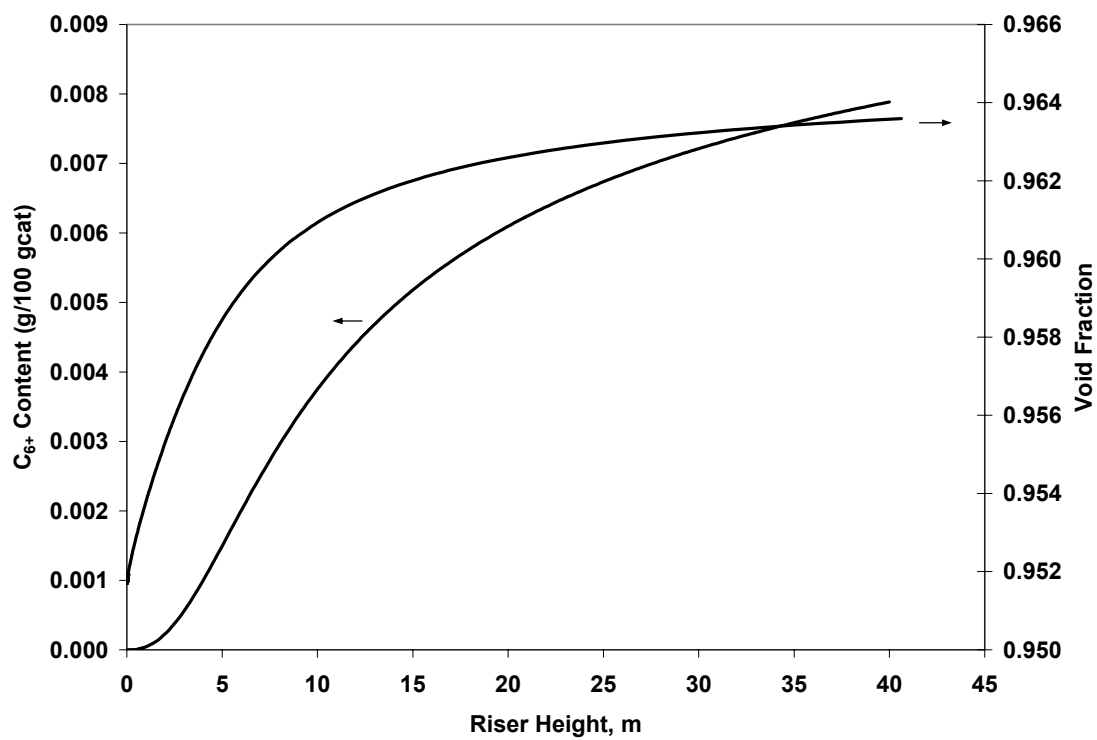


Figure VI-22. C₆₊ olefins content and void fraction profiles along the height of the riser. Feed temperature: 465°C. Methanol mole fraction in the feed: 1.0. Total pressure: 1.04 bar. Flow rates: solid = 4000 T/hr, gas = 28 T/hr.

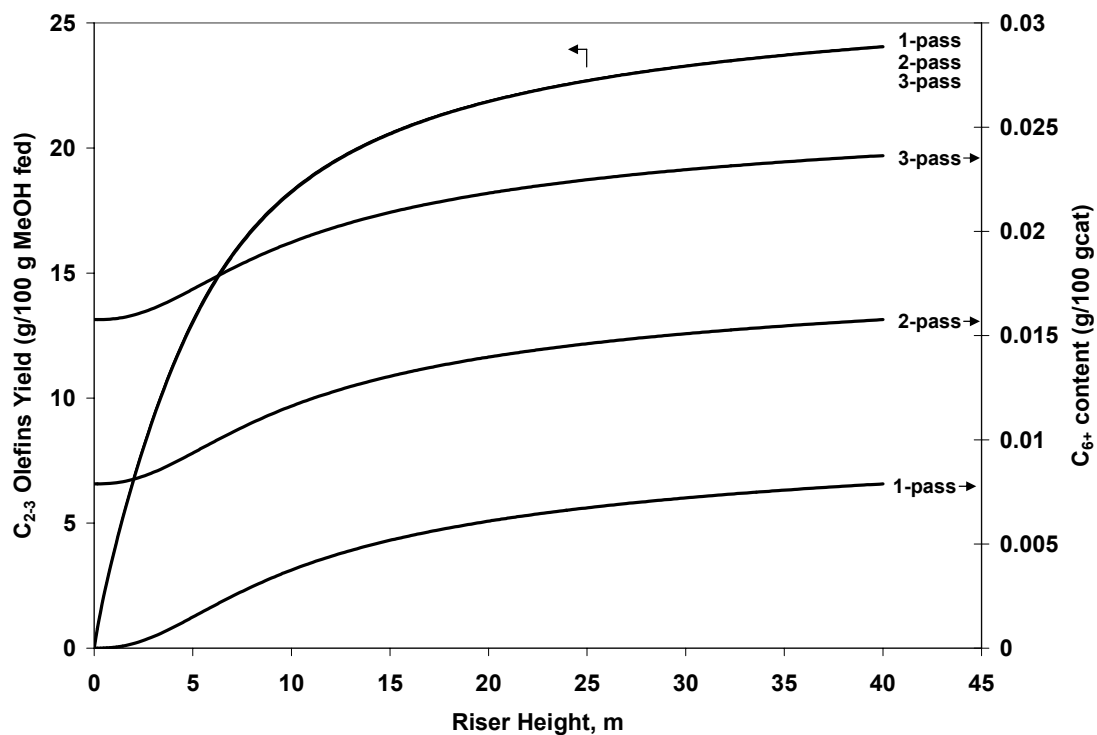


Figure VI-23. The effect of recycling the catalyst without regeneration on the light olefins yield and on the C₆₊ olefins content. Feed temperature: 465°C. Methanol mole fraction in the feed: 1.0. Total pressure: 1.04 bar. Flow rates: solid = 4000 T/hr, gas = 28 T/hr.

Figure VI-23 shows the effect of re-using the catalyst after each cycle, without burning the deposited C_{6+} , on the sum of the yields of ethylene and propylene. The catalyst C_{6+} content at the exit of each cycle is used in the feed of the next cycle. No effect was observed on the light olefins yield, even after 3 recycles. The yield profiles coincide.

Because of the use of high mass flow rate of solid, the amount of C_{6+} deposited on the catalyst is very small and the catalyst deactivation per pass is negligible. As a result, catalyst regeneration would only be required after a large number of passes. This makes the selection of a riser reactor, with its very large catalyst feed rate, for the MTO process unreasonable. A fluidized bed, with lower flow rates of gas and solid, is an alternate. That will be investigated next.

VI.5 Fluidized Bed Reactor

VI.5.1 Mathematical Modeling of MTO in a Fluidized Bed Reactor

In this work, the conversion of methanol to olefins in a bubbling fluidized bed has been modeled using the *two-phase model* developed by May⁶⁶ in 1959. The model was discussed in detail by Van Deemter⁶⁷ and briefly by Froment and Bischoff⁵⁸. According to the model, shown schematically in Figure VI-24, a fraction of the total flow rate through the bed in excess of the minimum fluidization velocity is considered to be in the bubble phase, the rest in the emulsion phase. Between both phases there is a certain interchange of gas. At the outlet, both streams, with their respective conversions, are hypothetically mixed to give the exit stream.

The following assumptions are incorporated in the development of the mathematical model:

- The emulsion phase and the bubble phase are in plug flow.
- The bubble phase is free of catalyst particles, and all reactions occur in the emulsion phase.
- The catalyst in the emulsion phase is completely mixed.
- The ideal gas law applies to the gas in both phases.
- Axial diffusion in the emulsion phase is negligible.
- Both solid and gas enter the reactor at the same temperature.
- An internal heat exchanger is required.
- Because of its high mass flow rate, temperature of the heat transfer medium stays constant.

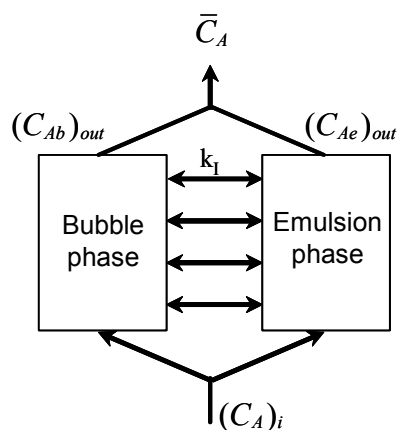


Figure VI-24. Two phase model for fluidized bed reactor.

The steady state continuity equation for component i in the bubble phase is,

$$\frac{dC_{ib}}{dz} = -k_{li} \frac{C_{ib} - C_{ie}}{u_b f_b} \quad (\text{VI-12})$$

In the emulsion phase,

$$\frac{dC_{ie}}{dz} = k_{li} \frac{C_{ib} - C_{ie}}{u_e f_e} + \frac{\mathfrak{R}_i}{u_e f_e} \rho_s \Phi_i f_s \quad (\text{VI-13})$$

where,

$$\Phi_i = \exp(-\alpha C_{C_{6+}}) \quad \text{for olefins formation} \quad (\text{VI-14})$$

$$\Phi_i = \frac{1}{(1 + \beta C_{C_{6+}})} \quad \text{for methanol conversion} \quad (\text{VI-15})$$

The initial conditions are

$$\begin{aligned} C_{ib} &= (C_i)_0 \\ & z = 0 \\ C_{ie} &= (C_i)_0 \end{aligned}$$

The concentration \bar{C}_i measured in the gas flow at the exit is given by,

$$\bar{C}_i = \left(\frac{1}{u_{s,g}} \right) (f_b u_b C_{ib} + f_e u_e C_{ie}) \quad (\text{VI-16})$$

Since the catalyst is assumed to be completely mixed, its C_{6+} olefins content is uniform over the whole bed. It is calculated from,

$$\dot{m}_s C_{C_{6+}} = \dot{m}_s (C_{C_{6+}})_0 + \int_0^Z r_c \rho_s \Phi_c f_s \Omega dz \quad (\text{VI-17})$$

where \dot{m}_s is the feed rate of the catalyst (kg/hr).

Similarly the uniform temperature over the whole bed can be calculated from,

$$T = T_F + \int_0^Z \left(\Omega \frac{\sum r_i (-\Delta H_i) f_s \rho_s \Phi_i - UA_t (T - T_a)}{\sum F_i C_{p_i} + \dot{m}_s C_{p_s}} \right) dz \quad (\text{VI-18})$$

The hydrodynamic and transport property correlations used in this study are given in Table VI-1.

The continuity equations V-12 to V-16 are integrated by the Gear routine. The uniform temperature and uniform concentration of C_{6+} olefins are calculated in an iterative way, starting from assumed values of T and $C_{C_{6+}}$.

Table VI-1. Hydrodynamic and Transport Property Correlations.

Parameter	Theoretical or Empirical Expressions	Ref.
Minimum Fluidization Velocity	$u_{mf} = 1.118 \times 10^{-13} \frac{d_p^{1.82} (\rho_s - \rho_g)^{0.94}}{\rho_g^{0.06} \mu^{0.88}} \quad (\text{VI-19})$	68
Bubble diameter	$d_b = 0.00853 [1 + 27.2(u_{s,g} - u_{mf})]^{1/3} (1 + 6.84z)^{1.21} \quad (\text{VI-20})$	69
Bubble rising velocity	<p>where</p> $u_b = u_{s,g} - u_{mf} + u_{br} \quad (\text{VI-21})$ $u_{br} = 1.6 \sqrt{d_b g}$	69
Emulsion gas velocity	$u_e = \frac{u_{mf}}{\varepsilon_{mf}} \quad (\text{VI-22})$	62
Bubble fraction	$f_b = \frac{u_{s,g} - u_{mf}}{u_b} \quad (\text{VI-23})$	62
Solid fraction	$f_s = \frac{u_{s,p}}{u_{s,p} + u_{s,g}} \quad (\text{VI-24})$	62
Emulsion gas fraction	$f_e = 1 - f_b - f_s \quad (\text{VI-25})$	62
Bubble-emulsion phase transfer coefficient	$k_I = f_b (k_{be})_{jb} \quad (\text{VI-26})$ $\frac{1}{(k_{be})_{jb}} = \frac{1}{(k_{bc})_{jb}} + \frac{1}{(k_{ce})_{jb}}$ $(k_{bc})_{jb} = 4.5 \frac{u_{mf}}{d_b} + 5.85 \left(\frac{D_{bcj}^{1/2} g^{1/4}}{d_b^{5/4}} \right)$ $(k_{ce})_{jb} = 6.78 \left(\frac{\varepsilon_{mf} D_{cej} u_b}{d_b^3} \right)^{1/2}$	62

Table VI-1. (Continued).

Parameter	Theoretical or Empirical Expressions	Ref.
Diffusivity of component j in the bubble gas mixture	$D_{bcj} = \frac{(1 - y_{jb})}{\left(\sum_{i=1, i \neq j}^n \left(\frac{y_{ib}}{D_{ji}} \right) \right)}$ (VI-27)	70
Diffusivity of component j in the emulsion gas mixture	$D_{cej} = \frac{(1 - y_{je})}{\left(\sum_{i=1, i \neq j}^n \left(\frac{y_{ie}}{D_{ji}} \right) \right)}$ (VI-28)	70
Binary diffusivity	$D_{ij} = \frac{0.00143T^{1.75}}{PM_{ij}^{1/2} \left[(\sum_v)_i^{1/3} + (\sum_v)_j^{1/3} \right]^2}$ (VI-29)	70
Gas components thermal conductivity	$\lambda_i = 3.75 \times 10^3 \frac{\mu_i \Psi_i R}{M_i}$ (VI-30) where $\Psi = 1 + \alpha \left\{ \frac{[0.215 + 0.28288\alpha - 1.061\beta + 0.26665Z]}{[0.6366 + \beta Z + 1.061\alpha\beta]} \right\}$ $\alpha = (C_v/R) - 3/2$ $\beta = 0.7862 - 0.7109\omega + 1.3168\omega^2$ $Z = 2.0 + 10.5T_r^2$	70
Gas mixture thermal conductivity	$\lambda_g = \frac{\sum_{i=1}^n y_i \lambda_i}{\sum_{j=1}^n y_j \phi_{ij}}$ (VI-31) $\phi_{ij} = \frac{\left[1 + (\mu_i / \mu_j)^{1/2} (M_j / M_i)^{1/4} \right]^2}{\left[8(1 + M_i / M_j) \right]^{1/2}}$	70
Gas components viscosity	$\mu_i = 40.785 \frac{F_c (MT)^{1/2}}{V_c^{2/3} \Omega_v}$ (VI-32)	70

Table VI-1. (Continued).

Parameter	Theoretical or Empirical Expressions	Ref.
Gas mixture viscosity	$\mu_g = \frac{\sum_{i=1}^n y_i \mu_i}{\sum_{j=1}^n y_j \phi_{ij}}$ <p style="text-align: right;">(VI-33)</p>	70
Gas mixture density	$\rho_g = \frac{1}{MV} \sum_{i=1}^n \frac{M_i}{w_i}$ <p style="text-align: right;">(VI-34)</p>	58
Heat transfer coefficient on the bed side	$\alpha = 0.033 \left(\frac{f_s \lambda_g}{d_p} \right) \left(\frac{\lambda_g}{C_{pg} \rho_g} \right)^{-0.43} \left(\frac{d_p G}{\mu} \right)^{0.23} \left(\frac{C_{ps}}{C_{pg}} \right)^{0.8} \left(\frac{\rho_s}{\rho_g} \right)^{0.66}$ <p style="text-align: right;">(VI-35)</p>	71
Heat transfer coefficient, heat transfer medium side	$\frac{\alpha_u d_{tu}}{\lambda_u} = 0.027 \left(\frac{d_{tu} G_u}{\mu_u} \right)^{0.8} \left(\frac{C_{pu} \mu_u}{\lambda_u} \right)^{1/3}$ <p style="text-align: right;">(VI-36)</p>	58

VI.5.2 Simulation Results

The simulation of the MTO process on SAPO-34 in a bubbling fluidized bed reactor was based on the two-phase model discussed before. Table VI-2 shows the reactor and the heat exchanger design data utilized in the simulation. Operating conditions were chosen based on a production rate of 55,000 tons/year of ethylene and propylene.

The output of the simulation was found to be very dependant on the bubble size. When Werther's correlation, Eq. VI-20, was used to calculate the bubble in the 15.0 m high fluidized bed reactor, the calculated bubble size was on the order of meters. Mass transfer from such an enormous bubble is so poor that it limits the ability of reaction to take place. This bubble size is not realistic and never takes place in an industrial vessel.⁷² Bubbles, certainly, grow as they rise inside the bed, eventually, however, they will reach a maximum size where they become unstable and start breaking up into smaller bubbles.

Unfortunately, Werther's correlation can only predict the bubble size in a small size laboratory bed.

In this work, the bubble size was estimated using Figure 6-7 in Kunii and Levenspiel⁶³. The figure presents the bubble growth profiles in a bed of fine particles. The bubble was shown to grow within a few centimeters in size above the inlet and stay at that size as a result of equilibrium between coalescence and splitting. A constant bubble size of 4 cm was chosen for the current fluidized bed.

Table VI-2. Data Used in the Fluidized Bed Reactor Simulation.

Reactor Geometry	
Reactor diameter, d_t	8.5 m
Reactor height, Z	15.00 m
Catalyst properties	
Catalyst average diameter, \bar{d}_p	8×10^{-5} m
Catalyst density, ρ_s	1500
Catalyst heat capacity, C_{ps}	1.003 kJ/kg K
Operating conditions	
Solid mass flow rate, \dot{m}_s	280 tons/hr
Gas mass flow rate, \dot{m}_g	28 tons/hr
Methanol feed mole fraction, y_M°	1.0
Feed temperature, T_f	430°C
Pressure, P	1.04 bar
Bed void fraction at minimum fluidization, ε_{mf}	0.55
Heat exchanger Geometry	
Height of cooling tubes, H	7.00 m
Diameter of cooling tubes, d_{tu}	0.035 m
Pitch (square tube arrangement)	0.25 m
Number of cooling tubes, N_t	910
Heat transfer medium properties	
Dowtherm A (liquid)	
Viscosity, μ_u	3.8×10^{-4} kg/m s
Heat capacity, C_{pu}	2.093 kJ/kg K
Thermal conductivity, λ_u	1.09×10^{-4} kW/m K
Density, ρ_u	902.5 kg/m ³
Cooling fluid mass flow rate, G_u	2.7×10^3 kg/m ² s
Cooling fluid temperature, T_u	205°C

Figure VI-25 shows the profiles of the bubble and emulsion gas velocities and volume fractions along the reactor. The profiles are almost flat except in a small region near the entrance of the bed where the gas is being heated by the catalyst.

The profiles of evolution of the conversion of methanol and the wt% yields of different products is shown in Figure VI-26 for a feed temperature of 430°C. Methanol conversion was limited to 90%. Propylene and ethylene yields amount to 13 and 12 wt% respectively. Methane yield, on the other hand, is less than 0.8 wt%.

Due to the exothermicity of the process, the uniform reaction temperature was found to be 451°C. On the other hand, the uniform C₆₊ concentration in the bed amounts to 0.15%. This has to be removed by controlled combustion in the regenerator. The bed temperature, 451°C, is relatively low. The size of the reactor could be decreased if the bed temperature were higher. However, higher temperature favors methane yield as well.

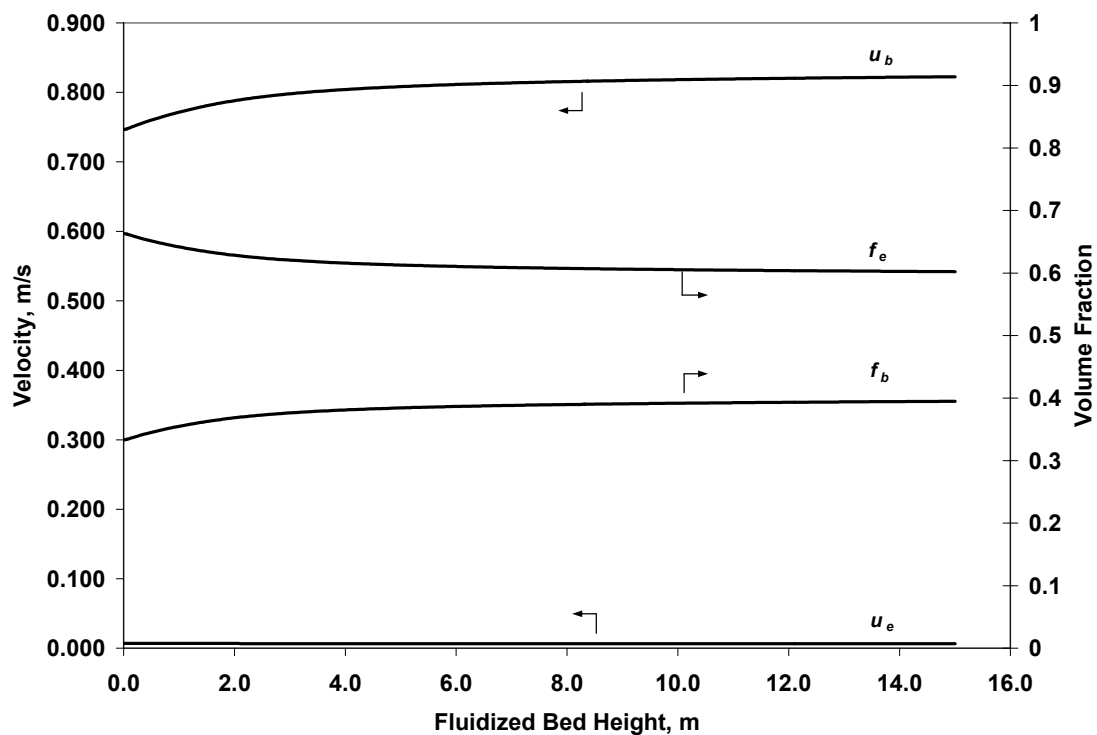


Figure VI-25. Evolution of the bubble and emulsion gas velocities and the volume fraction taken by the bubble phase and by the emulsion gas along the height of the fluidized bed reactor. Feed temperature: 430°C. Methanol mole fraction in the feed: 1.0. Total pressure: 1.04 bar.

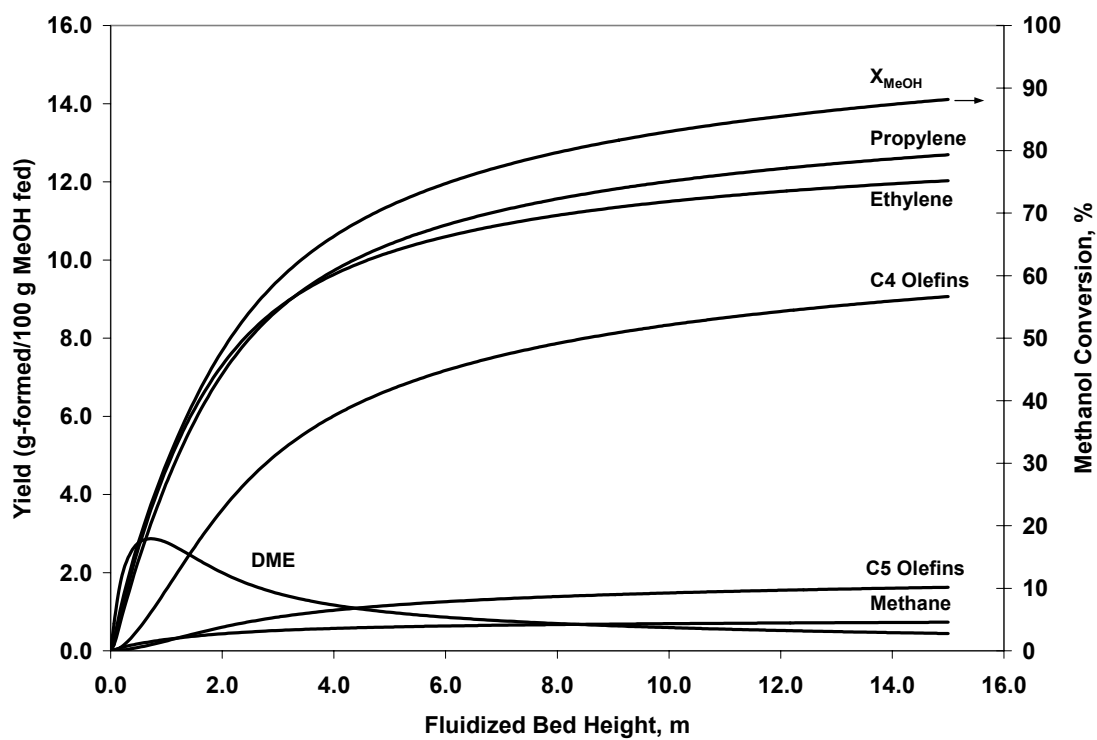


Figure VI-26. Evolution of methanol conversion and wt% yields of different products along the height of the fluidized bed reactor. Feed temperature: 430°C. Methanol mole fraction in the feed: 1.0. Total pressure: 1.04 bar.

CHAPTER VII

TECHNOLOGY EVALUATION

So far, two reactor configurations show good potential for the industrial process for the conversion of methanol to olefins, namely, fluidized bed and multi-bed adiabatic reactor configurations. The riser reactor option has been excluded for the reasons already discussed.

The comparison between the fluidized bed and the multi-bed adiabatic reactors was performed based on a production rate of 55,000 tons/year of ethylene and propylene.

Figure VI-9 was used to evaluate the performance of the MTO on SAPO-34 in a multi-bed adiabatic reactor after 40 minutes process time. In the simulation, the combined yield of ethylene and propylene was around 25% at a space time of 14.0 (g cat · hr/mol). The required flow rate of methanol to the reactor, then, becomes: $55000 / (25/100) = 220,000$ tons/year or 28 tons/hr with the 8,000 hrs/year basis.

The amount of catalyst needed is: $\frac{28000(\text{kg/hr})}{32(\text{kg/kmol})} \times 14(\text{kgcat} \cdot \text{hr/kmol}) = 12.25$ tons

At least two reactors are needed for cycling between reaction and regeneration, thus the total amount of catalyst needed is around 25 tons.

On the other hand, Figure VI-26 was used to evaluate the performance of the MTO process in the bubbling fluidized bed reactor. As in the case of the multi-bed reactor, the

combined yield of ethylene and propylene was 25%. Similarly, the required feed of methanol is: 28 tons/hr.

$$\text{Volume of the reactor: } \left(\frac{\pi d_i^2}{4}\right) \cdot Z = 56.7 \text{ m}^3$$

$$\text{Average bed density: } \rho_s \cdot f_s = 60 \text{ kg/m}^3$$

Therefore, the amount of catalyst at any time in the reactor is approximately,

$$60(\text{kg/m}^3) \times 56.7(\text{m}^3) \approx 3.4 \text{ tons}$$

A similar amount will be present at any time in the regenerator. Thus the total amount of catalyst needed is around 7 tons. This is a consequence of the heat transfer between the fluidized bed and the internal heat exchanger. The beds of the multi-bed adiabatic reactor have to be fed at low temperature to allow for the ΔT and keep the exit temperatures of the beds below a certain limit.

Therefore, to produce the same amount of ethylene and propylene in the multi-bed adiabatic reactor, the amount of catalyst needed will be roughly four times that in the fluidized bed reactor. This is of course at 40 minutes process time for the multi-bed reactor. If a longer process time is chosen, more catalyst will be required.

So if the amount of catalyst is the only factor in deciding which configuration to choose, the fluidized bed reactor is the more favorable option. However, more factors will have to be considered, mainly, construction and operational cost.

CHAPTER VIII

CONCLUSION AND RECOMMENDATIONS

The objectives of this research as stated earlier were as follows:

- 1) Develop a kinetic model for the formation of olefins from methanol on SAPO-34.
 - a) Write the model in terms of elementary steps without any lumping neither of components nor of steps.
 - b) Estimate the kinetic parameters using the experimental data of Abraha¹ and verify the model prediction using the experimental data of Marchi and Froment.²
- 2) Develop a deactivation model.
 - a) Relate the rate of coke production to the rate of production of C₆₊ olefins trapped inside the cavity of SAPO-34.
 - b) Estimate the deactivation parameters using the data of Marchi and Froment.
 - c) Use the model to explain the observed catalyst deactivation phenomena.
- 3) Combine the kinetic and the deactivation model and utilize them to:
 - a) Investigate the influence of the operating conditions on the product distribution in a multi-bed adiabatic reactor with plug flow.
 - b) Study the conceptual design of riser and fluidized bed reactors for MTO.

The kinetics of the formation of olefins from methanol on SAPO-34 was found to be well described by the model developed based upon oxonium methylene mechanism in the primary products formation followed by methylation, oligomerization, and cracking

based upon carbenium ion mechanism. The model not only agrees well with the experimental data, but also it was able to reproduce data obtained in a different lab and setup.

In the generated network, the number of elementary steps and the number of rate parameters was far too high to be determined accurately by conventional methods. The single-event concept and the Evans-Polanyi relation were essential in reducing the number of parameters to a tractable size.

The single-event concept, also, permitted prediction of the production rate of C_{6+} species, trapped inside the cavities of SAPO-34, and which can not be detected experimentally. The knowledge of the C_{6+} yield is essential for modeling the deactivation of the catalyst. The conversion of methanol to dimethylether and the subsequent conversion of the latter into olefins were found to be affected in a different way by deactivation. While olefins production decreases to zero, methanol conversion was found to drop and stabilize at a non-zero value. This was attributed to the easy nature of methanol conversion into DME, requires only weak acid sites, with respect to olefins production which requires strong acid sites. With deactivation, the strong acid sites are either covered or are not accessible because of blockage of pore structure. Weak acid sites, however, can be still found in the external surface of the catalyst.

The effect of water on the deactivation of SAPO-34 was also reflected in the developed deactivation model. Two different values of the deactivation parameters were found to be necessary to account for the effect of water.

In the conceptual design of the MTO reactor, multi-bed adiabatic, riser and fluidized bed technologies were evaluated. All but the riser configuration show good potential for the industrial process for the conversion of methanol to olefins.

The results of this research point to the following recommendations for future work:

- Investigate the effect of the acidity of SAPO-34 on increasing the rate of β -scission which is essential for decreasing the deactivation of the catalyst by C_{6+} components. Increasing the β -scission rate, however, should not affect the ethylene and propylene yields.
- Structure of the catalyst, as well, plays an important role in decreasing the deactivation of the catalyst. The catalyst structure can be chosen so as to reduce the C_{6+} production and therefore reduce the catalyst deactivation.
- In this work, the MTO process was simulated in a bubbling fluidized bed and in a riser reactor. Turbulent fluidized bed regime, which is an intermediate regime between the bubbling fluidized bed and the riser, might be recommended for commercial operation because of its high efficiency related to the absence of bubbles. Accurate modeling of turbulent fluidized bed would require computational fluid dynamics, beyond the scope of this thesis.

NOMENCLATURE

A'	Preexponential factor of an elementary step	
\tilde{A}	Single-event Preexponential factor	
A_t	Total heat exchange surface	m^2
C_{bs}^t	Total concentration of basic sites	$kmol/kg \text{ cat.}$
$C_{H^+}^t$	Total concentration of acidic sites	$kmol/kg \text{ cat.}$
$C_{C_{6+}}$	Weight content of C_{6+} olefins inside the catalyst	$kg/kg \text{ cat.}$
C_D	Drag coefficient for spheres	
C_{ib}	Concentration of component i in the bubble phase	$kmol/m_b^3$
C_{ie}	Concentration of component i in the emulsion phase	$kmol/m_{eg}^3$
\bar{C}_i	Concentration of component i at the exit of the of the bubble and emulsion phase	$kmol/m_f^3$
C_{pg}	Specific heat of gas	$kJ/kg \text{ K}$
C_{ps}	Specific heat of solid	$kJ/kg \text{ K}$
D_{ij}	Molecular diffusivity of i in a binary mixture of i and j	$m_f^2/m_f \text{ s}$
D_{bcj}, D_{cej}	Diffusivity of component j in the bubble and emulsion gas mixtures respectively	$m_f^2/m_f \text{ s}$
d_b	Bubble diameter	m
\bar{d}_p	Average particle diameter	m
d_t	Reactor diameter	m
E_a°	Intrinsic activation barrier in the Evans-Polanyi relation	$kJ/kmol$

f_b	Fraction of total fluidized bed volume occupied by bubble gas	m_b^3/m_r^3
f_e	Fraction of total fluidized bed volume occupied by emulsion gas	m_{eg}^3/m_r^3
f_s	Fraction of total fluidized bed volume occupied by solid	m_s^3/m_r^3
G	Superficial gas flow velocity	$kg/m_r^2 s$
g	Acceleration of gravity	m/s^2
h	Plank constant: 1.841×10^{-37}	J hr
H	Cooling tubes length	m
K_i	Equilibrium constant for an elementary step i	
k_B	Boltzmann constant: 1.381×10^{-23}	J/K
k'_i	Rate coefficient for an elementary step i	
$k'_i(j, k)$	Rate coefficient for an elementary step of type i at j th category and k th reaction	
\tilde{k}	Single-event rate coefficient	
k_I	Bubble-emulsion phase interchange coefficient	$m_r^3/m_b^3 s$
$(k_{bc})_b$	Mass transfer coefficient from bubble to interchange zone, referred to unit bubble volume	$m_r^3/m_b^3 s$
$(k_{be})_b$	Overall mass transfer coefficient from bubble to emulsion, referred to unit bubble volume	$m_r^3/m_b^3 s$
$(k_{ce})_b$	Mass transfer coefficient from interchange zone to emulsion, referred to unit bubble volume	$m_r^3/m_b^3 s$
M_j	Molecular weight of species j	kg/kmol
\dot{m}	Mass flow rate	kg/s
N_t	Number of cooling tubes	

n_e	Number of single events	
O_{ij}	An olefin with carbon number i and isomer index j	
P_i	Partial pressure of gas-phase species i	bar
$q(i)$	Heat of stabilization of species i	kJ/kmol
R_{ij}^+	An olefin with carbon number i and isomer index j	
S°	Standard entropy	kJ/kmol K
\mathfrak{R}_i	Net reaction rate for gas phase species i	kmol/kg cat . hr
R	Gas constant: 8.314	kJ/kmol K
$r_i(j, k)$	Reaction rate for an elementary step of type i at j th category and k th reaction	kmol/kg cat . hr
T_a	Cooling fluid temperature	K
u_b	Bubble rise velocity, absolute	m _r /s
u_{br}	Bubble rise velocity, with respect to emulsion phase	m _r ³ /m _r ² s
u_e	Emulsion gas velocity	m _r /s
u_{mf}	Minimum fluidization velocity	m _r /s
$u_{s,g}$	Superficial gas velocity	m _r ³ /m _r ² s
$u_{s,p}$	Superficial solid velocity	m _p ³ /m _r ² s
u_t	Terminal velocity of particle	m _r /s
W	Total catalyst mass	kg cat .
\hat{y}_i	Yield of species i	kg/100 kg MeOH fed

Greek Letters

α	Transfer coefficient in the Evans-Polanyi relation	
ν_i	Fractional coverage of surface species i	
ΔH^{\ddagger}	Standard enthalpy of activation	kJ/kmol
$\Delta H_f^\circ(i)$	Standard enthalpy of formation for species i	kJ/kmol
$\Delta H_i(j, k)$	Heat of reaction for an elementary step of type i at j th category and k th reaction	kJ/kmol
$\Delta H_{pr}^\circ(i)$	Heat of protonation for gas phase species i	kJ/kmol
ΔG_i	Standard Gibb's free energy change of reaction type i	kJ/kmol
ΔS^{\ddagger}	Standard entropy of activation	kJ/kmol K
σ	Symmetry number	
σ_{gl}^i	Global symmetry number of species i	
τ	Space time of methanol	kg hr/kmol

LITERATURE CITED

- 1 Abraha, M. *Methanol to Olefins: Enhancing Selectivity to Ethylene and Propylene Using SAPO-34 and Modified SAPO-34*. Ph.D. Dissertation, Chem. Eng. Dept., Texas A&M University, **2001**.
- 2 Marchi, A. J.; Froment, G. F. Catalytic Conversion of Methanol to Light Alkenes on SAPO Molecular Sieves. *Appl. Catal.* **1991**, 71, 139.
- 3 Ethylene Demand, Capacity to Rise Through 2010. *Oil & Gas J.* **1999**, 97, 48-.
- 4 CMAI World Propylene Supply Study. *CMAI Report* **2001** www.cmaiglobal.com.
- 5 Chenier, P. J. *Survey of Industrial Chemistry*, 3rd Edition, Kluwer Academic Publishers Inc. New York, New York **2002**.
- 6 Venner, R.; Kantorowicz, S. Metathesis: Refinery and Ethylene Plant Application, in *Proceedings of the European Petrochemical Technology Conference (EPTC)*, Vienna, Austria, **2001**.
- 7 Chen, T. J.; Ruziska, P. A.; Stuntz, G. F.; Ladwig, P. K. Multiple Feed Process for the Production of Propylene, *U.S. Patent* No. 6,339,181, January 15, **2002**.
- 8 Propylur Rout Boosts Propylene Production. *European Chemical News* **2000**, 72, 47.
- 9 Fu, A. Deep Catalytic Cracking Plant Produces Propylene in Thailand. *Oil & Gas J.* **1998**, 96, 49-52.
- 10 Picciotti, M. New Ethylene Routes are Available but Economics Inhibit Their Use. *Oil & Gas J.* **1997**, 95, 71-74.
- 11 *Kirk-othmer, Encyclopedia of Chemical Technology*, 4th edition, John Wiley & Sons publishers New York, New York **1993**.
- 12 Cavani, F.; Trifiro, F. The Oxidative Dehydrogenation of Ethane and Propane as an Alternative Way for the Production of Light Olefins. *Catal. Today* **1995**, 24, 307-313.
- 13 Weyten, H.; Luyten, J.; Keizer, K.; Willems, L.; Leysen, R. Membrane Performance: The Key Issues for Dehydrogenation Reactions in a Catalytic Membrane Reactor. *Catal. Today* **2000**, 56, 3-11.

- 14 Wolf, D.; Dropka, N.; Smejkal, Q.; Buyevskaya, O. Oxidative Dehydrogenation of Propane for Propylene Production – Comparison of Catalytic Processes. *Chem. Eng. Sci.* **2001**, 56, 713-719.
- 15 Keller, G. E.; Bhasin, M. M. Synthesis of Ethylene via Oxidative Coupling of Methane. *J.Catal.* **1982**, 73, 9.
- 16 Hinsien, W.; Bytyn, W.; Baerns, M. Oxidative Dehydrogenation and Coupling of Methane, In *Proceedings of the 8th International Congress on Catalysis*, Berlin **1984** 3, 581.
- 17 Ito, T.; Wang, J. X.; Lin, C. H.; Lunsford, J. H. Oxidative Dimerization of Methane over a Lithium-Promoted Magnesium Oxide Catalyst. *J.Am.Chem.Soc.* **1985**, 107, 5062.
- 18 Burch, R.; Squire, G. D.; Tsang, S. C. Role of Chlorine in Improving Selectivity in the Oxidative Coupling of Methane to Ethylene. *Appl. Catal.* **1989**, 46, 69-87.
- 19 Diddams, P. A.; Little, I. R.; Wade, S. R. Chemical Process and Catalyst to be Used Therein. *U.S. Patent* No. 5,051,390 September 24, **1991**.
- 20 Lunsford, J. H. Catalytic Conversion of Methane to more Useful Chemicals and Fuels: a Challenge for the 21st Century. *Catal. Today* **2000**, 63, 165-174.
- 21 Froment, G. F.; Dehertog, W. J. H.; Marchi, A. J. Zeolite Catalysis in The Conversion of Methanol into Olefins. *Catalysis* **1992**, 9, 1-64.
- 22 Keil, F. J. Methanol-to-hydrocarbons: Process Technology. *Micropor. Mesopor. Mat.* **1999**, 29, 49-66.
- 23 Dehertog, W. J. H.; Froment, G. F. Production of Light Alkenes from Methanol on ZSM-5 Catalysts. *Appl. Catal.* **1991**, 71, 153.
- 24 Chang, C. D. *Hydrocarbons from Methanol*, Marcel Dekker: New York 1983.
- 25 Hammon, U.; Kotter, M.; Riekert L. Production of Low Olefins from Methanol with Partial Conversion and Recycling. *Chem. Ing. Tech.* **1989**, 61, 151.
- 26 Chang, C. D. Methanol Conversion to Light Olefins. *Catal. Rev. Sci. Eng.* **1984**, 26, 323.
- 27 Kaiser, S. W. Production of Light Olefins. *U.S. Patent* No. 4,499,327, February 12, **1985**.

- 28 Socha, R. F.; Chang, C. D.; Gould, R. M.; Kane, S. E.; Avidan, A. A. Fluid-Bed Studies of Olefin Production from Methanol. *Am. Chem. Soc. Symp. Series* **1987**, 328, 34-41.
- 29 Vora, B. V.; Marker, T. L.; Barger, P. T.; Nilsen, H. R.; Kvisle, S.; Fuglerud, T. Economic Route for Natural Gas Conversion to Ethylene and Propylene. *Stud Surf Sci Catal* **1997**, 107, 87-98.
- 30 Vora, B. V.; Marker, T.; Arnold, E. C.; Nilsen, H.; Kvisle, S.; Fuglerud, T. Conversion of Natural Gas to Ethylene and Propylene: The Most-Profitable Option. *Stud Surf Sci Catal* **1998**, 119, 955-960.
- 31 Vora, B. V.; Lentz, R. A.; Marker, T. L. UOP/Hydro MTO Process: the Critical Link in Upgrading Natural Gas to Olefins. *World Petrochemical Conference Chemical Market Associates Inc.* Houston, TX, **1996**.
- 32 Kokotailo, G. T.; Lawton, S. L.; Olson, D. H.; Meier, W. M. Structure of Synthetic Zeolite ZSM-5. *Nature* **1978**, 272, 437-438.
- 33 Dent, L. S.; Smith, J. V. Crystal Structure of Chabazite, A Molecular Sieve. *Nature* **1958**, 181, 1794-1796.
- 34 Derouane, E. G. *Catalysis by Acids and Bases*. Elsevier: Amsterdam, **1985**.
- 35 Anderson, J. R.; Mole, T.; Christov, V. Mechanism of Some Conversions over ZSM-5 Catalyst. *J. Catal.* **1980**, 61, 477.
- 36 Wu, Xianchun.; Anthony, R. G. Effect of Feed Composition on Methanol Conversion to Light Olefins Over SAPO-34. *Appl. Catal.* **2001**, 218, 241.
- 37 Lok, B. M.; Messina, C. A.; Patton, R. L.; Gajek, R. T.; Cannan, T. R.; Flanigen, E. M. Silicoaluminophosphate Molecular-sieves : Another New Class of Microporous Crystalline Inorganic Solids. *J. Am. Chem. Soc.* **1984**, 106, 6092.
- 38 Rodewald, P. G. Manufacture of Light Olefins. *U.S. Patent* No. 4,066,714, January 3, **1978**.
- 39 Kaeding, W. W.; Butter, S. A. Conversion of Methanol and Dimethyl Ether. *U.S. Patent* No. 3,911,041, October 7, **1975**.
- 40 Al-Jarallah, A. M.; El-Nafaty, U. A.; Abdillahi, M. M. Effect of Metal Impregnation on the Activity, Selectivity and Deactivation of a High Silica MFI Zeolite When Converting Methanol to Light Alkenes. *Appl. Catal.* **1997**, 154, 117.

41 Inui, T.; Phatanasri, S.; Matsuda, H. Highly Selective Synthesis of Ethene from Methanol on a Novel Nickel Silicoaluminophosphate Catalyst. *J. Chem. Soc. Chem. Comm.* **1990**, 205.

42 Vanniekerk, M. J.; Fletcher, J. C. Q.; O'Connor, C. T. Effect of Catalyst Modification on the Conversion of Methanol to Light Olefins over SAPO-34. *Appl. Catal.* **1996**, 138, 135.

43 Inui, T.; Kang, M. Reliable Procedure for the Synthesis of Ni-SAPO-34 as a Highly Selective Catalyst for Methanol to Ethylene Conversion. *Appl. Catal.* **1997**, 164, 211.

44 Park, T. Y.; Froment, G. F. Kinetic Modeling of the Methanol to Olefins Process. 1. Model Formulation. *Ind. Eng. Chem. Res.* **2001**, 40, 4172.

45 Park, T. Y.; Froment, G. F. Kinetic Modeling of the Methanol to Olefins Process. 2. Experimental Results, Model Discrimination, and Parameter Estimation. *Ind. Eng. Chem. Res.* **2001**, 40, 4187.

46 Hutchings, G. J.; Hunter, R. Hydrocarbon Formation from Methanol and Dimethylether: A Review of the Experimental Observations Concerning the Mechanism of Formation of the Primary Products, *Catal. Today* **1990**, 6, 279.

47 Chen, N. Y.; Reagan, W. J. Evidence of Autocatalysis in Methanol to Hydrocarbon Reactions over Zeolite Catalysts. *J. Catal.* **1979**, 59, 123.

48 Chang, C. D. Kinetic Model for Methanol Conversion to Hydrocarbons. *Chem. Eng. Sci.* **1980**, 35, 619.

49 Schoenfelder, H.; Hinderer, J.; Werther, J.; Keil, F. Methanol to Olefins Prediction of the Performance of a Circulating Fluidized-Bed Reactor on the Basis of Kinetic Experiments in a Fixed-Bed Reactor. *Chem. Eng. Sci.* **1994**, 49, 5377.

50 Bos, A. N. R.; Tromp, P. J. J. Conversion of Methanol to Lower Olefins. Kinetic Modeling, Reactor Simulation, and Selection. *Ind. Eng. Chem. Res.* **1995**, 34, 3808.

51 Baltanas, M. A.; Van Raemdock, K. K.; Froment, G. F.; Mohedas, S. R. Fundamental Kinetic Modeling of Hydroisomerization and Hydrocracking on Noble-Metal Loaded Faujasites. *Ind. Eng. Chem. Res.* **1989**, 28, 899.

52 Vynckier, E.; Froment, G. F. Modeling of the Kinetics of the Complex Processes Based upon Elementary Steps. In *Kinetic and Thermodynamic Lumping of Multicomponent Mixtures*; Astarita, G., Sandler, S. I., Eds.; Elsevier: Amsterdam, Netherlands, 1991.

- 53 Feng, W.; Vynckier, E.; Froment, G. F. Single Event Kinetics of Catalytic Cracking. *Ind. Eng. Chem. Res.* **1993**, 32, 2997.
- 54 Svoboda, G. D.; Vynckier, E.; Debrabandere, B.; Froment, G. F. Single Event Rate Parameters for Paraffins Hydrocracking on Pt/US-Y Zeolite. *Ind. Eng. Chem. Res.* **1995**, 34, 3793.
- 55 Baltanas, M. A.; Froment, G. F. Computer Generation of Reaction Networks and Calculation of Product Distributions in the Hydroisomerization and Hydrocracking of Paraffins on Pt-containing Bifunctional Catalysts. *Comput. Chem. Eng.* **1985**, 9, 71.
- 56 Dewachtere, N.; Santaella, F.; Froment, G. F. Application of a Single Event Kinetic Model in the Simulation of an Industrial Riser Reactor for the Catalytic Cracking of Vacuum Gas Oil. *Chem. Eng. Sci.* **1999**, 54, 3653.
- 57 Evans, M.; Polanyi, M. Inertia and Driving Force of Chemical Reactions. *Trans. Faraday Soc.*, **1938**, 31, 11.
- 58 Froment, G. F.; Bischoff, K. B. *Chemical Reactor Analysis and Design*, 2nd ed.; John Wiley: New York, 1990.
- 59 Boudart, M.; Mears, D. E.; Vannice, M. A. *Ind. Chim. Belge.* **1967**, 32, 281.
- 60 Park, T.Y.; Froment, G. F. A Hybrid Genetic Algorithm for the Estimation of the Parameters in Detailed Kinetic Models. *Comput. Chem. Eng.* **1998**, 22, S103.
- 61 Hammond, G. S. A Correlation of Reaction Rates. *J. Am. Chem. Soc.* **1955**, 77, 334.
- 62 Soundararajan, S.; Dalai, A.K.; Berruti, F. Modeling of Methanol to Olefins (MTO) Process in a Circulating Fluidized Bed Reactor. *Fuel.* **2001**, 80, 1187.
- 63 Kunii, D.; Levenspiel, O. *Fluidization Engineering*, 2nd ed.; Butterworth: Boston, 1991.
- 64 Levenspiel, O. *Chemical Reaction Engineering*, 3rd ed.; John Wiley: New York, 1999.
- 65 Othmer, D. *Fluidization*, 1st ed.; Reinhold: New York, 1956.
- 66 May, W. G. Fluidized-Bed Reactor Studies. *Chem. Eng. Prog.* **1959**, 55, 49.
- 67 Van Deemter, J. J. Mixing and Contacting in Gas-Solid Fluidized Beds. *Chem. Eng. Sci.* **1961**, 13, 143.
- 68 Leva, M. *Fluidization*, McGraw-Hill: New York, 1960.

69 Werther, J. Mathematical-Modeling of Fluidized-Bed Reactors. *Chem. Ing. Techn.* **1978**, 50, 850.

70 Poling, B.; Prausnitz, J.; O'Connell, J. *The Properties of Gases and Liquids*, 5th ed.; McGraw-Hill: New York, 2001.

71 Wender, L.; Cooper, G. T. Heat Transfer between Fluidized-solid Beds and Boundary Surfaces, Correlation of Data. *A.I.Ch.E.J.* **1958**, 4, 15.

72 Pell, M. *Gas Fluidization*, Elsevier: Amsterdam, 1990.

APPENDIX A

Table A-1. List of Olefins Involved in the MTO Reaction Network Generated by Park.⁴⁴

O_{ij}	$c/t^a i^b j^c \sigma_{gl}^d$						
	- 2 - 4		{ t 7 12 27		{ t 8 17 27/2		- 8 57 27/2
	- 3 - 3		{ c 7 13 27		{ c 8 18 27/2		- 8 58 81
	- 4 1 3		- 7 14 9		{ t 8 19 27/2		{ t 8 59 162
	{ c 4 2 18		{ t 7 15 27/2		{ c 8 20 27/2		{ c 8 60 162
	{ t 4 3 18		{ c 7 16 27/2		- 8 21 9/2		- 8 61 27
	- 4 4 18		- 7 17 9/2		{ t 8 22 27/2		- 8 62 27/2
	- 5 1 3		- 7 18 9		{ c 8 23 27/2		- 8 63 27
	{ c 5 2 9		{ t 7 19 27		{ t 8 24 27		- 8 64 27
	{ t 5 3 9		{ c 7 20 27		{ c 8 25 27		{ t 8 65 243
	- 5 4 9		- 7 21 9		- 8 26 9		{ c 8 66 243
	- 5 5 27		- 7 22 81		{ t 8 27 27		- 8 67 729
	- 5 6 9		- 7 23 27/2		{ c 8 28 27		- 8 68 81
	- 6 1 3		{ t 7 24 81		{ t 8 29 27		- 8 69 243/2
	{ c 6 2 9		{ c 7 25 81		{ c 8 30 27		{ t 8 70 729
	{ t 6 3 9		- 7 26 81		- 8 31 9		{ c 8 71 729
	{ c 6 4 18		- 7 27 27		- 8 32 81/2		- 8 72 27
	{ t 6 5 18		- 7 28 27		{ t 8 33 81		- 8 73 81/2
	- 6 6 9/2		- 7 29 27/2		{ c 8 34 81		- 8 74 243
	- 6 7 9		- 7 30 27		{ t 8 35 81/2		- 8 75 81
	{ c 6 8 27		{ t 7 31 243		{ c 8 36 81/2		- 8 76 243
	{ t 6 9 27		{ c 7 32 243		{ t 8 37 81		- 8 77 81
	- 6 10 81		- 7 33 81		{ c 8 38 81		- 8 78 162
	- 6 11 27		- 7 34 243		- 8 39 9/2		- 8 79 243
	{ c 6 12 27		- 8 1 3		- 8 40 18		
	{ t 6 13 27		{ t 8 2 9		- 8 41 27/4		
	- 6 14 9		{ c 8 3 9		{ t 8 42 81/2		
	- 6 15 27		{ t 8 4 9		{ c 8 43 81/2		
	- 6 16 324		{ c 8 5 9		{ t 8 44 162		
	- 6 17 18		{ t 8 6 18		{ c 8 45 162		
	- 7 1 3		{ c 8 7 18		- 8 46 27/2		
	{ t 7 2 9		- 8 8 9/2		{ t 8 47 81		
	{ c 7 3 9		{ t 8 9 27		{ c 8 48 81		
	{ t 7 4 9		{ c 8 10 27		- 8 49 27/2		
	{ c 7 5 9		- 8 11 27		- 8 50 81		
	- 7 6 9/2		- 8 12 27		{ t 8 51 243		
	{ t 7 7 27		{ c 8 13 27		{ c 8 52 243		
	{ c 7 8 27		{ t 8 14 27		- 8 53 27/2		
	- 7 9 27		{ c 8 15 27		{ t 8 54 81		
	{ t 7 10 27		- 8 16 9		{ c 8 55 81		
	{ c 7 11 27				- 8 56 27		

^a c/t = cis/trans
^b i = carbon number
^c j = isomer index
^d σ_{gl} = global symmetry number

Table A-2. List of Carbenium Ions Involved in the MTO Reaction Network Generated by Park.⁴⁴

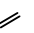
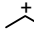
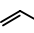
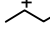
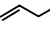

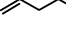
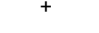

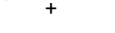
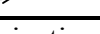
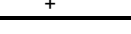
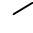
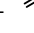


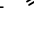






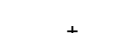
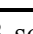










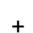
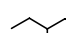

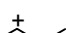

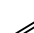
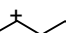



R_j^+	i^a	j^b	σ_{gl}^c												
	1	-	6		7	1	9		8	3	27/2		8	25	81
	2	-	6		7	2	9		8	4	27		8	26	27/2
	3	1	18		7	3	27/2		8	5	9		8	27	81/2
	3	2	18		7	4	27		8	6	27/2		8	28	81
	4	1	9		7	5	18		8	7	27/2		8	29	81
	4	2	162		7	6	27/2		8	8	27		8	30	27
	4	3	6		7	7	27		8	9	54		8	31	81
	5	1	9		7	8	54		8	10	27		8	32	243
	5	2	18		7	9	27		8	11	81/2		8	33	729
	5	3	27		7	10	162		8	12	81/2		8	34	729/2
	5	4	54		7	11	81/2		8	13	27/2		8	35	162
	6	1	9		7	12	27/2		8	14	54		8	36	486/2
	6	2	9		7	13	81		8	15	27/2		8	37	486
	6	3	27/2		7	14	81		8	16	81/4		8	38	729
	6	4	27		7	15	162/2		8	17	81/2		8	39	243
	6	5	54		7	16	243		8	18	81		8	40	243
	6	6	54		7	17	27		8	19	162/2		8	41	243
	6	7	27		7	18	162		8	20	243		8	42	1458
	6	8	162		7	19	243		8	21	27				
	6	9	243		7	20	1458		8	22	81				
					8	1	9		8	23	81/2				
					8	2	9		8	24	162/2				

^a i = carbon number
^b j = isomer index
^c σ_{gl} = global symmetry number

Table A-3. Rates and Equilibrium Constants for the Elementary Steps of the Primary Products Formation in the MTO Process on SAPO-34 at Different Temperatures.

Elementary Steps		Rate or Equilibrium Constants	Values			Unit	
			380°C	440°C	480°C		
DME Formation							
$MeOH + H^+$	\rightleftharpoons	$MeOH_2^+$	$K_{Pr}(MeOH)$	4.6670E+00	1.1994E+00	5.4676E-01	dimensionless
$MeOH_2^+$	\rightleftharpoons	$R_1^+ + H_2O$	$k'_F(R_1^+)$	1.1834E+03	1.3502E+03	1.4571E+03	$s^{-1} \cdot bar^{-1}$
			$k'_C(R_1^+)$	8.7018E+01	8.8401E+01	8.9210E+01	$s^{-1} \cdot bar^{-1}$
$R_1^+ + MeOH$	\rightleftharpoons	DMO^+	$k'_F(DMO^+)$	2.5740E+01	2.6141E+01	2.6376E+01	$s^{-1} \cdot bar^{-1}$
			$k'_C(DMO^+)$	5.8085E-04	1.0698E-03	1.5228E-03	$s^{-1} \cdot bar^{-1}$
DMO^+	\rightleftharpoons	$DME + H^+$	$K_{Pr}(DME)$	4.7924E+05	1.0446E+05	4.3294E+04	dimensionless
Methane Formation							
$R_1^+ + MeOH$	\rightarrow	$CH_4 + HCHO + H^+$	$k'_F(CH_4)$	7.6073E-02	1.1725E+00	5.7000E+00	$s^{-1} \cdot bar^{-1}$
Primary Olefins Formation							
$R_1^+ + bs$	\rightleftharpoons	$OM + H^+$	$k'_{Sr}(R_1^+; bs)$	1.0392E+02	1.6289E+03	7.9967E+03	s^{-1}
			$k'_{Sr}(OM; H^+)$	5.4556E+05	5.1185E+06	1.8676E+07	s^{-1}
$OM + DMO^+$	\rightarrow	$R_2^+ + MeOH + bs$	$k'_{Sr}(OM; DMO^+; R_2^+)$	6.0431E+02	9.8567E+02	1.3079E+03	s^{-1}
R_2^+	\rightleftharpoons	$O_2 + H^+$	$k'_{De}(R_2^+)$	2.4036E-02	2.1419E-01	7.5860E-01	$s^{-1} \cdot bar^{-1}$
			$k'_{Pr}(O_2)$	1.1865E-03	4.4373E-03	9.5127E-03	$s^{-1} \cdot bar^{-1}$
$OM + DMO^+$	\rightarrow	$R_3^+ + H_2O + bs$	$k'_{Sr}(OM; DMO^+; R_3^+)$	4.8509E+02	5.5275E+02	5.9610E+02	s^{-1}

Table A-4. Single Event Rate Constants of the Elementary Steps for the Formation of Higher Olefins in the MTO Process on SAPO-34 at Different Temperatures.

Elementary Steps				Rate Constants in s ⁻¹			
				380°C	440°C	480°C	
Methylation							
R_1^+	+		→		1.1336E-02	5.0813E-02	1.2099E-01
R_1^+	+		→		1.2200E-02	5.4273E-02	1.2865E-01
R_1^+	+		→		1.1989E-02	5.3404E-02	1.2668E-01
R_1^+	+		→		1.2011E-02	5.3493E-02	1.2688E-01
R_1^+	+		→		1.5113E-02	6.6024E-02	1.5487E-01
R_1^+	+		→		1.6557E-02	7.1789E-02	1.6766E-01
Oligomerization							
	+		→		1.1336E-02	5.0816E-02	1.2101E-01
	+		→		1.4200E-02	6.2352E-02	1.4667E-01
	+		→		1.4335E-02	6.2894E-02	1.4787E-01
	+		→		1.8197E-02	7.8265E-02	1.8190E-01
	+		→		2.0199E-02	8.6116E-02	1.9914E-01
β-scission							
	→		+		8.6224E-15	7.2915E-14	2.5139E-13
	→		+		9.2136E-21	3.1502E-19	2.4483E-18
	→		+		6.1587E-22	2.7259E-20	2.4593E-19
	→		+		1.7159E-22	1.1352E-20	1.2913E-19
	→		+		1.3268E-24	1.1382E-22	1.5030E-21
	→		+		7.8318E-24	6.6233E-22	8.6873E-21

VITA

Saeed M. Al Wahabi was born in Riyadh, Saudi Arabia on September 13, 1969. In 1992 he received a Bachelor of Science in chemical engineering from King Saud University in Riyadh, Saudi Arabia. In the same year, he joined SABIC R&T in Riyadh and worked as a catalyst engineer. In 1998 he received a Master of Science in chemical engineering from King Saud University. In 2000 he received a scholarship from SABIC to study in the USA for a Ph.D. in chemical engineering. In the spring of 2000, he began graduate studies towards his Ph.D. at Texas A&M University in College Station, TX. After graduation he will return to work at SABIC R&T.

He can be reached in the following address:

SABIC R&T, P.O. Box 5101, Riyadh 11422, Saudi Arabia